Contribution to the Estimation of Uncertainties in Assembly Operations Assisted by 3D Metrology

by

Moloud JAFARI

THESIS PRESENTED TO ÉCOLE DE TECHNOLOGIE SUPÉRIEURE IN PARTIAL FULFILLMENT FOR A MASTER'S DEGREE WITH THESIS IN MECHANICAL ENGINEERING
M.A.Sc.

MONTREAL, JANUARY 12, 2026

ÉCOLE DE TECHNOLOGIE SUPÉRIEURE
UNIVERSITÉ DU QUÉBEC

BOARD OF EXAMINERS

THIS THESIS HAS BEEN EVALUATED

BY THE FOLLOWING BOARD OF EXAMINERS

Mr. Souheil-Antoine Tahan, Thesis Supervisor
Department of Mechanical Engineering at École de technologie supérieure

Mr. Louis Rivest, Thesis Co-supervisor
Department of Systems Engineering at École de technologie supérieure

Mr. Sasan Sattarpanah Karganroudi, Thesis Co-supervisor
Department of Mechanical Engineering at Université du Québec à Trois-Rivières

Mrs. Julia Guérineau, President of the Board of Examiners
Department of Systems Engineering at École de technologie supérieure

Mr. Lucas Hof, Member of the jury
Department of Mechanical Engineering at École de technologie supérieure

THIS THESIS WAS PRENSENTED AND DEFENDED

IN THE PRESENCE OF A BOARD OF EXAMINERS AND PUBLIC

ON DECEMBER 11, 2025

AT ÉCOLE DE TECHNOLOGIE SUPÉRIEURE

FOREWORD

In memory of my father,

To my mother, for her love,

To my brother, Reza, for his support,

And to my magic friend, for always being there.

ACKNOWLEDGEMENTS

First, my heartfelt thanks go to the esteemed Professor Tahan, whose guidance and wisdom have always illuminated my path, offering me support as caring father. I am also immensely thankful to Professor Sattarpanah and Professor Rivest, my co-supervisors, for their precise insights and guidance in steering me in the right direction.

I would like to extend my gratitude to the respected juries for their dedication in reviewing and providing valuable feedback on this thesis. I also wish to thank Mr. Joël Grignon for his invaluable technical assistance, responsiveness, and unwavering support. Thank you to Mr. Hubert Krempa and 7DK for dedicated iGPS support, timely help, and technical guidance.

I am deeply grateful to my family to my mother for her unconditional love, calming presence, and constant support; to my brother Reza, dear Gelareh and my sisters for their continuous help, encouragement, and enduring kindness.

I would also like to warmly thank my colleagues at the Metrology Laboratory, especially Mohamed Hosame Kanali and William Babin, for their daily collaboration, team spirit, and the many insightful exchanges we shared. Their presence made this experience much richer.

Finally, I would like to thank all those who, directly or indirectly, supported me or contributed to the progress of this research through their encouragement, advice, or simply being present when needed especially Majid Yazdani, whose support is sincerely appreciated. To each and every one of you, I extend my deepest gratitude.

CONTRIBUTION À L'ESTIMATION DES INCERTITUDES DANS LES OPÉRATIONS D'ASSEMBLAGE ASSISTÉES PAR LA MÉTROLOGIE 3D

Moloud JAFARI

RÉSUMÉ

L'assemblage sur gabarit est une méthode très employée dans les industries automobiles et aéronautiques. Parmi ses avantages, nous pouvons mentionner sa robustesse et ses performances métrologiques (bonne répétabilité). Aussi, même des non spécialistes peuvent l'utiliser, les composants sont immobilisés avec des butées avant de finaliser l'assemblage. Finalement, la qualité est garantie par une certification du gabarit employé. Par contre, les désavantages sont nombreux. En plus de l'important coût de fabrication et d'étalonnage de ces gabarits, ces derniers sont prévus pour un usage spécifique ; dès qu'il y a une modification ou une altération du modèle ou des composants, des modifications coûteuses doivent être réalisées.

Depuis environ deux décennies, le développement des systèmes de mesures 3D est impressionnant. Aujourd'hui, nous avons accès à des technologies qui permettent le suivi simultané d'un ensemble de cibles (>30) dans l'espace de travail (jusqu'à 100×100 m) avec une bonne précision (<0.5 mm @ 95%). Le principe de l'assemblage sans gabarit (Jigless Assembly) exploite les capacités des équipements de meure 3D (ex. iGPA, Laser Tracker…) pour positionner et orienter les composants selon les requis exigés. L'idée est donc de proposer une nouvelle méthode d'assemblage, dite « Assemblage Assisté par Métrologie » (AAM), qui se veut une alternative à celle de l'assemblage sur gabarit. L'AAM offrira une très bonne flexibilité qui peut se traduire par des gains de productivité.

Toutefois, pour un déploiement industriel, il faut résoudre un verrou technologique qui est l'assurance qualité de l'assemblage qui sera obtenu par AAM. En effet, il faut estimer et consigner l'incertitude inhérente à une opération d'assemblage réalisée par AMM. Ainsi, la principale question est de développer une approche pour chiffrer le doute associé sur le résultat obtenu par AAM sur une caractéristique critique (KC)? Ce mémoire a pour principal objectif le développement d'une méthodologie générale permettant d'estimer l'incertitude sur une opération d'assemblage AAM en utilisant un système iGPS.

Mots-clés : Assemblage sans gabarit, Assemblage assisté par métrologie (AAM), iGPS, Laser Tracker, Incertitude de mesure

CONTRIBUTION TO THE ESTIMATION OF UNCERTAINTIES IN ASSEMBLY OPERATIONS ASSISTED BY 3D METROLOGY

Moloud JAFARI

ABSTRACT

Jig -based assembly is a method widely used in the automotive and aerospace industries. Among its advantages, its robustness and its metrological performance (good repeatability) can be mentioned. In addition, even non-specialists can use it; the components are immobilized using stops before finalizing the assembly. Finally, quality is guaranteed through certification of the fixture used. On the other hand, the disadvantages are numerous. In addition to the significant cost of manufacturing and calibrating these jig, they are intended for a specific use; as soon as there is a modification or an alteration of the model or the components, costly modifications must be carried out.

For approximately two decades, the development of 3D measurement systems has been impressive. Today, we have access to technologies that allow the simultaneous tracking of a set of targets (>30) within the workspace (up to 100×100 m) with good accuracy (<0.5 mm @ 95%). The principle of jigless assembly (Jigless Assembly) exploits the capabilities of 3D measurement equipment (e.g., iGPS, laser tracker…) to position and orient components according to the required specifications. The idea is therefore to propose a new assembly method, referred to as "Metrology-Assisted Assembly" (MAA), which is intended as an alternative to jig-based assembly. MAA will offer very good flexibility, which can translate into productivity gains.

However, for industrial deployment, it is necessary to resolve a technological barrier, which is the quality assurance of the assembly that will be obtained by MAA. Indeed, it is necessary to estimate and document the uncertainty inherent to an assembly operation carried out using MAA. Thus, the main question is to develop an approach to quantify the uncertainty associated with the result obtained by MAA on a critical characteristic (KC)? The main objective of this thesis is the development of a general methodology to estimate the uncertainty of a metrology-assisted assembly operation using an iGPS system.

Keywords: Jigless Assembly, Metrology-Assisted Assembly (MAA), iGPS, Laser Tracker, Measurement Uncertainty

TABLE OF CONTENTS

Page

LIST OF TABLES

Page

LIST OF FIGURES

LIST OF ABBREVIATIONS AND ACRONYMS

AMM	Assemble-Measure-Move
ADM	Absolute Distance Meters
AIAG	Automotive Industry Action Group
ANOVA	Analysis of variance
ASME	American Society of Mechanical Engineers
AIAG	Automotive Industry Action Group
AIFM	Absolute Interferometer
BIM	Building Information Modeling
BIPM	International Bureau of Weights and Measures
CAD	Computer-Aided Design
CAM	Computer-Aided Manufacturing
CDF	Cumulative Distribution Function
CI	Confidence Interval
CMM	Coordinate Measuring Device
DA	Determinate Assembly
DOF	Degree of Freedom
ÉTS	École de technologie supérieure
F-Statistic	Fisher-Statistic
GD&T	Geometric and Dimensional Tolerancing
GCS	Global Coordinate System
GPS	Geometrical Product Specifications
GUM	Guide to Expressing Measurement Uncertainty
iGPS	Indoor Global Positioning System
ISO	International Organization for Standardization
IFM	Laser Interferometers
KC	Key characteristic
LCS	Local Coordinate System
LSM	Large-Scale Metrology

LT	Laser Tracker
MAA	Metrology-Assisted Assembly
MADA	Measurement Assisted Determinate Assembly
MC	Monte Carlo
MCS	Measurement Coordinate System
MPE	Maximum Permissible Error
MSA	Measurement System Analysis
PDF	Probability Density Function
RMSE	Root Mean Square Error
R&R	Repeatability and Reproducibility

LIST OF SYMBOLS AND UNITS OF MEASUREMENT

a, b	Estimated Coordinates of Circle Center
Hz	Hertz
μm	Micrometer
mm	Millimetre
m	Meter
s	Second
(°)	Degrees
θ	Horizontal Angle
Φ	Zenith Angle
d	Distance
d_{ij}	Euclidean Distance between Points i and j
$\hat{e}_{\mathrm{i}}$	Radial Residual of Point i $(\hat{p}_{\mathrm{i}} - \hat{R})$
$J(a, b, R)$	Objective Function in Circle Fitting (Least-Squares Residuals)
P	Point
$\hat{p}_{\mathrm{i}}$	Distance of Point i from Estimated Center
$\mathbb{R}^n$	The n-Dimensional Space of Real Numbers
$\mathbb{R}_+$	Non-negative Real Numbers
$\mathbb{R}$	Set of Real Numbers
R	True and Estimated Circle Radius
u_c	Measurement reference uncertainty
u_m	Uncertainty of Measurement Equipment Error
u_i	Indicator uncertainty
u_{Rep}	Repeatability Uncertainty
u_{X_i}	Standard uncertainties of each X_i
u_x	Standard deviation of repeated measurements (repeatability)
$u_{\bar{x}}$	Standard uncertainty of the mean
U_Y	Expanded uncertainty (at 95% CI level)
$\mathcal{N}(0, u_x)$	Normal Distribution

$\bar{x}$	Estimated average
x_i	i^{th}measured value
s	The sample standard deviation
σ^2	Estimated variance
σ	Estimated standard deviation
n	Sample size
H_0	Null hypothesis
H_1	Alternative hypothesis
p_value	Probability of making a Type I error
t	Time

INTRODUCTION

Mechanical assembly is a fundamental process in manufacturing, involving the integration of various components to form a complete product or a significant part of a product (Fiedler et al., 2024). Assembly processes can be performed using different methodologies, each tailored to specific product requirements and production scales. Among different assembly methods, jig-based assembly has been a traditional and widely used approach in large-scale industries due to its precision, robustness, and ease of use. Jigs ensure accurate positioning and alignment of components, enabling high-quality results even with minimal operator training.

Despite their effectiveness, jigs have significant limitations, including high costs and limited flexibility. Jigless assembly eliminates the need for physical jigs, offering greater flexibility and cost efficiency. In jigless assembly, the absence of physical jigs necessitates alternative methods to ensure that components are accurately positioned relative to one another.

To address this challenge, 3D metrology emerges as a promising solution. By leveraging advanced 3D measurement devices, such as the iGPS system, it is possible to determine the position of each part in real time. These systems enable the real-time measurement of multiple targets, allowing operators to achieve precise alignment, gap measurement, and other key characteristics (KCs) required during assembly. However, the implementation of such technologies is not without its own difficulties. The measurement uncertainty in 3D devices can impact the reliability of the results, especially when strict tolerances must be maintained.

This research focuses on developing a methodology for jigless assembly by using 3D metrology with uncertainty management to achieve precise and reliable results. By addressing these challenges, the study aims to enhance the efficiency and adaptability of mechanical assembly processes while maintaining high standards of quality.

Chapter 1 sets the context, problem statement, and scope. Chapter 2 provides a literature review on relevant topics and concepts, identifying existing gaps in prior studies. Chapter 3 focuses

on defining the objectives and methodology of this study. Chapter 4 develops the uncertainty estimation and propagation model for jigless assembly using iGPS. Chapter 5 presents the experimental setup, data, and validation results. Chapter 6 concludes and outlines future work. Together, these chapters provide a comprehensive framework to develop a general method for estimating measurement uncertainty in 3D metrology using iGPS for jigless assembly operations.

CHAPTER 1

PROBLEM STATEMENT

1.1 Overview of Assembly Challenges in Industries

The automotive and aerospace industries are facing increasing demands for flexible, efficient, and cost-effective production systems. These sectors are characterized by structural and operational complexity and precision required in their assembly processes, which are critical not only for product functionality but also for maintaining competitiveness. Assembly accounts for a significant portion of production costs, particularly in large-scale manufacturing. In this context, the rising customer demand for customized products creates a fundamental challenge: the need to maintain the cost-efficiency of mass production while delivering unique, high-quality products (Pilati, Lelli, Regattieri, & Ferrari, 2022).

Traditional manufacturing paradigms, such as mass production, focused on standardized workflows to achieve cost efficiency. However, the shift towards mass customization has introduced the need for flexible production systems capable of handling a wide range of product variants. For example, the automotive industry requires up to 1,032 variants for a single compact car model, necessitating the adoption of assembly-to-order strategies. These systems demand real-time information and precise coordination to minimize errors and maintain efficiency (Pilati et al., 2022). Moreover, the need to inspect and rework defective products adds to production complexity, highlighting the importance of flexible systems that can adapt to changing requirements (Ganguly, Dey, Pareek, & Sarkar, 2023).

Jigs have historically played a pivotal role in manufacturing, providing essential positioning and alignment capabilities during assembly. However, their limitations are becoming increasingly evident. Jigs constitute up to 29% of capital expenditure and lack flexibility, as each new product design requires a unique jig, adding to costs and delays. These inefficiencies are particularly pronounced in high-volume and rapidly changing manufacturing environments, where flexibility is critical (Fiedler et al., 2024).

In the aerospace industry, the reliance on jigs for accurate alignment during assembly further underscores the limitations of traditional methods. Aircraft assembly, which accounts for more than 50% of the manufacturing workload, relies heavily on jigs to meet stringent accuracy and coordination requirements. As illustrated in (Figure 1.1), these structures can be massive and complex, exemplified by a large-scale wing jig used in facilities like Bombardier Aerospace®. However, this dependence introduces significant costs and inflexibility, as each new aircraft design requires the development of dedicated jigs, adding to production expenses and time (Mei & Maropoulos, 2014).

The concept of jigless assembly, enabled by advanced technologies such as 3D metrology, offers a solution to these challenges. Systems like iGPS allow for real-time measurement and positioning without the need for physical jigs, enhancing flexibility and reducing costs.

Incorporating 3D metrology into assembly processes, known as Metrology-Assisted Assembly (MAA), has emerged as a promising approach. MAA leverages dimensional measurements to guide assembly operations, enhancing precision, flexibility, and quality. This approach aligns with the principles of Industry 4.0, integrating advanced technologies to improve efficiency and productivity (J. E. Muelaner, Martin, & Maropoulos, 2013).

Despite these advancements, several challenges remain, including the lack of standardized measurement systems and the need to manage uncertainties in key characteristics. Addressing these issues is essential for the successful implementation of jigless assembly and the broader adoption of flexible production systems in the automotive and aerospace industries. By overcoming these challenges, these industries can achieve greater efficiency, cost effectiveness, and adaptability, ensuring their competitiveness in an increasingly demanding market.

Figure 1.1 Large-scale wing jig, from Bombardier Aerospace

1.2 Research Challenges

In industrial assembly, jigs are highly precise tools widely used in large-scale industries to facilitate assembly processes. However, they present significant challenges in terms of production costs. Jigs are not only expensive to design and manufacture but also require extensive time and costs for calibration and inspection. Another critical drawback is their lack of flexibility; any modification to the product design necessitates changes to the jig itself, leading to additional expenses and delays. Despite these issues, jigs remain robust tools that ensure excellent quality assurance, require minimal operator training, and do not demand a highly specialized workforce.

On the other hand, advancements in technology have opened new opportunities to address these challenges, steering the industry toward jigless assembly. The primary question, however, is how to effectively leverage this opportunity to implement jigless assembly while maintaining or even improving assembly performance.

Advanced 3D measurement systems, such as iGPS, offer significant potential for jigless assembly. These systems can simultaneously detect multiple targets, are cost-effective, and are

easy to calibrate. However, the absence of defined standards for 3D measurements using iGPS raises concerns about its reliability in jigless assembly operations, particularly regarding two critical challenges:

i. Quantification of measurement uncertainty: How can the intrinsic uncertainty of iGPS measurements be characterized and quantified within a defined work volume?

ii. Propagation of uncertainty to key assembly characteristics (KCs): How does the uncertainty of individual iGPS measurements affect the accuracy of key characteristics in Metrology-Assisted Assembly (MAA)?

Addressing these challenges requires the following steps:

- Quantifying the measurement uncertainty of iGPS for single points along each coordinate axis (X, Y, Z) within a work volume.
- Developing a methodology for propagation uncertainty to given key characteristics (KCs) in MAA operations to ensure reliable and accurate assembly operations.

In jig-based processes, measurements are inherently precise with tightly controlled tolerances. In contrast, jigless assembly relies on measurements accompanied by inherent uncertainties. The challenge lies in ensuring that measurement uncertainty remains within the specified tolerance range.

In summary, traditional jigs provide precision and reliability, but their high cost and limited flexibility reduce their effectiveness in modern manufacturing. Advanced 3D metrology systems like iGPS offer a promising alternative to jigless assembly. However, challenges remain, particularly in ensuring measurement accuracy and developing a method to estimate uncertainty for key characteristics (KCs) in MAA. Managing these uncertainties is essential to enable more efficient and flexible assembly processes.

CHAPTER 2

STATE OF ART

In this chapter, we will review the relevant literature and explore key concepts related to the topic, while identifying existing research and highlighting the gaps in the current body of knowledge. First, we will delve into the concepts of assembly using jigs and jigless assembly. We will then examine the application of 3D metrology technologies and advanced assembly techniques, focusing on the use of iGPS as a measurement tool. Additionally, we will explore the concept of measurement uncertainty, including the methods used to quantify and statistically analyze it. Finally, this chapter is concluded by discussing the research gaps in current literature and laying the groundwork for the contributions of this study.

2.1 Methods of Assembly

The term "assembly" in a manufacturing context refers to the process of putting together various components or parts to form a complete product or a significant part of a product (Fiedler et al., 2024).

In the following, the two assembly methods of Jig and Jigless assembly will be explained.

2.1.1 Jig Assembly

A jig is a highly precise tool used to hold and position the part during assembly, ensuring that the part is maintained with great accuracy. Its primary function is to guarantee the precision of the product (Naing, Burley, Odi, Williamson, & Corbett, 2000).

A jig serves to accurately position and secure parts during assembly or machining, ensuring the correct operation of the process. It employs positioning mechanisms to support and assemble components, often using clamps to prevent movement. In the aircraft industry, dedicated jigs are critical for ensuring product quality and maintaining tight tolerances.

However, due to increasing competition, there is a growing need for cost reduction and efficiency improvements through the adoption of advanced technologies. Approximately 10% of the costs associated with airframe manufacturing are related to the production and maintenance of jigs (de Mello et al., 2020).

In the past, particularly in large-scale aerospace assemblies, skilled craftsmen manually positioned parts using general tools. However, this method proved inefficient, leading to the use of rigid and costly jigs. Despite advancements in engineering and technology within the aerospace industry, the use of such jigs persists due to the difficulty of maintaining tight tolerances in large structures. Precise alignments, particularly in drilling patterns, are challenging to achieve, and the common solution has been the use of jigs during assembly. This reliance on jigs, however, introduces limitations such as decreased production efficiency (Jody E Muelaner, Kayani, Martin, & Maropoulos, 2011).

In large aerospace assemblies, jigs are essential for ensuring precision and stability, compensating for the limitations of manual craftsmanship. These tools maintain accuracy in complex operations, yet each unique assembly requires a specific. Jigs require precise calibration to meet standards and involve substantial production, set up, and storage costs, where frequent adjustments for design changes further challenge efficiency. While these tools are critical for quality, their high costs, limited adaptability, and long preparation times create logistical obstacles, especially for short production runs. Consequently, the aerospace industry is increasingly seeking flexible, reconfigurable solutions that can eliminate the need for jigs (Mozzillo, Iaccarino, Vitolo, & Franciosa, 2019 ; Naing et al., 2000).

These challenges lead us to seek a solution that eliminates the need for a jig, which will be explained in detail later.

2.1.2 Jigless Assembly

The Jigless Assembly Concept is designed to implement a jigless approach by integrating management strategies, design tools, and manufacturing processes. It unifies various techniques to form a cohesive assembly system, promoting flexibility and reducing setup times (Naing et al., 2000).

Jigless Assembly aims to minimize the use of product-specific assembly tooling by incorporating supportive technologies. This approach does not eliminate all tooling but significantly reduces dependence on jigs.

Figure 2.1 Jigless assembly process utilizing 3D metrology (iGPS) is used for the alignment and joining of large aircraft components (Mei & Maropoulos, 2014)

As shown in (Figure 2.1), the jigless assembly concept relies on 3D metrology systems such as iGPS to guide the alignment and joining of large aircraft parts. The use of these measurement systems enables accurate positioning without the need for physical jigs.

Jigless assembly increases flexibility and reduces setup times, making it a more efficient and scalable option in industries such as aerospace. By utilizing a Universal Magnetic Table

(UMT) and lean manufacturing in a robotic cell, this approach minimizes reliance on complex jigs and improves efficiency in later stages of production, offering more streamlined assembly processes. This significant role of automation within jigless assembly can reduce labor costs by 50-80% and lower overall product costs by 25-75%. However, the process still faces challenges such as the need for skill development and establishing effective human-machine interaction. To achieve successful automation, it is crucial to design products with automation as a key consideration).(de Mello et al., 2020).

Jigless assembly for aeronautical structures, specifically the "Integrated Main Landing Gearbox," has been investigated to reduce costs and enhance precision by eliminating jigs. This approach involves ergonomic analysis, digital modeling, and statistical tolerance prediction, leading to a flexible assembly process optimized through virtual simulations; however, real-world testing remains necessary to confirm its practical feasibility (Mozzillo et al., 2019).

In the context of industrial products requiring precise alignment, a fully jigless robotic assembly method has been introduced using a universal robotic hand. This system utilizes a self alignment technique and closed-loop control to achieve high accuracy and repeatability without traditional jigs, making it particularly beneficial for small and medium scale productions. Despite these advantages, the system’s adaptability to diverse part shapes is limited, suggesting a need for more universal alignment strategies (Fukuda et al., 2023).

Furthermore, a jigless production system for the automotive industry has been proposed that integrates jig features directly into the parts themselves to increase flexibility and reduce costs in body shop production. However, as the concept is still in early development, further research is required to fully integrate it into automotive production lines and evaluate its feasibility across varied automotive manufacturing environments (Fiedler et al., 2024).

Recent studies on position-control-based robots have also demonstrated an increase in assembly speed, though the overall assembly approach continues to require more detailed examination (Fiedler et al., 2024 ; Fukuda et al., 2023).

The need for control tools in jigless assembly arises from the challenge of maintaining precise alignment and positioning without relying on jigs. In these systems, real-time adjustments are crucial to ensure accuracy throughout the assembly process. Control tools play an essential role by enhancing part alignment and enabling continuous adjustments as assembly progresses. Additionally, these tools are fundamental to adapting jigless assembly within Industry 4.0 environments, where data integration and automation are key. Research also highlights that incorporating digital twin simulations and artificial intelligence within control systems can predict maintenance needs and optimize workflows, effectively substituting for the precision traditionally provided by jigs. In summary, control tools are indispensable in jigless assembly, bridging the gap left by jigs and delivering flexibility, precision, and compatibility with advanced manufacturing. They are central to making assembly operations more efficient and adaptive, meeting the stringent precision demands of sectors like aerospace and automotive (Dalle Mura & Dini, 2021).

In jigless assembly, in-process geometric control and real-time pose tracking are essential; 3D metrology provides the measurements and registration to achieve this. The next section introduces 3D metrology.

2.2 3D Metrology

3D metrology covers techniques and tools that rapidly capture precise 3D data from object surfaces. It is now integral to industrial workflows, especially for quality control, rapid prototyping, and reverse engineering (Mochizuki, 2010). Measurement systems must track multiple targets in real time (≈40-50Hz) and display their 3D positions. Since operators move frequently during assembly, distributed systems are preferred, eliminating the need to move equipment between stations (Maisano et al., 2008).

Metrology often relies on multiple systems, making data fusion essential for improving accuracy and coverage. In competitive fusion, systems independently measure 3D coordinates and merge results; in cooperative fusion, sensors share data to determine a common position, improving efficiency. Current trends include multi-sensor architectures that combine dimensional sensors with environmental ones (e.g., temperature, humidity) to reduce errors. Persistent challenges remain in calibration, uncertainty evaluation, and point registration, with cooperative approaches requiring further research (Schmitt et al., 2016).

Large-Scale Metrology (LSM) refers to measuring object geometry according to Geometrical Product Specifications (GPS), particularly for objects with linear dimensions ranging from one metre to several hundred metres (Schmitt et al., 2016).

In a review of scientific literature dating back to 1995, LSM systems were classified by noting object size and scope as key factors distinguishing them from conventional metrology. Typically, LSM involves objects ranging from 10 to 100 metres in size, with accuracy targets between 0.1 mm and 100 mm (Franceschini, Galetto, Maisano, & Mastrogiacomo, 2014).

In this work, the LSM size definition of Schmitt et al. (2016) (≈1 m to several hundred metres) and the accuracy targets of Franceschini et al. (2014) (sub-millimetre to tens of millimetres) are adopted.

In large-scale assembly and quality assurance, manufacturers select suitable devices, define measurement fields, and acquire data on position, orientation, shape, and interfaces. These are transformed into a common coordinate system to align components. Since no single device meets all requirements, integrated measurement networks are used, requiring knowledge of device principles, characteristics, and uncertainties (Chen & Du, 2017). In aerospace and other low-rate large-scale manufacturing, 3D metrology is indispensable, though challenges persist due to hardware limits and the need to set tolerances based on measurement uncertainty (Francis, Maropoulos, Mullineux, & Keogh, 2016).

Thus, the principles and capabilities of 3D metrology directly enable the concept of metrology-assisted assembly (MAA).

2.3 Measuring Systems for 3D Metrology-Assisted Assembly

3D Metrology-Assisted Assembly (MAA) is an assembly method that utilizes 3D metrology to actively observe crucial dimensional and geometric features during assembly processes. Originating in the UK through the efforts of JE Muelaner and PG Maropoulos as a component of the industry 4.0 evolution, this technique has garnered significant attention, prompting numerous researchers and institutions to engage in further exploration and advancement in this field.

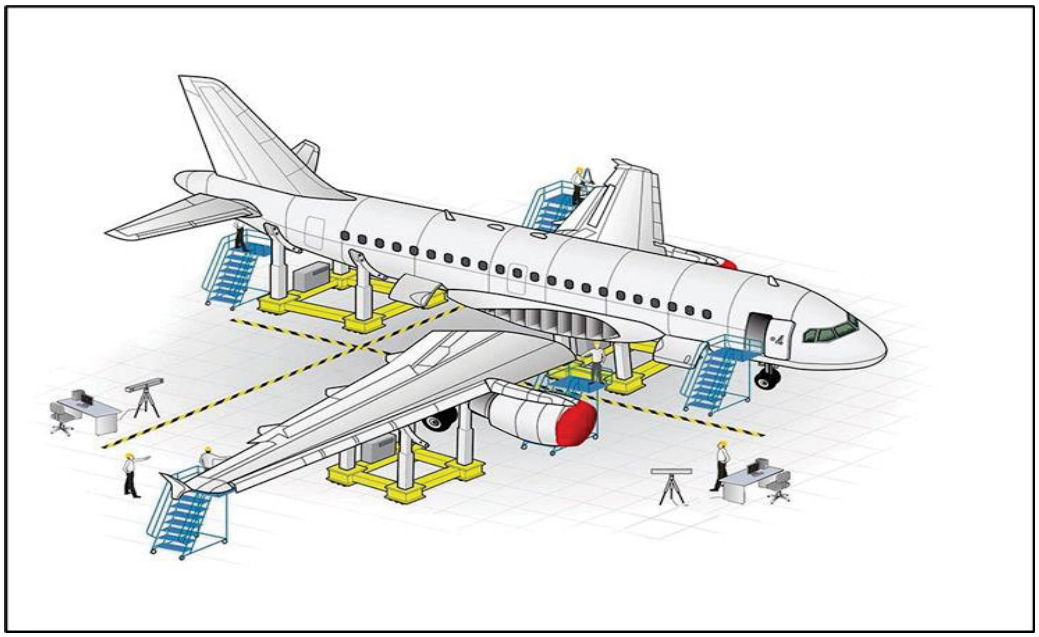

Figure 2.2 The assembly process assisted by 3D metrology
(« Metrolog X4 - Metrologic Group », 2019)

Figure 2.2 illustrates how MAA uses 3D metrology to guide real-time positioning and alignment of large aircraft components, reducing reliance on jigs and improving flexibility.

The 3D metrology-assisted assembly (MAA) process uses dimensional measurements to guide assembly operations and thus improve the economic performance and speed of the process. To respect the requirements linked to quality management in a company, MAA requires a guarantee of metrological traceability (metrological connection, procedures, proofs and evidence), which means that an analysis of uncertainties and a study of capability (performance) must be carried out to ensure that the assembly is correctly constructed from the start (J. E. Muelaner et al., 2013).

The MAA suggests incorporating 3D metrology into assembly processes to enhance precision, flexibility, and production quality.
It is essential to highlight that metrology-assisted assembly requires a device capable of dynamic tracking and real-time measurement of the components during assembly. In this project, two devices, iGPS and Laser Tracker, have been used, as shown in Table 2.1.

Table 2.1 Comparison of specifications of Laser Tracker and iGPS

	iGPS	**Laser Tracker**
Manufacturer	7 DK Metrology	Hexagon Metrology
Measurement Range	$2\text{m} - 40\text{ m}$	40 m
Accuracy	$\pm 200\ \mu\text{m} + 20\mu\text{m/m}$	$\pm 15\ \mu\text{m} + 6\ \mu\text{m/m}$
Interface Software	Metris Surveyor	Innovmetric Polyworks

2.3.3 Laser Tracker (LT)

The Laser Tracker (LT) is a portable system for large-scale measurements based on spherical coordinates. Essentially, it functions as a spherical coordinate measuring machine. Using a laser beam, it tracks a mirrored spherical probe to measure 3D coordinates. The control unit calculates the 3D coordinates of a reference target by combining distance data from a laser interferometer with angular data from encoders. The Laser Tracker (LT) measures three key values to determine the position of a target point (P): the distance (d) to the point, the horizontal angle (θ), and the zenith angle (φ), as shown in Figure 2.3.

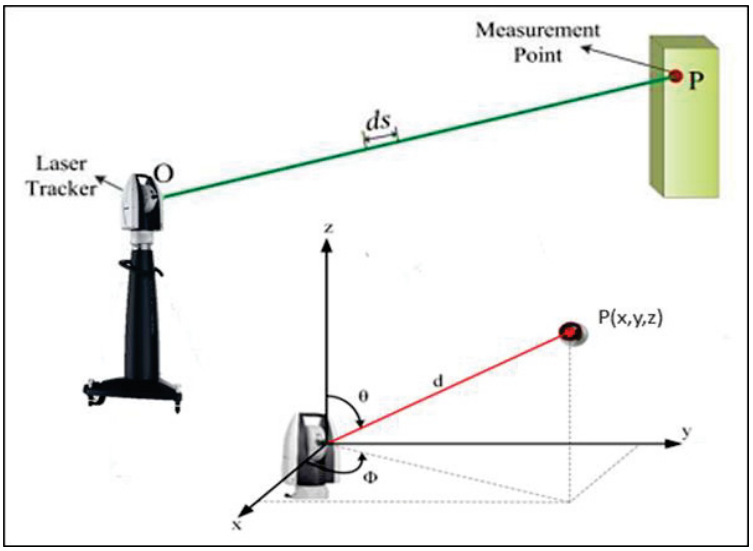

Figure 2.3 Measurement principle of Laser Tracker
(Zhu, Zheng, & Tang, 2016)

The distance is measured using a laser interferometer, while the angles are calculated using high-precision angle encoders (Zhu et al., 2016).

The relationship between the LT measurements and the Cartesian coordinates of points p_i is a function of the spherical coordinates q_i:

$$p_i = f(q_i) = f(d_i, \theta_i, \varphi_i) \tag{2.1}$$

As shown in Figure 2.3, the laser tracker measures three parameters for each target point: the radial distance d_i is from the tracker to point p_i; the azimuth angle θ_i (rotation in XY-plane); and the elevation angle φ_i from XY-plane toward the Z-axis. Based on these measurements, the Cartesian coordinates of the point in a three-dimensional space are calculated using the following formulas:

$$\begin{bmatrix} x_i \\ y_i \\ z_i \end{bmatrix} = \begin{bmatrix} d_i \cos\theta_i \sin\varphi_i \\ d_i \sin\theta_i \sin\varphi_i \\ d_i \cos\varphi_i \end{bmatrix} \tag{2.2}$$

2.3.4 Indoor GPS (iGPS)

The iGPS (indoor GPS) system is an advanced coordinate measurement machine that operates over a large area without a conventional frame. It includes transmitters that emit rotating laser signals and sensors that detect these signals. The system determines azimuth and elevation angles by analyzing the arrival times of these signals (See Figure 2.4)(J. E. Muelaner, Wang, Jamshidi, & Maropoulos, 2010).

The system operates using triangulation by calculating differences in signal arrival times and features a flexible, mobile setup. Multiple transmitters can function simultaneously, with layouts optimized for various applications (Schmitt et al., 2016).

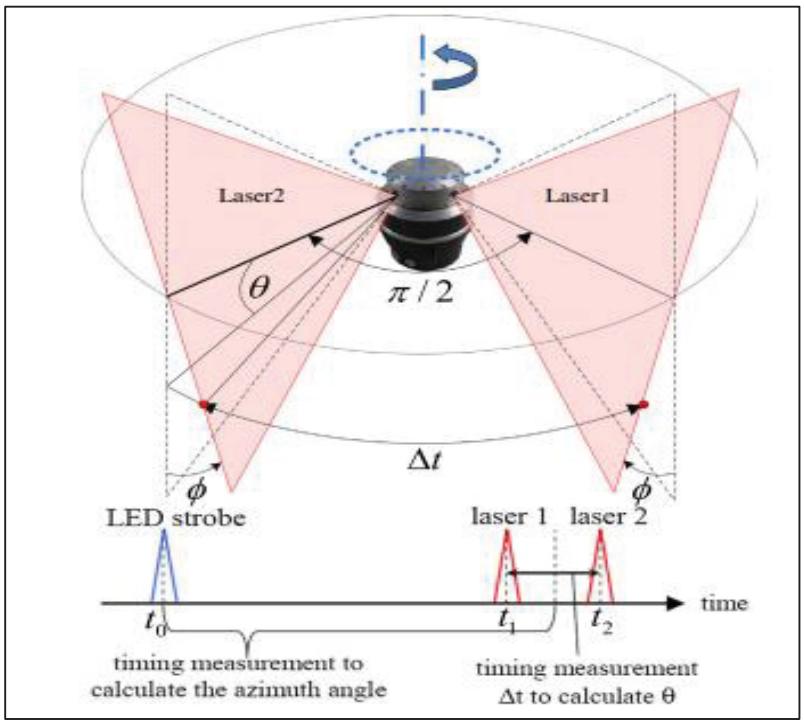

Figure 2.4 Description of the light signal from the transmitter
(Chen & Du, 2017)

iGPS Transmitter: The transmitter emits two fan-shaped laser beams and an infrared strobe, with its head rotating at a specific frequency. Sensors detect these signals to calculate angles, covering an area of up to 40 m² (See Figure 2.5)(https://7dkmetrology.com/, 2024).

Figure 2.5 iGPS Transmitter
(https://7dkmetrology.com/, 2024)

Integrated Sensor (i5): The i5 is a 5-degree of freedom (5DOF) sensor that converts optical signals into digital data for iGPS software. It supports 3D point measurements, automatic setup, monitoring, and 6DOF tracking when used with another sensor. It is designed for quick and easy deployment (See Figure 2.6)(https://7dkmetrology.com/, 2024).

Figure 2.6 i5 Integrated Sensor
(https://7dkmetrology.com/, 2024)

Long Reach Probe G6 Kit: The i6 Long Reach Probe delivers wireless 6DOF measurements within the iGPS system and is also utilized for the system calibration It is designed to provide high-accuracy measurements for large-scale inspection tasks and supports wireless operation for improved mobility during measurement (See Figure 2.7) (https://7dkmetrology.com/, 2024).

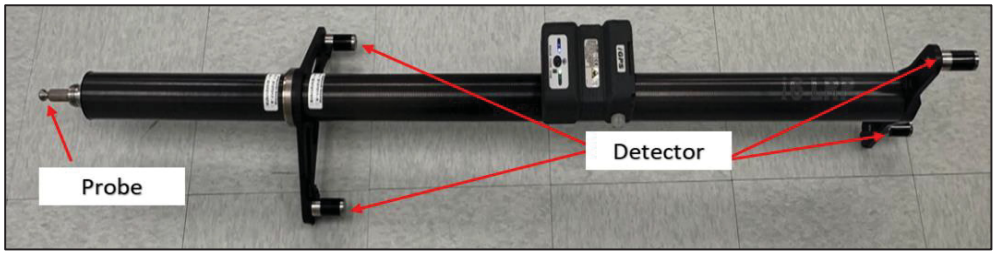

Figure 2.7 Long Reach Probe G6 Kit

The iGPS has been widely studied for its potential to enhance precision and flexibility in large-scale industrial applications, particularly in aerospace and robotics. Despite its advantages,

several challenges remain in terms of accuracy, integration, and dynamic performance. The following articles explore various aspects of iGPS, addressing both its improvements and the ongoing issues that need further investigation.

iGPS-assisted assembly techniques in the aerospace industry were examined, focusing primarily on improving assembly accuracy rather than directly addressing uncertainty. The main challenge identified in this study was balancing accuracy with efficiency in large-scale production (Drouot, Zhao, Irving, Sanderson, & Ratchev, 2018).

Precise tracking techniques were improved by integrating iGPS into industrial robots. Although the study aimed to enhance iGPS's dynamic performance, challenges such as integrating iGPS with other systems and improving dynamic capabilities remained unresolved (Han, Dunker, Trostmann, & Xu, 2024).

Statistical models were developed to assess iGPS system settings, which helped optimize configurations and reduce uncertainty. However, the study did not fully test the models in real-world conditions, nor did it compare iGPS with other systems. Additionally, issues related to user interaction and cost-benefit analysis were not adequately addressed (Ferri, Mastrogiacomo, & Faraway, 2010).

A multi-dimensional model for measurement planning in digital manufacturing was developed, improving the accuracy and efficiency of measurement processes. Although this model was optimized using iGPS, further integration of emerging technologies, such as artificial intelligence, was needed to further reduce uncertainty (Tang & Chen, 2015).

Genetic algorithms were used to optimize the placement of iGPS trackers, successfully reducing measurement uncertainty without increasing the number of stations. Although the approach improved accuracy, it did not fully explore the effects of environmental conditions and dynamic complexities, leaving room for further investigation (Ren, Fu, Liu, & Zhang, 2019).

The dynamic performance of iGPS in aerospace and industrial robots was examined, showing that the new iGPS software version reduced dynamic bias errors. However, bias errors persisted in more complex dynamic conditions and at higher speeds, and the new software was not fully evaluated in such scenarios (Wang, Mastrogiacomo, Franceschini, & Maropoulos, 2011).

The accuracy of the iGPS system was confirmed by comparing its data with laser tracker measurements and using Monte Carlo simulations to analyze uncertainty. Although the system showed acceptable performance at a 95% confidence level, further real-world testing and long-term uncertainty assessments in industrial environments were needed (J. E. Muelaner et al., 2010).

iGPS and laser tracker systems were integrated to align large aerospace structures, achieving high measurement accuracy. While the study succeeded in reducing uncertainty, challenges related to error propagation and the complexity of calibration processes remained unresolved (Zhao, Zhang, & Xiao, 2018).

A virtual iGPS model was developed to simulate and predict measurement uncertainty in large-scale assembly environments. By optimizing transmitter placement, the model significantly reduced measurement uncertainty. However, further validation in real-world assembly environments and the challenge of achieving uniform uncertainty distribution across complex environments remained (Nicksch, Sabzehi, & Schmitt, 2022).

These studies highlight advancements in reducing uncertainty and enhancing the performance of the iGPS system. However, challenges persist, such as assessing the uncertainty related to the iGPS device, evaluating how uncertainty propagates in 3D space, improving integration with other systems, and achieving real-world validation. These unresolved issues require further research and lay the groundwork for a more in-depth examination of uncertainty and its implications in the upcoming section.

2.4 Uncertainty of a Measurement System

Various guides and standards provide instructions to help analyze the performance of measurement systems. Two key documents often referenced are:
Guide to the Expression of Uncertainty in Measurement (GUM), which outlines theoretical principles for expressing uncertainty, published by the Bureau International des Poids et Mesures (BIPM) (« JCGM - Joint Committee for Guides in Metrology », 2008).
Measurement System Analysis (MSA), developed by the Automotive Industry Action Group (AIAG), specifically for the North American manufacturing sector.
These guidelines can be broken down into the following steps.

2.4.5 Definition of the Measurement System

A measurement system includes all tools, equipment, procedures, operations, software, operators, environments, and assumptions used to quantify a measurement unit or assess a characteristic. The system must consider all factors affecting the measurement process to identify potential sources of variation, quantify them, and understand their impact on the system.

2.4.6 Measurement Function

Once the components of the measurement system are identified, a measurement function representing the system may be defined. A direct measurement involves assessing a quantity Y using a device that directly measures the physical quantity. In indirect measurements, the device cannot provide Y directly; instead, it relies on several physical quantities X_i. The measurement function is expressed as:

$$Y = f(X_1, X_2, \dots, X_n) \tag{2.3}$$

This function describes the relationship between all the measurements required to evaluate a physical quantity. Since no measurement is perfectly accurate, all physical quantities X_i are measured and then estimated x_i to calculate the final value y, which is influenced by the uncertainty of each measurement u_{x_i}. This relationship can be rewritten as:

$$y = f(x_1, x_2, \dots, x_n) \tag{2.4}$$

2.4.7 Standard Uncertainties

According to GUM, uncertainties u_{x_i} for each measurement component x_i can be broken down into (4) components:

- **Measurement reference uncertainty** (u_c)**:** Linked to the reference standard used during calibration. The value is negligible; therefore, it will assume it to be neglected $(u_c \approx 0)$.
- **Equipment error uncertainty** (u_m)**:** Typically provided by the manufacturer.
- **Indicator uncertainty** (u_i)**:** Related to the instrument's resolution, calculated as $u_i = \sqrt{\frac{\delta^2}{12}}$, where δ is the smallest division on the indicator. This value is typically very small, and it can be assumed to be neglected as well $(u_i \approx 0)$.
- **Repeatability uncertainty** (u_{Rep}): Repeatability refers to the system's ability to consistently produce in constant and unchanged conditions the same results under the same conditions.

The standard uncertainties of each x_i are considered independent. Therefore, they combine as:

$${u_{x_i}}^2 = u_c^2 + u_m^2 + u_i^2 + u_{Rep}^2 \tag{2.5}$$

2.4.8 Performance of the Measurement System

Depending on the types of measurement errors (systematic or random), several performances can be defined:

Bias: The difference between the true value (reference value) and the mean of the measured observations (See Figure 2.8).

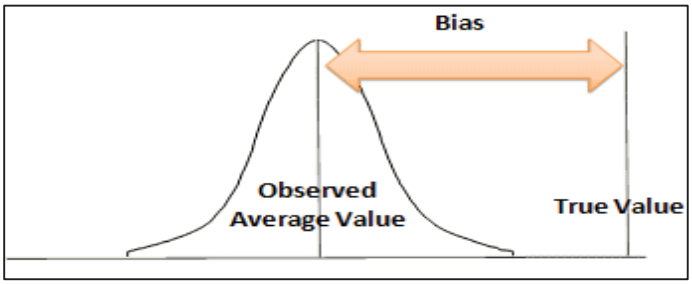

Figure 2.8 Schematic illustration of Bias error
(Ted Hessing, 2014)

After collecting and verifying the measurement data (ensuring no outliers), the bias for each measurement can be calculated using the following formula:

$$bias_i = x_i - Ref \tag{2.6}$$

where x_i represents the i^{th} measured value, and Ref is the reference value. A histogram can be used to visually detect any outliers. The average bias is then calculated as:

$$bais_m = \frac{1}{n}\sum_{i=1}^{n} bais_i \tag{2.7}$$

where $bais_m$ represents the overall mean bias calculated from all samples, n is the number of measurements, and the subscript m denotes the mean bias value.

Linearity: Reflects how well the measurement data across the device's measurement range agrees with the reference value (See Figure 2.9).

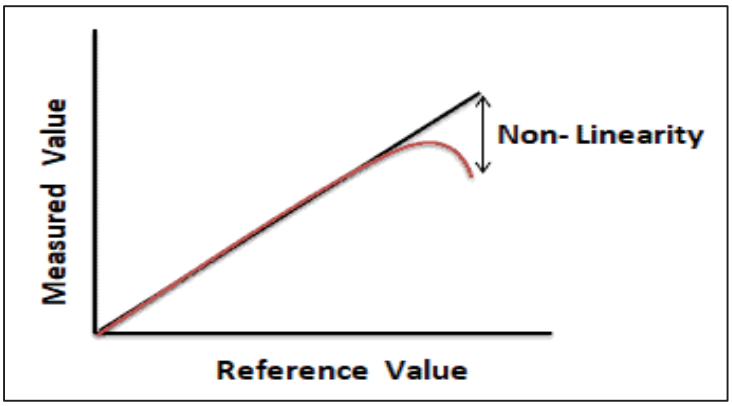

Figure 2.9 Schematic representation of Linearity error
(Ted Hessing, 2014)

Stability: The system's ability to maintain its metrological performance over time.

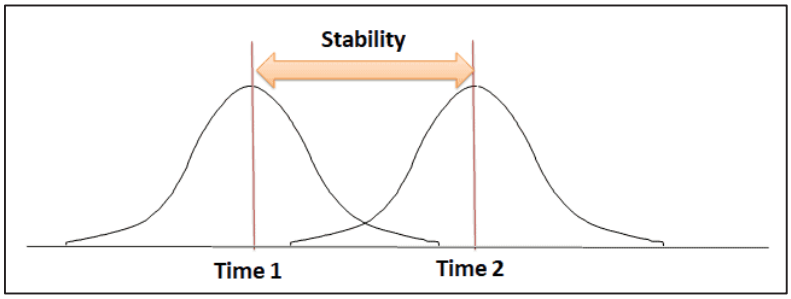

Figure 2.10 Schematic illustration of Stability
(Ted Hessing, 2014)

2.4.9 Propagation of Uncertainties

According to the principle of uncertainty propagation, the estimate of a measured (y) depends on a set of input quantities (x_i), each associated with its own measurement uncertainty (u_{x_i}). As expressed in the Equation (2.4) and illustrated in Figure 2.11, the combined uncertainty (u_y) of (y) is directly linked to the uncertainties of these inputs. In many cases, the explicit form of the measurement function is too complex to express, yet assessing (u_y) remains essential. This evaluation is carried out through the propagation of uncertainties.

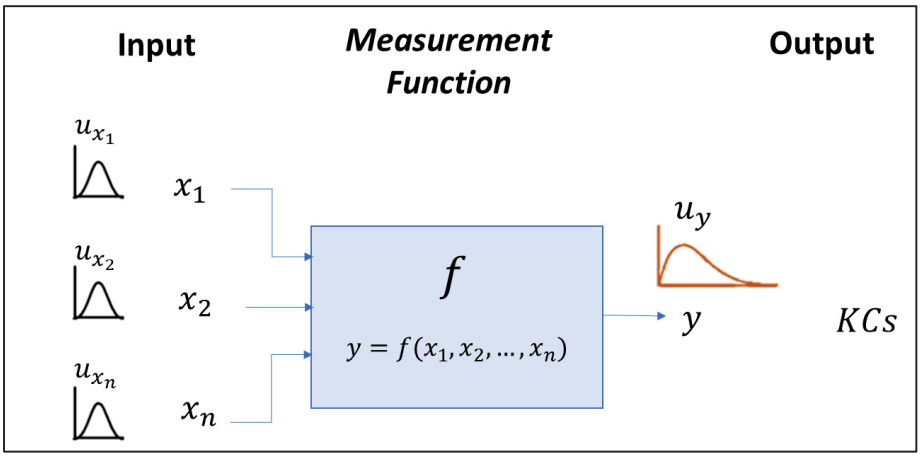

Figure 2.11 Function of the measuring system

According to the Guide to the Expression of Uncertainty in Measurement (GUM), there are three strategiesfor propagating uncertainties, each suited to different conditions that is shown in Figure 2.12 that is inspired by (Émond-Girard, 2022).

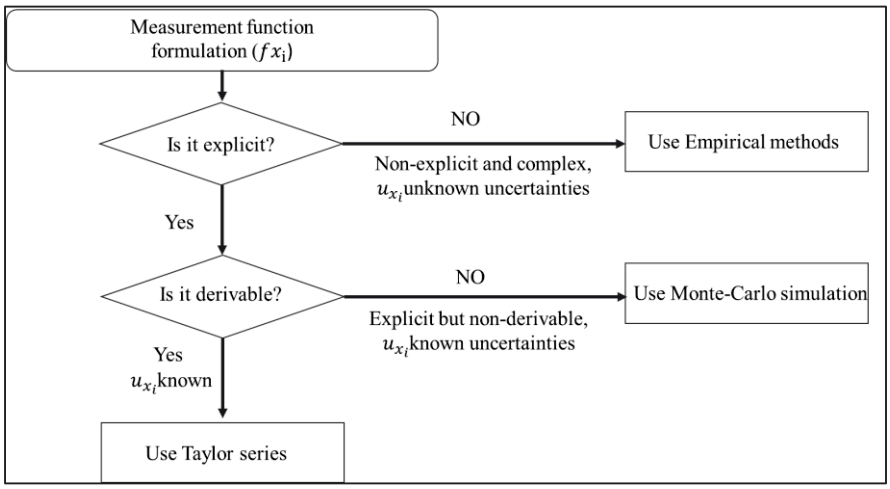

Figure 2.12 Uncertainty propagation methods

2.4.9.1 Taylor Series Expansion Method

The Taylor Series Expansion Method is a key approach for calculating combined uncertainty when a measurement result is influenced by multiple input variables. Each of these input

variables carries its own measurement uncertainty, and the goal is to determine how these uncertainties affect the overall measurement result.

To calculate the combined uncertainty of the output (f), which results from the uncertainties of the input quantities, the Taylor series expansion method can be utilized. In this approach, the measurement function (f) is expanded as a Taylor series around the point of measurement. For simplicity, we limit the expansion to the first order and ignore higher-order terms.

Uncorrelated

In situations where the input variables x_i and x_j are not correlated, the uncertainty formula is the same as the combined uncertainty (See Eq (2.8)).

$$u_y^2 = \sum_{i=1}^{n} (\frac{\partial f}{\partial x_i})^2 \, u_{x_i}^2 \tag{2.8}$$

where u_y^2 is the combined uncertainty of the output,u_{x_i} represents the uncertainties of the input variables and $\frac{\partial f}{\partial x_i}$ is the derivative of the measurement function with respect to each input variable. This means that the combined uncertainty is obtained by summing the squares of the uncertainties of each independent input variable.

Correlate

When there is a correlation between the input variables, the correlation effect must be included in the calculation.

$$u_y^2 = \sum_{i=1}^{n} \left(\frac{\partial f}{\partial x_i}\right)^2 u_{x_i}^2 + 2 \sum_{i=1}^{n-1} \sum_{j=i+1}^{n} (\frac{\partial f}{\partial x_i} \frac{\partial f}{\partial x_j}) u_{x_i} u_{x_j} \rho_{x_i x_j} \tag{2.9}$$

where $\rho_{x_i x_j}$is the correlation coefficient between the input variables $x_i$and x_j. The $u_{x_i}$and u_{x_j} are the uncertainties of each input variable. The additional term 2Σ represents the effect of the

correlation between the variables. The stronger the correlation (values of ρ close to 1 or -1), the greater its influence on the combined uncertainty.

The Taylor Series Expansion Method is a powerful tool for calculating combined uncertainty, helping to determine how the uncertainties of the input variables affect the final measurement result. It works differently, depending on whether the input variables are independent or correlated and can be applied to both simple and complex calculations.

According to the GUM, the Taylor series method for uncertainty propagation requires specific conditions to provide a consistent estimate of the standard uncertainty u_y. The measurement function f must be explicit, differentiable, and continuous; the input uncertainties u_{x_i} should be standard deviations of symmetric distributions (skewness = 0); and the distribution of the output uncertainty in y is assumed to be asymptotically Gaussian, often treated as a Student t-distribution in practical analysis.

2.4.9.1 Monte Carlo Simulation for Uncertainty Propagation

Monte Carlo simulation is a numerical method used for calculating combined uncertainties. This method is particularly useful when the measurement model or function is not explicit, not differentiable, or when the uncertainty distributions are non-Gaussian (non-normal).

Monte Carlo is a simulation-based approach in which calculations are performed by generating many random samples from the input variables. The impact of these samples on the output is then evaluated. This method allows us to compute the uncertainty of the output based on the distributions of the inputs, without relying on mathematical approximations like the Taylor series.

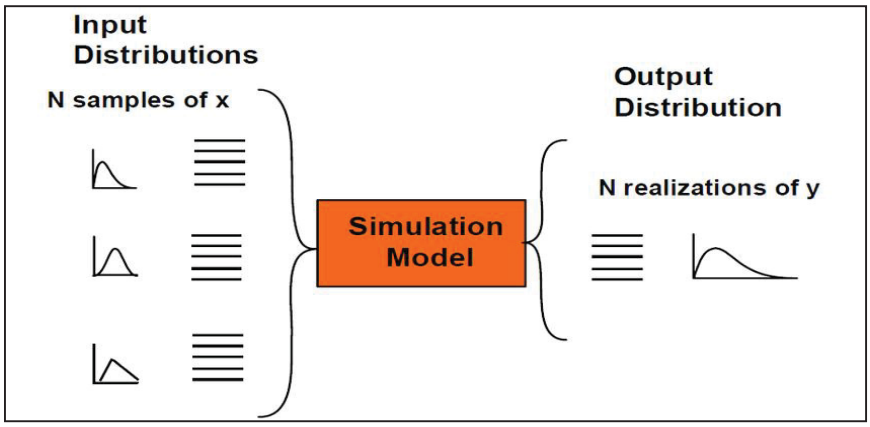

Figure 2.13 Monte Carlo sampling used for aleatory uncertainty propagation (Turnadge, Mallants, & Peeters, 2018)

For each input variable that has uncertainty, random data are generated. These data are sampled from probability distributions that correspond to the uncertainty of each variable.

The measurement model or function is applied to each set of random data. This simulation is repeated many times (usually thousands or millions of times) to observe the variation in the output data.

After the simulation, the output data from all simulations are analyzed. This analysis includes:
- calculating the mean of the outputs;
- determining the standard deviation and uncertainty of the outputs;
- estimating the distribution of the output based on the simulated data.

The output of the Monte Carlo simulations is used to estimate the combined uncertainty of the system. This uncertainty is typically expressed as the standard deviation of the outputs.

2.4.10 Empirical Evaluation of combined uncertainty

When the measurement system is complex, the measurement function cannot always be explicitly defined, making deterministic uncertainty evaluation infeasible. In such cases, the

uncertainty can be estimated experimentally and modeled statistically, often using a parametric distribution such as the normal distribution.

First, a part that will be measured repeatedly is selected. This part will be used throughout the entire experiment. In addition, the environmental conditions (such as temperature and humidity) and the measurement device must remain constant and consistent.

To perform the repeatability study, the selected part must be measured multiple times. The number of measurements can vary depending on the required accuracy and the type of measurement system, but typically, between 30 and 50 measurements are taken. All measurements must be carried out by the same operator, using the same measurement device, and under identical environmental conditions.

After performing the measurements, the first step in data analysis is calculating the mean of the measured values. The mean ($\bar{x}$) represents the central value of the data and is calculated as follows:

$$\bar{x} = \frac{1}{n}\sum_{i=1}^{n} x_i \tag{2.10}$$

where x_i represents the measured data points, ranging from $x_1,\ x_2,\ x_3$, ..., x_n, and n is the total number of measurements.

After calculating the mean, the next step is calculating the standard deviation of the data. The standard deviation indicates the spread or dispersion of the data around the mean and tells us how far the data points deviate from the mean. The formula for the standard deviation (u_x), is as follows:

$$u_x = \sqrt{\frac{\sum_{i=1}^{n} (x_i - \bar{x})^2}{n-1}} \tag{2.11}$$

The standard uncertainty of the mean is calculated using the following formula:

$$u_{\bar{x}} = \frac{u_x}{\sqrt{n}} \tag{2.12}$$

And if is given $u_{\bar{x}}$, to obtain u_x, we assume:

$$u_x = u_{\bar{x}}\sqrt{n} \tag{2.13}$$

One-Way ANOVA in Repeatability Studies

In repeatability studies, all conditions remain the same (part, operator, device, and environment) because it reflects only the intrinsic variation of the measurement system. However, when data are collected under different levels of one factor (for example, time intervals), s (the sample standard deviation) alone cannot reveal whether the mean values differ significantly across these groups. In such cases, a One-Way ANOVA is applied to separate the total variation into within-group and between-group components and to test if the observed differences are statistically significant. A Two-Way ANOVA, on the other hand, is unnecessary here because only one factor is varied, while all others remain constant; it is used only when two independent factors (e.g., operator and time) are both studied simultaneously.

ANOVA (Analysis of Variance) is a statistical method used to assess differences between groups. In repeatability studies of measurement systems, ANOVA helps determine whether a measurement device can produce consistent results under identical conditions.

To conduct ANOVA in a repeatability study, data from multiple measurements of the same part is required. For instance:

- An operator measures the same part multiple times.

- All external factors, such as temperature, operators, and equipment, must remain constant throughout the measurements.

In ANOVA, variance represents the degree of variability in the data. The mean of each group's measurements (e.g., those taken immediately after the calibration vs. those taken several hours later) is presented, which allows for examining the variability across different conditions.

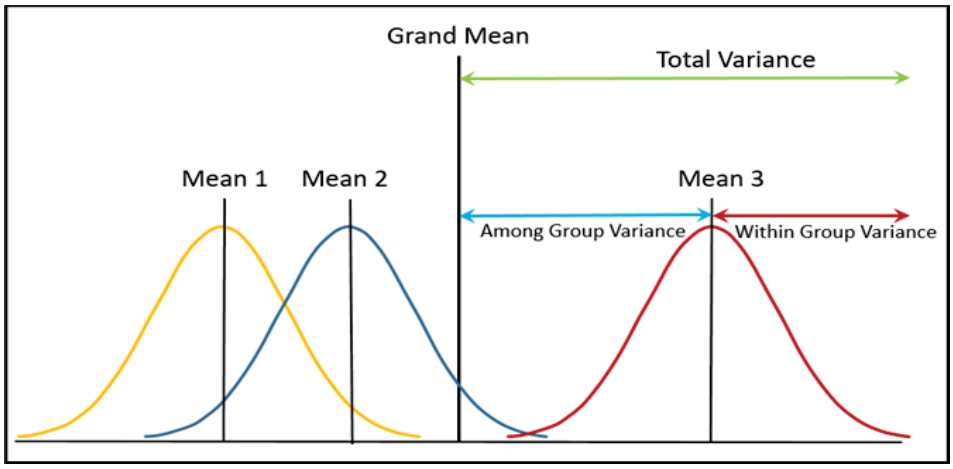

Figure 2.14 Concept for analysis of variance (ANOVA) showing total variance is the sum of variance for among groups and variance for within groups (« Analysis of Variance for Completely Randomized Designs », 2024)

The Fisher-Statistic (F-Statistic) reveals whether the observed differences between groups are substantial enough that they cannot be attributed to the random error alone. This test determines if factors like time or conditions have a statistically significant effect on measurement outcomes. The P-Value is a metric for evaluating the statistical significance of the differences between groups. If the P-Value is < 0.05, it indicates that the null hypothesis $H_0: \mu_{level\_1} = \mu_{level\_2} = \cdots$) can be rejected (differences are statistically significant), meaning the factor being studied (such as time or distance) has a measurable impact on measurement accuracy.

2.4.11 Expanded Uncertainty

The combined standard uncertainty can be expanded using a coverage factor $k = 1.96$ (typically 2 for 95% confidence):

$$U = \pm k u_{total} \tag{2.14}$$

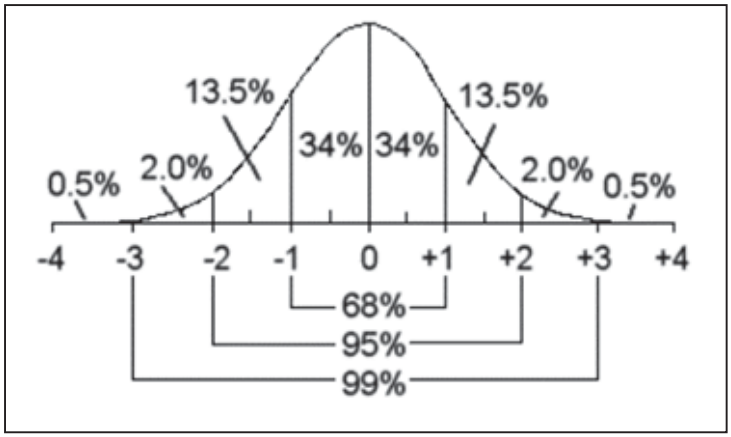

Figure 2.15 Confidence intervals for various confidence levels in a normal distribution (Moses, Golos, & Bennett, 2015)

2.5 Synthesis of Chapter 2

This chapter aims to provide a comprehensive review of the literature and key concepts related to the topic, focusing on precise assembly methods and measurement tools. It begins with the definition and explanation of traditional assembly methods, such as those using jigs to stabilize and align components. The challenges associated with these methods, including high costs, reduced flexibility, and lengthy setup times, have also been examined. Subsequently, newer approaches like Jigless Assembly are introduced, which aim to reduce the need for specific assembly tools by leveraging advanced technologies to enhance precision and minimize costs.

Additionally, the chapter examined the application of 3D metrology technologies, particularly the iGPS system, in jigless assembly processes. The iGPS system, a critical tool for precise

measurement in large-component assemblies, allows simultaneous monitoring of multiple targets in real time, significantly improving both accuracy and efficiency. Despite these advancements, key gaps in research remain unaddressed.

One critical gap lies in the absence of comprehensive methods for estimating and propagating measurement uncertainty associated with iGPS, particularly within work volumes and key characteristics (KCs). Additionally, the need for a continuous information flow between the iGPS system and the operator is crucial for creating an effective communication interface. Measurement uncertainty remains a significant concern, as it can directly affect assembly quality and the final product's performance.

To address these gaps, this thesis proposes the following approaches:

i. Uncertainty Estimation: Developing methods to evaluate measurement uncertainties in iGPS.
ii. Uncertainty Propagation: Developing methods to propagate uncertainties in iGPS, particularly for key characteristics in assembly processes, in compliance with GUM recommendations.

By addressing these challenges, the proposed approach aims to improve the efficiency and flexibility of assembly operations while maintaining high-quality standards. These issues will be explored further in subsequent chapters.

CHAPTER 3

OBJECTIVES AND OVERALL METHODOLOGY

3.1 General Objective

To develop a general method for estimating measurement uncertainty in 3D metrology using iGPS for jigless assembly operations. The method will involve: (i) estimating the measurement uncertainty of iGPS, and (ii) analyzing the propagation of this uncertainty through a defined measurement function, such as the position parameter in geometric dimensioning and tolerancing (GD&T), within MAA operations with the goal of reducing jig costs, improving flexibility, and ensuring assembly quality.

3.2 Specific Objectives

- **Objective 1:** Estimating the uncertainties (U_X, U_Y, U_Z) at one single point (P) within a work volume, inherent in the use of iGPS. These uncertainties should include equipment errors, repeatability errors, and reference errors. The calculation and expression of these uncertainties must adhere to the guidelines provided by GUM (Guide to the Expression of Uncertainty in Measurement).
- **Objective 2:** Define and validate methods to calculate the uncertainty of a key characteristic (KCs) (such as position) in Metrology-Assisted Assembly (MAA) operations according to ASME Y14.5. KCs are measurement functions that include various GD&T (Geometric Dimensioning and Tolerancing) requirements (e.g., Euclidean distance, position, etc.).

3.3 General Methodology

To address the objectives, a structured methodology is proposed. Below is the detailed methodology for each objective.

For objective 1 the methodology is:

To address the absence of a standard for 3D measurements, the uncertainty along the X, Y, and Z-axes will be calculated using a laser tracker as a reference device. In this method, measurements from the iGPS and the laser tracker will be compared, and statistical methods will be applied to calculate the uncertainty of the iGPS system. The main steps are:

- Identify and categorize all sources of uncertainties in iGPS measurements, including environmental factors, references and system-related errors.
- Collect data and conduct controlled experiments (calibration, repeatability) to quantify uncertainties for one single point in 3D space.
- Validate results through practical testing and comparisons with the real world iGPS measurements

For objective 2 the methodology is:
A Monte Carlo simulation will be employed to analyze the propagation of uncertainty of position as a key characteristic (KCs) during assembly, validating the accuracy of the iGPS system in jigless assembly according to ASME Y14.5. The main steps are:

- Implement the Monte Carlo algorithm to model and define methods for uncertainty calculation within the iGPS system on position Key characteristics (KC) in assembly operations.
- Validate the methods by comparing measured uncertainties with the results from both the model and experimental data.

CHAPTER 4

EXPERIMENTAL SETUP AND MEASUREMENT PROCEDURES

This chapter presents the experimental framework designed to implement the methodology proposed in Chapter 3. It describes the principles, setup, and procedures used to evaluate and validate the performance of the iGPS measurement system. The experimental activities aim to estimate the measurement uncertainty of iGPS (Objective 1) and to analyze the propagation of position uncertainty as a key characteristic (Objective 2). The chapter first introduces the working hypotheses, reference standards, and measurement equipment, followed by the experimental setup and calibration steps. It then details the procedures for data collection, statistical analysis, and simulation used to ensure traceability, repeatability, and compliance with GUM recommendations.

4.1 Principles and Experimental Setup

In this section, the operating principles and experimental setup are presented, the reference standards are defined, the primary equipment is introduced, the references and the coordinate system are established.

4.1.1 Working Hypotheses

1) The ASME Y14.5 (2009) standard will be used for defining and interpreting dimensional and geometric requirements.
2) The system analysis should conform to ISO 10360 standards, with meticulous uncertainty evaluation for each axis (u_x, u_y, u_z).
3) Systems are turned on 1 hour before use to ensure measurement stability and to reach the required operating temperature.
4) iGPS is calibrated before each measurement (as recommended).
5) Parts are considered rigid (no compliance).

4.1.2 Measuring Equipment

Absolute Laser Tracker AT960 AIFM: The model, developed by Leica Geosystems, is an advanced 3D measuring device with 6 degrees of freedom (6DoF) capability. It offers accuracy for Maximum Permissible Error (MPE) $\pm 15\mu m + 6\mu m/m$. Measurements are conducted using a laser tracker device with PolyWorks® software.

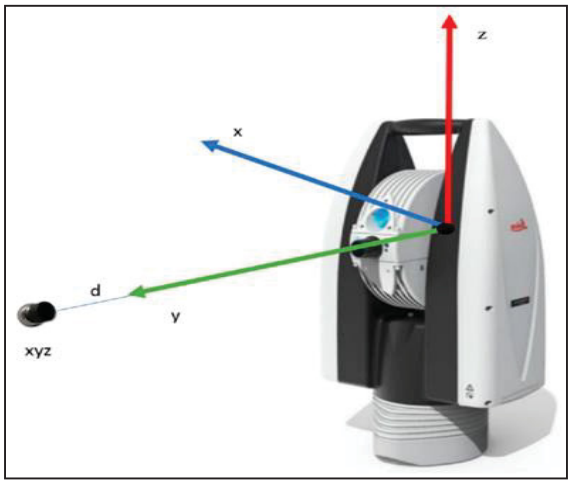

Figure 4.1 Absolute Laser Tracker AT960

7D Kinematic Metrology's iGPS System: The iGPS system provides a high-precision solution for large-scale measurements, utilizing six transmitters to detect reflective targets on i5 units or reflectors. The precision of the iGPS with a one-meter i6 Long Reach Probe is $\pm 200\mu m + 20\mu m/m$ at a 95% confidence level. Measurements are conducted using a laser tracker device with Surveyor ® software.

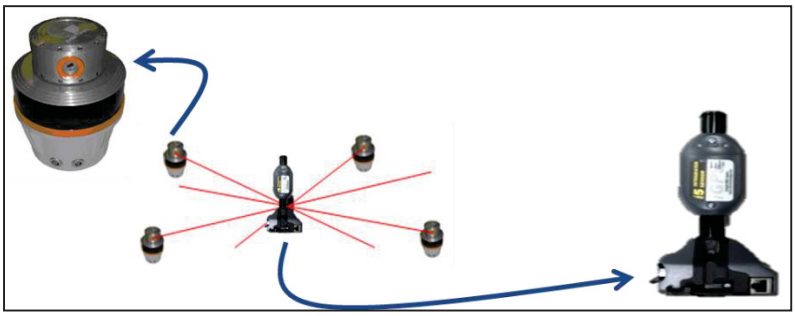

Figure 4.2 Measurement using iGPS system

4.1.3 Development of a Measurement System

As previously mentioned, the goal is to develop a method for identifying the metrological functions of a 3D measurement system using iGPS, which is particularly suited for MAA on a large scale, such as in the aerospace industry. Figure 4.3 illustrates the operational diagram of such a system.

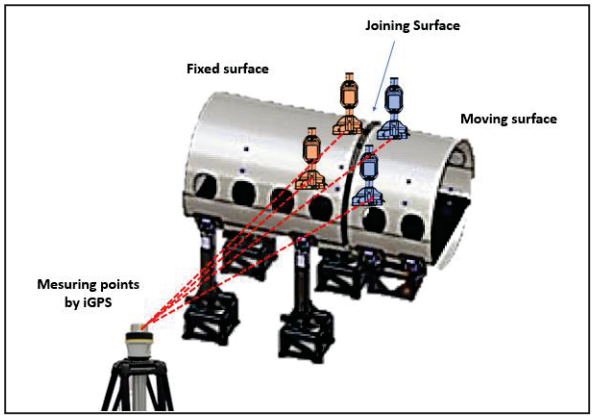

Figure 4.3 iGPS Measurement System

In this figure, the iGPS device is shown utilizing its orange reflectors, which are fixed onto a stationary part, while the blue reflectors are moved along the mobile part until the correct alignment for connecting the two parts is achieved.

After outlining the iGPS-based measurement system and its operating principle, the next step focuses on verifying its reliability and accuracy before implementation in jigless assembly. The measurement uncertainty is first quantified within a controlled work volume and compared against a high-accuracy reference to establish confidence in the system's precision. Subsequently, the influence of these uncertainties on position as a key characteristic is analyzed. Together, these stages form a consistent and traceable framework that connects system evaluation to its practical application in MAA.

4.2 Uncertainty of iGPS for Each Single Measurement Point

This section focuses on improving the performance of the iGPS system, which currently lacks a defined standard for 3D measurements. Currently, this system lacks a specific standard for three-dimensional measurements, making it essential to determine its uncertainty. For this, the uncertainty of each point along the X, Y, and Z-axes must be estimated. This process requires a reference device with established accuracy and standards for which a laser tracker is used. The process begins by calibrating the bar with the laser tracker; once calibrated, the bar serves as the reference and its measurement uncertainties are computed. These results serve as a reference for the iGPS system. Subsequently, the same bar is measured with the iGPS system under identical conditions, and the results are compared to those from the laser tracker. Finally, using statistical methods, the uncertainty of the iGPS in each axis and the overall uncertainty of the system within the work volume will be estimated.

4.2.4 Bar Design as Reference

To effectively manage the positioning and orientation of parts within the study area, a reference bar is essential. This bar acts as a calibrated tool for calculating uncertainties along axes and their associated planes. The bar measures $2294.990\ mm$ and is used with two auxiliary bases to form a triangular setup with one $90°$ angle and two $45°$ angles, enabling coverage of horizontal, vertical, and diagonal orientations. This design conforms to the ISO 10360 standard, ensuring comprehensive orientation coverage.

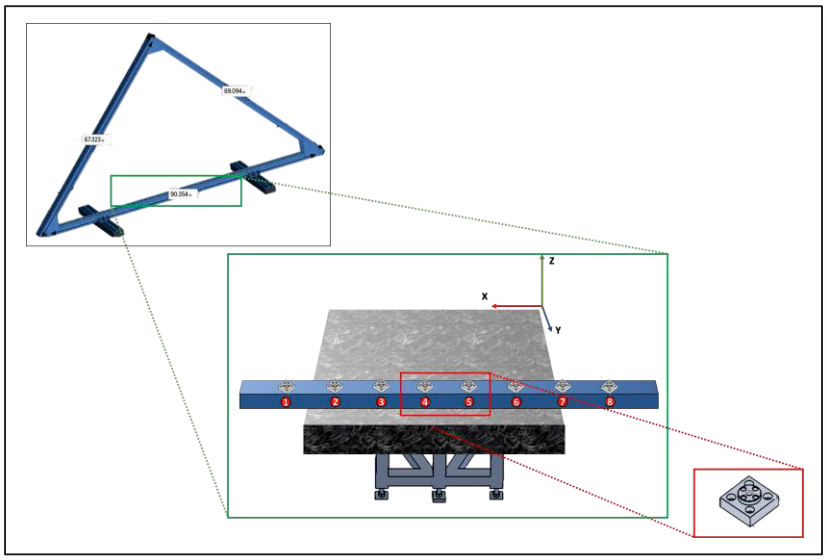

Figure 4.4 A view of designing the bar

As shown in Figure 4.4, the bar (not yet calibrated) forms the base of the triangular setup and two auxiliary bases attach to it to complete the configuration. After calibration, this bar will serve as the reference bar. The upper view is a zoom of the setup, while the lower view shows the same base of the triangular setup on the granite table with eight tool pads for mounting iGPS detectors and laser-tracker targets. This setup used to evaluate uncertainties along the X, Y, and Z axes within the work volume.

4.2.5 Definition of the Measurement Function of Euclidean Distance

The measurement function calculates the distance (d_{ij}) between two points (i and j) based on the absolute value of their vector components, as expressed by the following formula:

$$d_{ij} = \left|\vec{r}_i - \vec{r}_j\right| \tag{4.1}$$

An important point is that for simplicity, will first explain this process using two points as an example, but in reality, the measurement will be performed with 8 points.

Euclidean distance is a simple and common method to calculate the distance between two points in two-dimensional or three-dimensional space. This distance is calculated based on the coordinates of each point in space (See Eq (4.2)).

For two points in three-dimensional space with coordinates x_i, y_i, z_i and x_j, y_j, z_j, the Euclidean distance ($\mathbb{R}^6 \longrightarrow \mathbb{R}_+$) between these two points is calculated using the Euclidean distance formula as follows:

$$d_{i,j} = f(x_i, y_i, z_i, x_j, y_j, z_j) = \sqrt{(x_i - x_j)^2 + (y_i - y_j)^2 + (z_i - z_j)^2} \qquad (4.2)$$

Stable environmental conditions are critical for accurate measurements. The bar as a reference bar is fixed to prevent any angular deviation. The bar is not yet calibrated; it will become the reference bar after laser calibration. Environmental factors such as temperature, pressure, and humidity are controlled to ensure high precision. Each point is measured three times to thoroughly assess the system's accuracy and repeatability.

The test will be conducted in a controlled laboratory environment at LIPPS Labo (Montréal, ÉTS, Metrology Laboratory) with a temperature maintained at $20 \pm 1°C$ (See Figure 4.5).

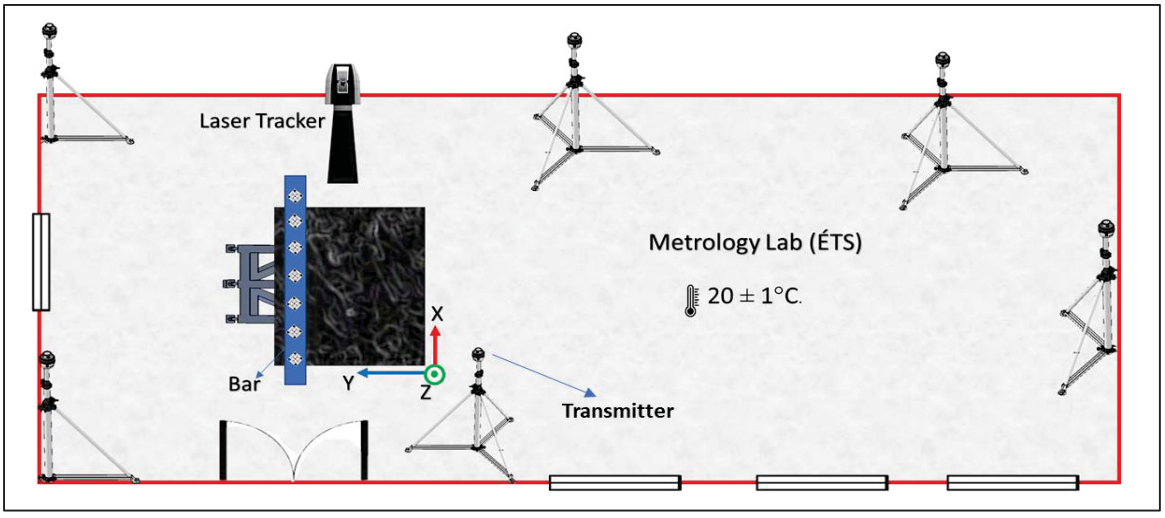

Figure 4.5 A general description of how measuring devices are placed in the laboratory

4.2.6 Calibration of the Bar as a Reference Using the Laser Tracker

The lack of a measurement standard for the iGPS device necessitates the use of a laser tracker, which follows established calibration and measurement standards. The calibration of the bar is performed using the laser tracker. In this process, the bar is used to precisely measure the X, Y, and Z-coordinates of the points. Due to the high accuracy of the laser tracker, the uncertainty of the points must first be calculated and then compared to the iGPS system's uncertainty.

First, the coordinates of each point are randomly measured using a laser tracker. These measurements are taken three times per day at specific intervals. The purpose of repeating the measurements three times each day is to minimize repeatability errors and calibration inaccuracies. Once the point coordinates are obtained for each repetition of the day, the distances between points are calculated using the Euclidean distance formula. The Figure 4.6 illustrates the bar and the Euclidean distance from point 1 to the other points during the laser tracker measurement process. This process is repeated in the same manner for every point.

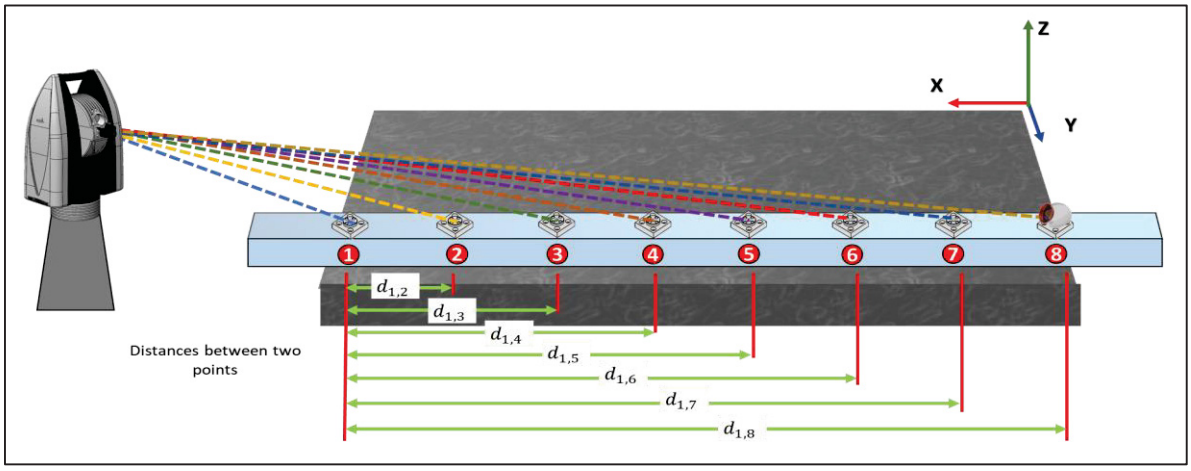

Figure 4.6 A laser tracker is used to measure the bar and make it a reference, with Euclidean distances from point 1 to all other points

4.2.6.1 Steps for Calculating Laser Tracker Uncertainty

After the Euclidean distances are calculated for each repetition, the average distance between points is determined. Next, the uncertainty for each point along the x-axis is calculated by following the steps used to determine the laser tracker uncertainty. These steps include:

Step 1: Standard Uncertainty Calculations: These include the following sources

- Measurement reference uncertainty and index uncertainty, which are negligible for the laser tracker and typically assumed to be zero.
- Equipment error uncertainty, which, according to the laser tracker specifications, is $MPE_{LT} = \pm 15\mu m + 6\mu m/m$. When using the Maximum Permissible Error (MPE) and assuming that the error follows a rectangular distribution (meaning that the probability of any error occurring within the range of ±MPE is equal), the MPE must be converted to the standard uncertainty. This conversion is done using the following formula:

$$u_{device} = \frac{MPE}{\sqrt{3}} \tag{4.3}$$

This division is necessary to convert the MPE (which represents the maximum error in a rectangular distribution) into the standard deviation. The division by $\sqrt{3}$ reflects the transformation from a maximum error to the standard deviation, which is recommended by the GUM Guide.

Step 2: Calculating Repeatability Uncertainty using section 2.4.10.
Step 3: Compute the combined standard uncertainty for each point using Eq (2.5).

This uncertainty serves as a reference for future measurements using the iGPS system. By following this method, the reference points are established as part of a calibrated system that can be used to assess the accuracy and performance of the iGPS device. Therefore, from this

stage onward, the bar is referred to as the reference bar. Before calibration, it is simply the bar, not a reference and after laser calibration it becomes the reference bar.

4.2.7 Measurement of the Reference Bar Using the iGPS

In the previous section, the uncertainty of each point was calculated using a laser tracker. The laser tracker is a precise measuring device with specific standards for measurement. A reference bar was calibrated using this device, and measurements were repeated three times over three consecutive days.

The primary goal of this measurement was to use the laser tracker-calibrated reference bar to assess the uncertainty of the iGPS system and determine the uncertainty at each point. The laser tracker was chosen due to its accuracy being ten times higher than that of the iGPS system, making it suitable for calibrating the reference bar. Since the iGPS does not have a defined standard, the ISO 10360 was applied. According to metrological principles, the reference device must be more accurate than the device under test, which ensures reliable results.
The manufacturer advises calibrating the iGPS system every 24 hours or after each power off cycle. According to the Surveyor® manual for the following bundling guidelines to ensure effective results:

- Maintain a consistent walking pace; avoid variations in speed.
- Hold the i6 Long Reach Probe at a slight 10-degree tilt rather than keeping it perfectly vertical.
- Carefully and slowly raise and lower the i6 Long Reach Probe to ensure precise measurements.
- Record a minimum of 100 bundle reference points.
- Spread the reference points evenly throughout the iGPS environment to encompass each transmitter's full field of view.
- Keep the i6 Long Reach Probe visible to as many transmitters as possible during data collection.

- Avoid collection near reflective surfaces, such as windows and mirrors, to minimize accuracy distortions.

4.2.7.2 Measurement Process

Without changing the position of the reference bar, iGPS measurements were performed at eight points using G6 detectors. After a one-hour warm-up period, the device was calibrated with the i6 Long Reach Probe (See Figure 4.7).

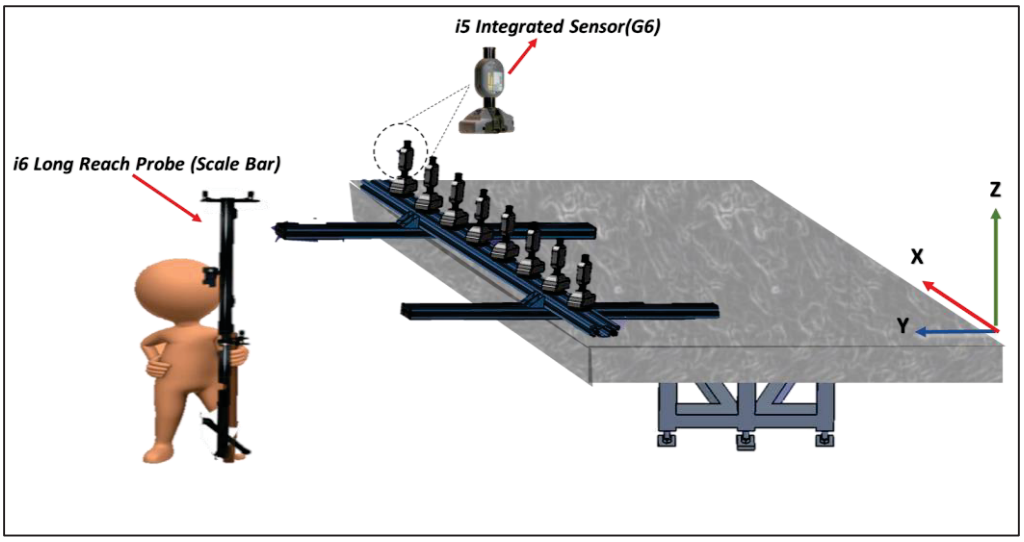

Figure 4.7 Reference bar set up during the iGPS measurement process

As per the manufacturer's recommendation:

1. The calibration of the iGPS system should be performed after 4 to 6 hours of operation (unless monuments are used and the system remains stable).
2. The warm-up time is approximately 20-30 minutes.

Therefore, it is essential to assess whether the time elapsed since the last calibration of the iGPS system affects the accuracy and reliability of the measurements. To address this, measurements were taken at different intervals, after a one-hour warm-up iGPS is calibrated by i6 Long Reach Probe and then, measurements were taken immediately (0+1 hour warm-up iGPS), 3 hours (3+1 hour warm-up iGPS), and 5 hours (3+1 hour warm-up iGPS) after the

calibration of iGPS. Additionally, it is essential to assess whether repeating the measurements using the same protocol on different days affects the measurements. Accordingly, measurement uncertainty and system stability were evaluated by repeating this protocol over three consecutive days.

Measurement data was collected for each axis (e.g., X-axis), and the Euclidean distance for each time was calculated. Factors such as day, time, and distance could affect uncertainty or bias. Therefore, distances calculated from iGPS were compared with the Euclidean distances obtained from the laser tracker (using the formula (4.2)). One-way ANOVA (Analysis of Variance) was used to evaluate the effects of measurement uncertainty across three consecutive days, time, and distance on iGPS measurements. The measurements were divided into three categories:

1. Comparison of repetitions across three consecutive days.
2. Comparison based on time.
3. Comparison based on Euclidean distance intervals between points.

ANOVA is a statistical method used to compare the means of different groups of data. One-way ANOVA is used when an independent factor (such as time, day or distance) affects a dependent variable (such as measurement uncertainty). One-way ANOVA was used to evaluate the effects of three different factors on iGPS measurements:

Factors Analyzed with ANOVA:

1. **Day:** Compare the average of three repetitions of measurements across days.
2. **Time:** Evaluate the effect of different intervals immediately (0+1 hour warm-up iGPS), 3 hours (3+1 hour warm-up iGPS), and 5 hours (3+1 hour warm-up iGPS) after the calibration of iGPS.
3. **Distance:** Compare measurements taken at various distances to evaluate their effect on iGPS measurement uncertainty across 8 different sections (Totaling 28 conditions).

ANOVA Outputs:

1. Group Mean: Displays the average for each group (e.g., measurements at different times or distances).
2. F-Statistic: Indicates if the differences observed between groups are significantly larger than random variations.
3. P-Value: If the p-value <0.05, it indicates that the differences between groups are statistically significant, meaning that the examined factors (e.g., time, day or distance) have a meaningful effect.

If the p-value is ≤ 0.05, it concludes that factors like time, day or distance have a significant effect on measurement uncertainty. If the p-value is greater than 0.05, it suggests that these factors do not significantly affect the measurements.

4.2.7.3 iGPS Uncertainty Calculation

The iGPS uncertainty calculation follows the same steps as those for the laser tracker, with the standard uncertainty for each point being a combination of the following factors:

1. Uncertainty of the iGPS system, as specified by the manufacturer.
2. Uncertainty of the reference device, which is the laser tracker.
3. Uncertainty of repeatability, which includes the mean and variance of repeated measurements.
4. Calculate the combined uncertainty for the distance between points.

To achieve this, the Taylor series expansion method was initially applied to compute the combined uncertainty of the distance. Once the measurement uncertainty for each point is determined, the standard uncertainties are combined to calculate the combined uncertainty for each distance. The uncertainty of the distance (u_d) between two points (A and B) is then calculated using the uncertainty of both points by applying the law of uncertainty propagation:

$$u_d = \sqrt{\left[\frac{\partial f}{\partial x_A}\, u(x_A)\right]^2 + \left[\frac{\partial d}{\partial y_A}\, u(y_A)\right]^2 + \left[\frac{\partial d}{\partial z_A}\, u(z_A)\right]^2 + \cdots + \left[\frac{\partial d}{\partial z_B}\, u(z_B)\right]^2} \qquad (4.4)$$

Once the standard uncertainties are combined, they contribute to the overall Combined Uncertainty for each point. This process is carried out separately for the X, Y, and Z-axis. Then, calculate the expanded uncertainty for each interval at a 95% confidence level using the equation (2.14).

If a set of uncertainty values U_d is obtained for different distances and a single final uncertainty is required, the maximum U_d is reported. The maximum uncertainty value is selected because a conservative estimate is desired in order to account for the highest possible uncertainty. This ensures that the reported overall uncertainty will never be less than the actual uncertainties of any of the distances.

$$U_{Final} = Max\ (U_d) \qquad (4.5)$$

This approach is especially useful when precision is critical and the worst-case scenario must be accounted for.

After the uncertainty for each axis of the iGPS system has been calculated, the overall uncertainty of the system is determined. To this end, the Taylor series expansion method is initially used to compute the combined uncertainty.

It is assumed that the uncertainties of each axis are independent and uncorrelated. Therefore, Equation (2.8) is utilized to calculate the total uncertainty as the square root of the sum of the squared uncertainties of each axis. This approach assumes that the uncertainty in one axis does not influence the others, allowing each axis to be treated as an independent variable.

Once it is determined which formula is appropriate, the overall uncertainty of the iGPS system is calculated. This value represents the total system uncertainty across the entire work volume,

which is crucial for assessing the accuracy and reliability of the system in various applications, including assembly processes.

4.3 Propagating Uncertainty of Position as a Key Characteristic in MAA

This section focuses on assessing the uncertainty of position as a key characteristic in the assembly process. Key characteristics are critical throughout the assembly, and control processes will be applied based on specific standards. In jigless assembly, due to the absence of physical jigs and the lack of fixed parts, these characteristics become even more important. Therefore, in this stage, the propagation of uncertainty in one of the key characteristics, which is positioned during assembly, will be examined. The Monte Carlo simulation method, a technique used for complex models, will be applied. This simulation will assess the uncertainty of position as a key characteristic and compare it with real-world models for validation. These results will significantly aid the jigless assembly process using iGPS.

4.3.8 Estimating the Propagation of Uncertainty iGPS Measurements

Once the uncertainty of the iGPS system has been determined for each single measurement point, the next step is to evaluate how this uncertainty propagates throughout the assembly process. This assessment is crucial for ensuring the effective implementation of iGPS in production.

Key Characteristics (KCs) are critical features, dimensions, or properties of components and products that directly impact the performance, functionality, and safety of the final product. Inadequate control of these characteristics can result in significant issues affecting product quality or safety.

Key characteristics are important during the product design process and require continuous monitoring throughout the entire process. For this reason, it is proposed to analyze the propagation of uncertainty in key characteristics (KCs) using Monte Carlo simulations. This

technique is particularly useful for complex models, allowing for a detailed analysis of the uncertainties that might arise during both measurement and assembly.

After modeling, the results obtained are compared with the results of measured tests. This comparison helps verify the accuracy and reliability of the assembly process by identifying any errors or deviations that could potentially affect overall system performance.

We analyze the propagation of uncertainty in one of the key assembly characteristics, namely position, using a dedicated case study.

4.3.8.4 Design of the Artifact

To evaluate the propagation of uncertainty in a key assembly characteristic, specifically the position, a dedicated physical artifact was designed. The artifact consists of a hexagonal aluminum plate with a central circular hole of 50 mm radius, which represents the key feature under evaluation. The objective is to determine the position of this circular hole's center using iGPS measurements under controlled conditions.

The hexagonal shape was selected for cost efficiency and ease of manufacturing, without compromising geometric functionality. Due to limitations in the iGPS system, particularly the difficulty of placing detectors directly around the circular feature because of overlapping measurement zones and spatial constraints, six detector positions were predefined around the central hole. These locations are arranged along a concentric circle of 117.5 mm radius, allowing for indirect estimation of the hole center. While the Z-axis (height) is not analyzed in this stage, the plate thickness is 25.4 mm, providing structural rigidity and minimizing deformation during measurement (See Figure 4.8).

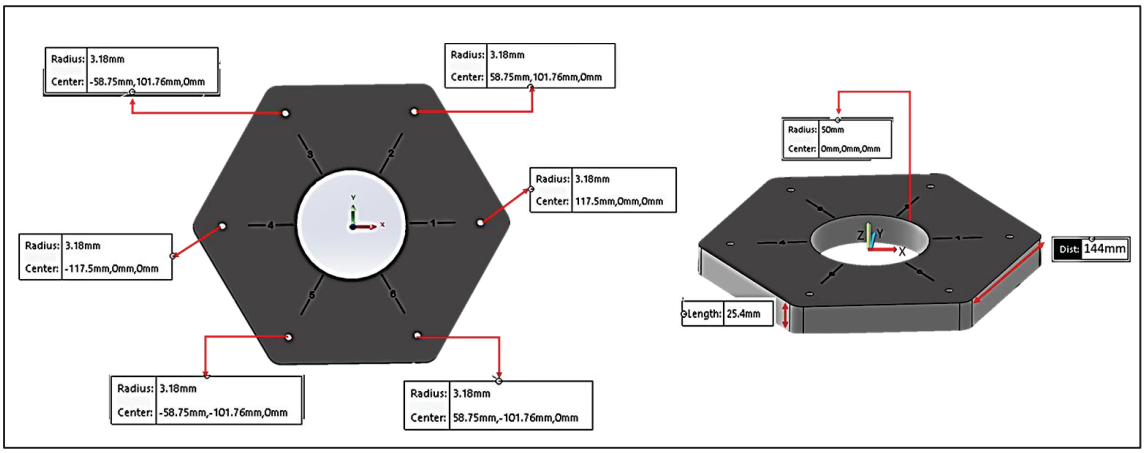

Figure 4.8 The artifact designed in CAD software

The detector positions are clearly marked and numbered (1 to 6) on the surface of the artifact. These reference points were machined with a CNC system, ensuring accurate and repeatable placement.

This artifact serves as the foundation for subsequent measurement experiments using both iGPS and laser tracker systems. The comparison between the two will enable statistical estimation of uncertainty propagation in determining the position of the hole's center.

4.3.8.5 Experimental Setup

The artifact is inspected on a CMM to establish the nominal data for subsequent iGPS tests. The CMM acts as the high-accuracy reference.

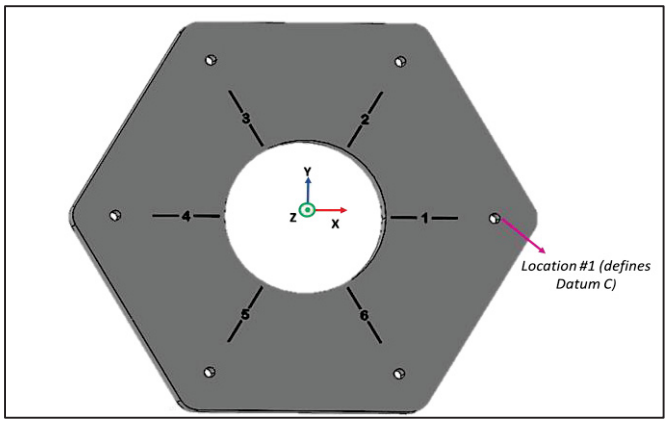

Figure 4.9 Artifact and datum setup on the CMM

The plate is rigidly fixtured to the CMM table. The top face is sampled to define Datum A (plane). The central hole is measured to fit its axis and define Datum B. One small detector hole (location #1) is measured to define Datum C, locking in-plane rotation. The reference frame is A|B|C the origin at the center of the large hole, Z normal to Datum A, and X oriented toward location #1 (See Figure 4.9).

The CMM provides the origin and axes per these datums, the large-hole center as (0,0,0), and the XY coordinates of the six detector locations (with their distances to the hole center). These data are imported into the iGPS software as nominal frame data so that, during iGPS experiments, the position of the artifact's center is tracked on screen relative to the same reference.

iGPS and Calibration

The iGPS system is powered on and allowed to warm up for 1 hour. Calibration is performed with the i6 Long Reach Probe and coordinate system aligned by Plane–Line–Line according to the manufacturer's instructions. To remove the scale-bar offset (≈ 6.35 mm in each direction) for fixing this matter the iGPS tool pad is mounted to the precision metrology plate, and is measured and calibrated with a CMM to eliminate the offset. The reference artifact is placed on the lab table; its orthogonal edges are aligned with the axes, and offset corrections are

applied and zeroed in the software so that the (X,Y) axes are exactly aligned with the A|B|C reference frame.

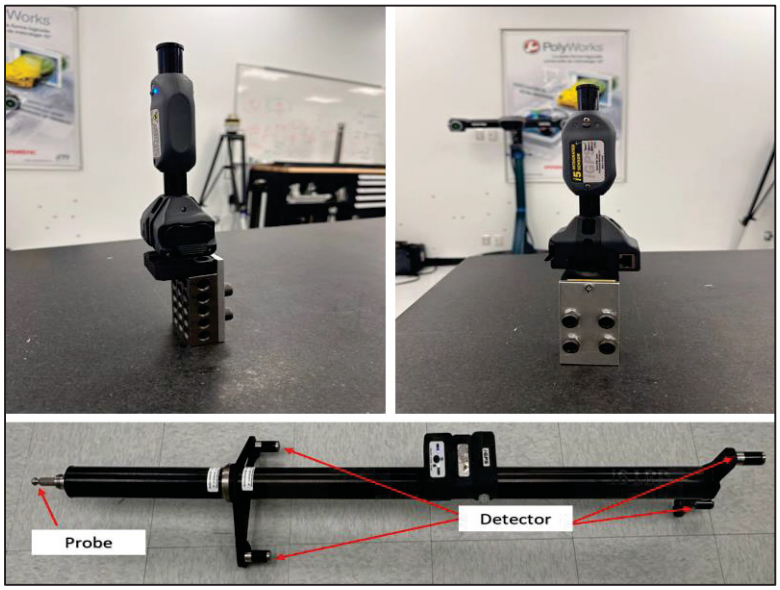

Figure 4.10 Setup used for offset removal of i6 Long Reach Probe iGPS calibration

Frame Creation in Surveyor®

In Surveyor®, the i5 Frame option is selected (recommended for frames attached to moving objects) (See Figure 4.11).

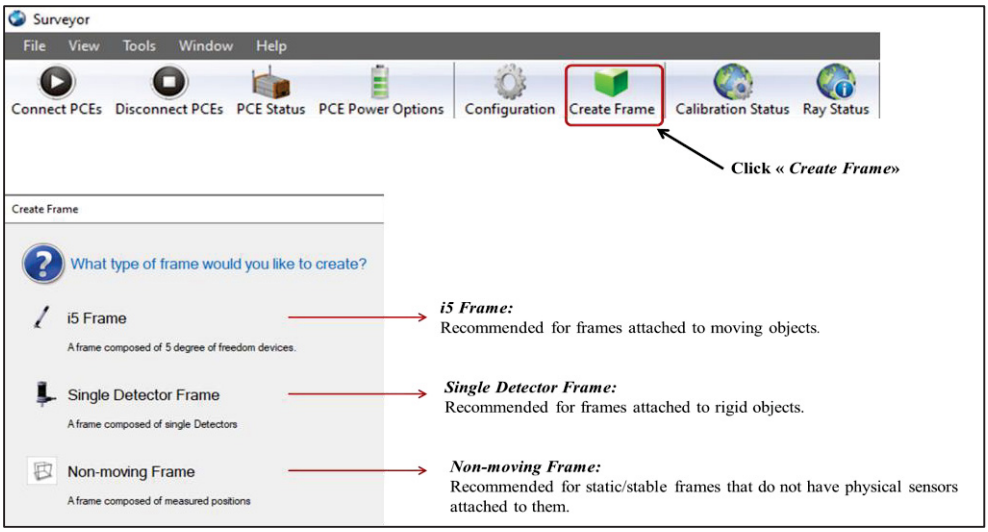

Figure 4.11 Surveyor frame setup using the i5 Frame option for detector mapping and coordinate assignments

The nominal coordinates of points 1–6 are entered (units: millimetres). Each i5 detector is mapped to its corresponding point using its unique hardware ID. The detectors are mounted so that their degrees of freedom (translation and rotation) are locked (See Figure 4.12).

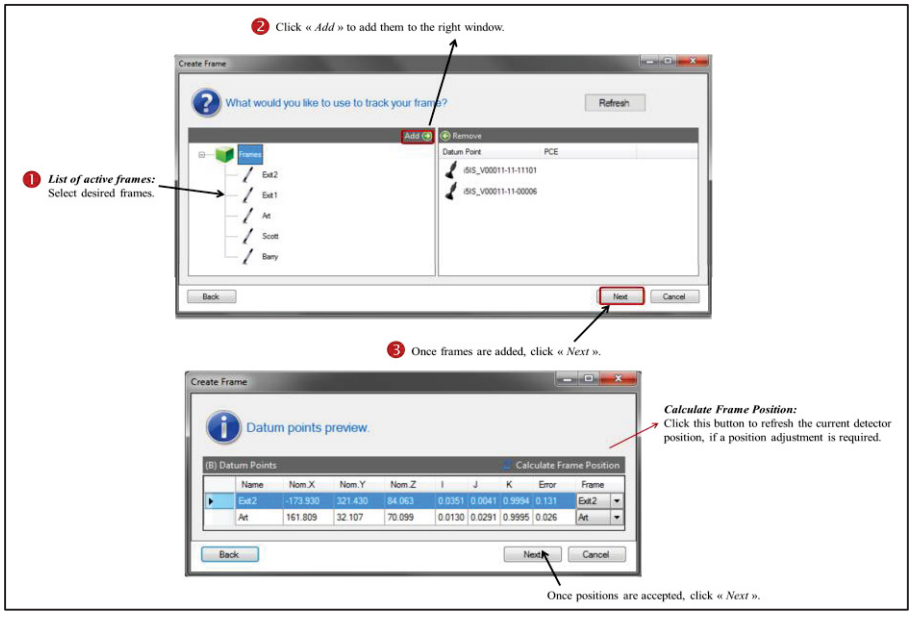

Figure 4.12 Nominal point entry and i5 detector mapping in Surveyor

Work Volume and Target Selection

The (XY) work volume is defined based on the same granite table in the methodology of objective 1. Five random (XY) target locations within this area are chosen under edge-clearance and minimum-separation constraints, and their coordinates are recorded.

Detector Scenarios

To assess the effect of the number of detectors since increasing detector redundancy is expected to improve geometric constraint and reduce measurement uncertainty, four scenarios are executed on the numbered artifact locations: 3, 4, 5 and 6 detectors. The order of scenarios is randomized.

Test Protocol

1. The artifact centre is guided from the coordinate to the (XY) target until the on-screen reaches the best achievable display value; the artifact is then fixed.
2. The (X, Y, Z) coordinates of active points, detector IDs, and frame time are recorded from iGPS.
3. The artifact is measured with the laser tracker and the readings are validated (details provided subsequently).
4. The artifact is, returned to the coordinate (0, 0, 0), and repositioned on the same target.
5. Steps 1–4 are repeated three times to evaluate positional repeatability.

Validation with the Laser Tracker

In PolyWorks®, a Plane–Line–Line alignment is applied so that the laser-tracker frame matches the iGPS frame (the selected (X, Y) axes are co-linear with iGPS). Points 1-6 around the large inner hole are then measured with the laser tracker. This dataset serves as a higher-accuracy independent reference of the iGPS results.

The following quantities are computed: Estimated centre and radius. The computation details and uncertainty propagation are presented in the Monte Carlo section.

4.3.9 Monte Carlo Method Propagates Uncertainties

After calculating the uncertainty for each point, it is necessary to apply these uncertainties to the assembly process models and simulate how they propagate. The Monte Carlo simulation method is used for this purpose, where the chosen function is based on key characteristics (KCs) of the assembly. This function can be simple (such as the Euclidean distance between two points) or highly complex.

The Monte Carlo algorithm uses key points, defined according to geometric standards, and runs them through a high number of iterations (e.g., thousands or even millions of times) to achieve an accurate distribution of the results. In each iteration, the calculated uncertainties for the axes (obtained in the previous step) are added to the function's inputs. This introduces random variations in the input points, resulting in a distribution of output results.

This process allows us to accurately and randomly simulate the behavior of uncertainties throughout the assembly process, ensuring the proper performance of the key characteristics.

The Monte Carlo Simulation method propagates uncertainties through a measurement function by generating random samples.

The steps of the simulation process are as follows:

1. Generating Random Samples: For each point x, a random sample is drawn from a normal distribution $\mathcal{N}(0, u_x)$, where u_x represents the uncertainty associated with x.

2. Measurement Function: The measurement function is applied to these random samples to calculate the resulting uncertainty.

3. Repeating the Simulation: This process is repeated m times, producing a distribution of the resulting uncertainties.

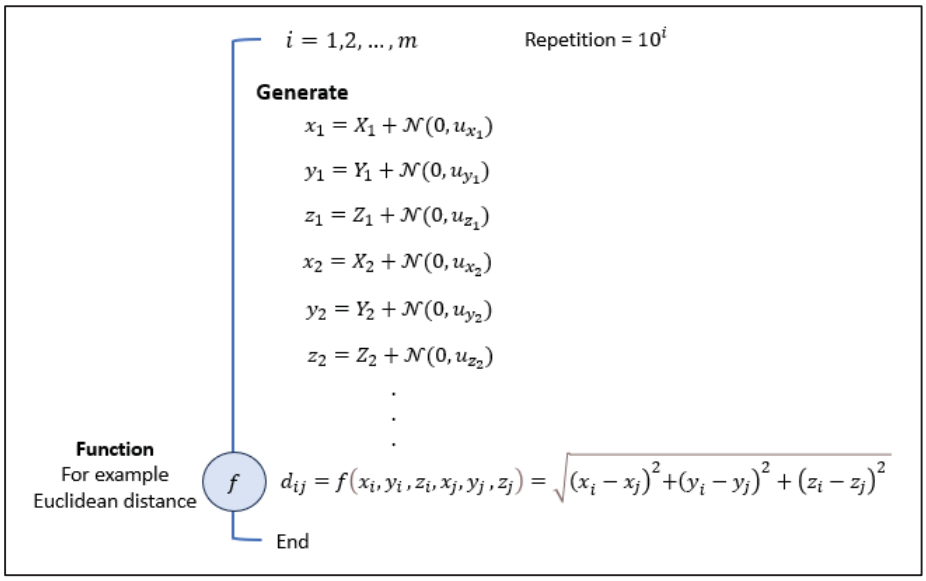

Figure 4.13 The framework of the calculation model using the Monte Carlo algorithm

4.3.9.6 Monte Carlo Propagation of Position Uncertainty (KC) in iGPS Measurements

The aim is to analyze how measurement uncertainty propagates during assembly, focusing on one key characteristic: the position (position of the artifact center) and the radius of the circle is defined by the iGPS detector points on the artifact. Estimate of propagation uncertainty are produced from iGPS data using a Monte Carlo simulation, and results are validated by Laser Tracker (LT). The confidence level is 95%.

Inputs

The six detector holes (1–6) form a circular pattern around the central hole. The nominal radius (r_{CMM}) corresponds to the distance between the center of the large hole and the fitted circle passing through these detector locations.

1. **Measured points (iGPS):** 3D coordinates of active detector locations on the artifact, labeled #1 to #6.

2. **Uncertainties of each axis for one single measurement point:** From Objective 1, uncertainties of each axis for one single measurement point in the work volume (U_X, U_Y, U_Z) . Axes are treated as independent.
3. **Nominal radius (CMM):** Reference radius (r_{CMM}) from CMM.

Monte Carlo

Five random (X-Y) target locations were selected on the granite table within the work volume. For each target location and each detector-number scenario (3i5–6i5), three independent repetitions were performed separately. A Monte Carlo simulation was then executed independently for each repetition (and thus for each location–scenario–repeat combination) to propagate the iGPS per-axis uncertainties and compute the resulting uncertainty of the estimated parameters.

For each run:

1. **Uncertainty sampling**: For each iGPS point (x,y,z), draws a sample that models measurement uncertainty.
2. **Refit:** Maps the set to the best-fit function and recompute the best-fit circle.

   Measurement function: The measurement function is the least- square best-fit circle. For circle, the objective is to minimize the sum of squared radial residuals.

   For a point set, (x_i, y_i) estimate the circle by minimizing the sum of squared radial residuals:

$$\left(\hat{a}, \hat{b}, \hat{R}\right) = \arg\ min_{a,b,R} = J(a, b, R) \tag{4.6}$$

Where is a, b are center coordinates of the circle and R is circle radius.

$$J(a, b, R) = \sum_{i=1}^{n} \sqrt{(x_i - a)^2 + (y_i - b)^2} - R^2 \tag{4.7}$$

Distance of each point to the center:

$$\hat{p}_i = \sqrt{(x_i - \hat{a})^2 + (y_i - \hat{b})^2} \quad (4.8)$$

If a point lies exactly on the circle, then $p_i = R$. Radial difference (residual) of each point:

$$\hat{e}_i = \hat{p}_i - \hat{\mathrm{R}} \quad (4.9)$$

If $\hat{e}_i = 0$: point on the circle and if $\hat{e}_i > 0$ point outside $\hat{e}_i < 0$ point inside the circle.

3. **Iterations:** Monitors convergence of the mean, standard deviation, and RMSE of radius and the center coordinates.

Outputs

Mean and standard deviation for the radius and the center coordinates for each repetition from each location, compare the four detector scenarios (3/4/5/6 detectors) at the 95% CI.

Validation with Laser Tracker (LT)

Measure points 1 to 6 with LT as an independent, higher-accuracy reference to assess of iGPS results. LT data are used only for validation.

4.4 Synthesis of Chapter 4

This chapter explained the experimental framework for evaluating the iGPS measurement system and its use in metrology-assisted assembly. The working hypotheses, reference standards, and measurement equipment were defined to ensure traceability and compliance with ISO and GUM standards.

For Objective 1, the uncertainty of each single iGPS measurement point was quantified using a laser-tracker calibrated reference bar. The calibration steps, measurement -collection

protocol, and statistical analyses (including one-way ANOVA) were detailed to evaluate the effects of time and distance, with the protocol repeated over three consecutive days.

For Objective 2, an artifact was designed to investigate the propagation of measurement uncertainty to position as a key assembly characteristic. Monte Carlo simulation was used to model how point uncertainties affect the estimated circle center and best-fit radius, and the results were validated using independent laser-tracker measurements.

Together, these procedures provide a consistent, traceable basis linking single-point measurement uncertainty to its propagation in assembly-level key characteristics (here, position). The next chapter presents the results, examining single-point uncertainty, the resulting propagated uncertainties for jigless assembly.

CHAPTER 5

EXPERIMENTS & RESULTS

Following the experimental framework and calibration protocols detailed in Chapter 4, this chapter presents the results of the iGPS uncertainty evaluation and its propagation to a key assembly characteristic in a Metrology-Assisted Assembly (MAA) context. The results are organized into two main sections that correspond to the research objectives defined in the methodology.

The first section (Objective 1) quantifies the iGPS measurement uncertainty at the single-point. Measuring the bar using a laser-tracker and make it a reference. Repeatability, device, and reference uncertainties are evaluated and combined, and the effects of measurement day (three consecutive days), elapsed time after calibration, and distance between measured points are assessed to examine system stability and identify the dominant contributors to uncertainty. This section then provides representative uncertainty values along the X, Y, and Z axes for the defined work volume.

The second section (Objective 2) uses these representative axis uncertainties as inputs to model uncertainty propagation to position as a key assembly characteristic. Using the CNC-fabricated hexagonal artifact, the circle center and best-fit radius are estimated from iGPS measurements under different detector-number scenarios (3, 4, 5, and 6 detectors). Monte Carlo simulations are performed to propagate the single-point uncertainties through the circle-fitting model, and the results are validated using independent Laser Tracker measurements. Overall, the chapter establishes a consistent link between single-point measurement uncertainty and its propagation to assembly-level position, and it demonstrates how detector redundancy influences measurement reliability in jigless assembly applications.

5.1 Uncertainty of iGPS for Each Single Measurement Point

This section quantifies the iGPS uncertainty for each single measurement point. A reference bar is designed and calibrated using a laser tracker. Repeatability and device uncertainties are then estimated and combined with the reference uncertainty. The effects of three factors day (three consecutive days), time, and distance between measured points are evaluated and reported. Finally, representative uncertainties along the X, Y, and Z axes are computed.

5.1.1 Design of the Reference Bar

A bar as reference was securely attached to the surface. As previously mentioned, the base of the designed artifact triangle served as the reference bar (See Figure 5.1)

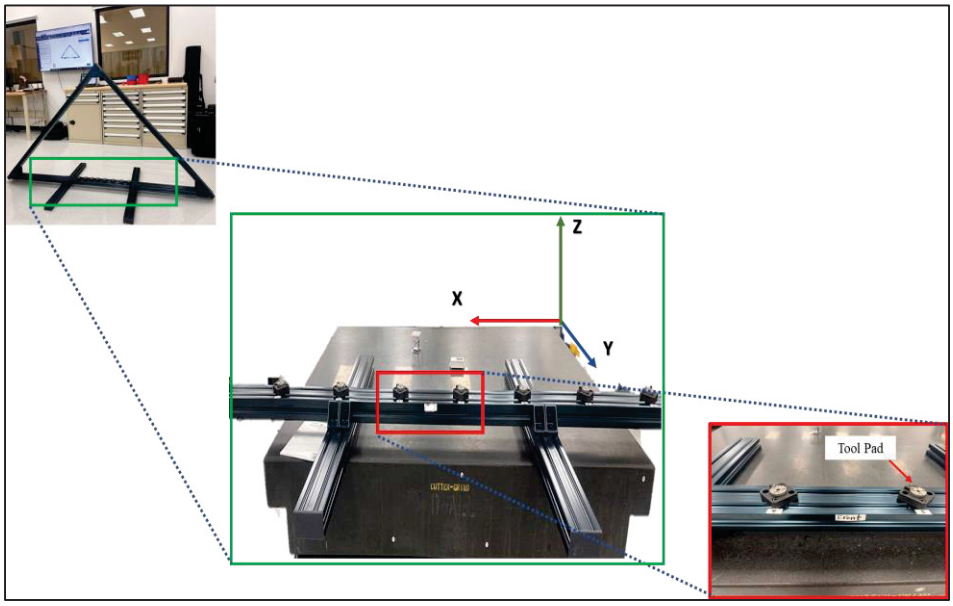

Figure 5.1 Design of a bar as reference with tooling pads for measurement

5.1.2 Calibration of the Bar as Reference Bar Using the Laser Tracker

At first, the bar is calibrated using a laser tracker and and make it a reference. The bar as a reference is positioned in front of the laser tracker (See Figure 5.2).

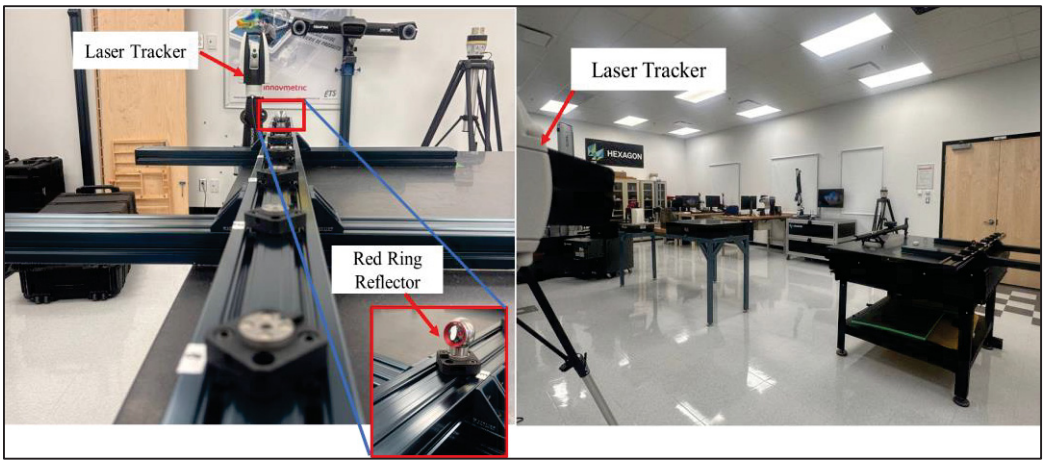

Figure 5.2 Calibration of the bar and make it a reference with the Absolute Laser Tracker 960

The Red Ring Reflector is placed on the tooling pads on the reference bar. These points are measured using a laser tracker, and the Euclidean distance between each pair of points is then calculated (Eq (4.2)). This Euclidean distance formula is used because when comparing two devices (laser tracker and iGPS), there is no need for coordinate system alignment, allowing points to be compared directly regardless of their reference systems. At this stage all (x, y, z) are considered when calculating the Euclidean distance to account for any misalignment of the reference bar with the X-axis.

To minimize the effect of random and environmental errors (such as temperature fluctuations), the measurements are repeated over three consecutive days, with three repetitions each day. After gathering all the measurements, the Euclidean distance between two points measured on different days is calculated, and the mean distance is taken.

Then, the uncertainty for each point along the X-axis is determined by applying the same procedure used for the laser tracker uncertainty evaluation. The following steps are considered:

Step 1: Standard Uncertainty Calculations

According to the laser tracker brochure, the maximum device uncertainty ($u_{x_{device}}$) increases with the measurement distance from the laser tracker, as presented in Table 5.1 and Eq (4.3).

Therefore, the uncertainty of each point is calculated relative to its distance from the laser tracker.

Step 2: Calculating Repeatability Uncertainty for the Laser Tracker

After collecting the coordinates, the next step is to calculate the repeatability uncertainty of the laser tracker:

The average coordinates for each point were calculated using Eq. (2.10), as shown in Table 5.1.

The standard deviation of the coordinates (σ_x) was then computed using Eq. (2.11).

Finally, the standard error for each coordinate ($u_{x_{rep}}$) was obtained from Eq (2.12) and Eq (2.13).

Step 3. Combining Standard Uncertainties for Each Point

The combined standard uncertainty for each point (u_{x_i}) was obtained by combining repeatability and device uncertainties using Eq. (2.5) as shown in Table 5.1.

To calculate the uncertainty for each point, the combined uncertainty is multiplied by the square root of 2, as shown in Table 5.1 (Eq (2.8)).

Table 5.1 Uncertainty of reference points

Meas. point number	$\bar{x}$	**Average point distance from LT**	σ_x	$u_{x_{rep}}$	$u_{x_{device}}$	u_{x_i}	$u_{x_{point}}$
1	-373.164	2247.786	0.011	0.004	0.016	0.017	0.024
2	-387.554	2499.447	0.010	0.003	0.017	0.018	0.025
3	-401.495	2747.526	0.010	0.003	0.018	0.018	0.026
4	-415.790	2998.249	0.008	0.003	0.019	0.019	0.027
5	-429.818	3249.298	0.010	0.003	0.020	0.020	0.029
6	-444.013	3499.202	0.009	0.003	0.021	0.021	0.030
7	-458.914	3748.071	0.008	0.003	0.022	0.022	0.031
8	-472.803	4000.000	0.014	0.005	0.023	0.023	0.032

To ensure a conservative estimation, the maximum point uncertainty obtained from the laser tracker is considered as the reference uncertainty in the iGPS uncertainty, as shown in Figure 5.3 and Eq.(4.5).

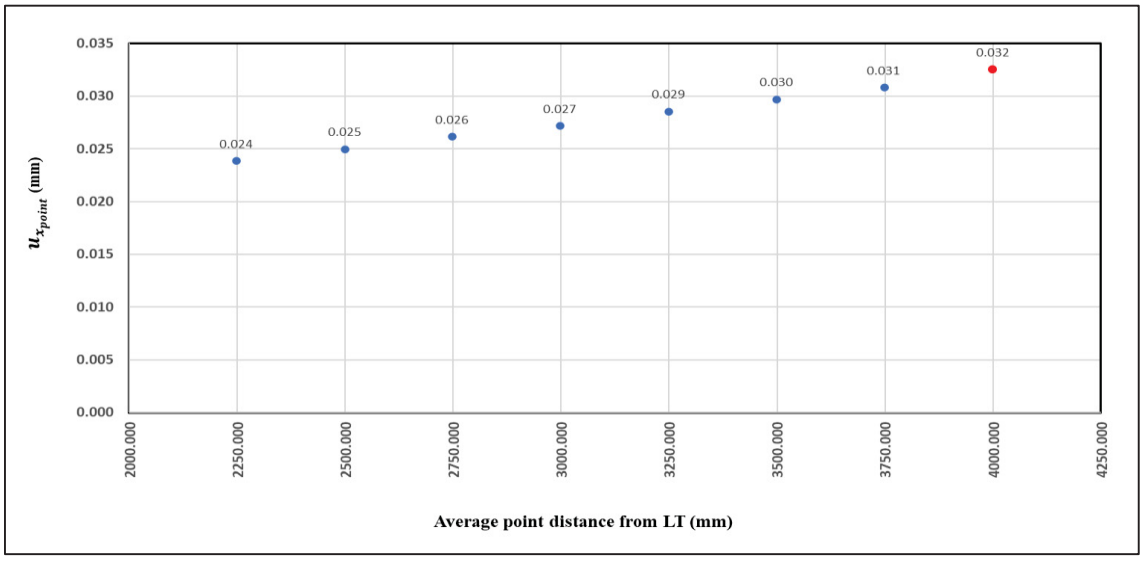

Figure 5.3 Graph of combined uncertainty of points measured by the laser tracker versus their average distance to the laser tracker

The graph illustrates the maximum uncertainty of a point measured by the laser tracker along the x-axis, with a value $u_{max_{LT}} = 0.032\ mm$.

5.1.3 Measurement of the Reference Bar Using the iGPS

The iGPS system measurements are repeated using the reference bar in the same setup, ensuring consistency and minimizing variable factors. Here's a detailed description of the process.

Step 1: Calculating Bias (Systematic Uncertainty)

- Bias Determination: The bias, representing the systematic difference between measurements from the laser tracker and the iGPS, is calculated by comparing the Euclidean distances obtained by both devices using Eq (4.2).

Step 2: Reducing Random and Environmental Errors

- Repeated Measurements: To mitigate the effects of random variables and environmental factors such as temperature fluctuations, measurements are repeated over three consecutive days, with each day consisting of three repetitions.
- Analysis of Repeated Data: The Euclidean distances between corresponding points measured on different days are calculated, and the mean distance is derived to ensure consistent results. The iGPS measurement setup used for this step is shown in Figure 5.4.

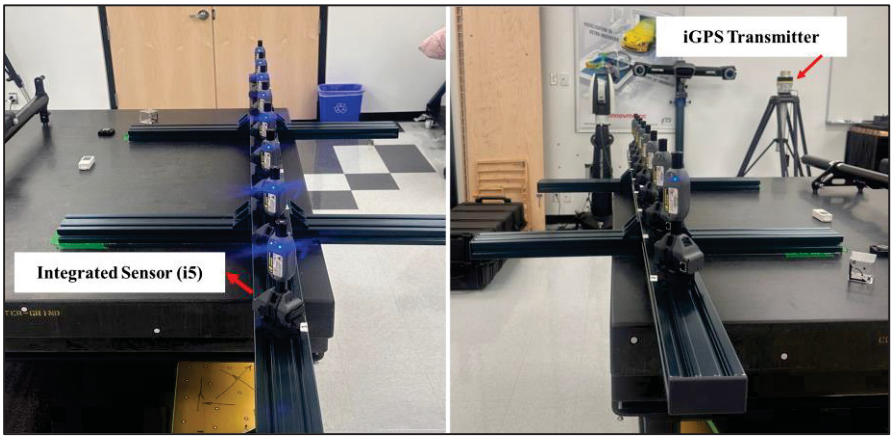

Figure 5.4 Measurement with the iGPS system

Step 3: Analysis of factors influencing measurement uncertainty

- Investigation of Influencing Factors: Factors such as (i) day, (ii) time, and (iii) the distance between measurement points are examined for their potential impact on uncertainty.
- Statistical Analysis: Data are analyzed for standard deviations and means. A one-way ANOVA is performed using Minitab software to further assess the effects of these factors.

i. **Effect of Day on Measurement Uncertainty**: This result indicates that the measurement day does not have a statistically significant effect on the mean iGPS

measurement uncertainty. In other words, the iGPS system exhibits statistically stable behavior across the three consecutive measurement days.

This stability implies that day factors such as normal laboratory environmental variations or routine system recalibration do not contribute significantly to the measurement uncertainty (See

One-way ANOVA:

Method

Null hypothesis	All means are equal
Alternative hypothesis	Not all means are equal
Significance level	α = 0.05

Equal variances were assumed for the analysis.

Analysis of Variance

Source	DF	Adj SS	Adj MS	F-Value	P-Value
Day	2	0.019	0.009	2.294	0.107
Error	81	0.327	0.004		
Total	83	0.346			

Means

Evaluation of Measurement Uncertainty	N	Mean	StDev	95% CI
Day1	28	0.064	0.075	(0.040, 0.088)
Day2	28	0.028	0.061	(0.004, 0.052)
Day3	28	0.040	0.052	(0.016, 0.064)

Pooled StDev = 0.0635779

Figure 5.5 Comparison of the effect of day on iGPS measurement uncertainty across three consecutive days

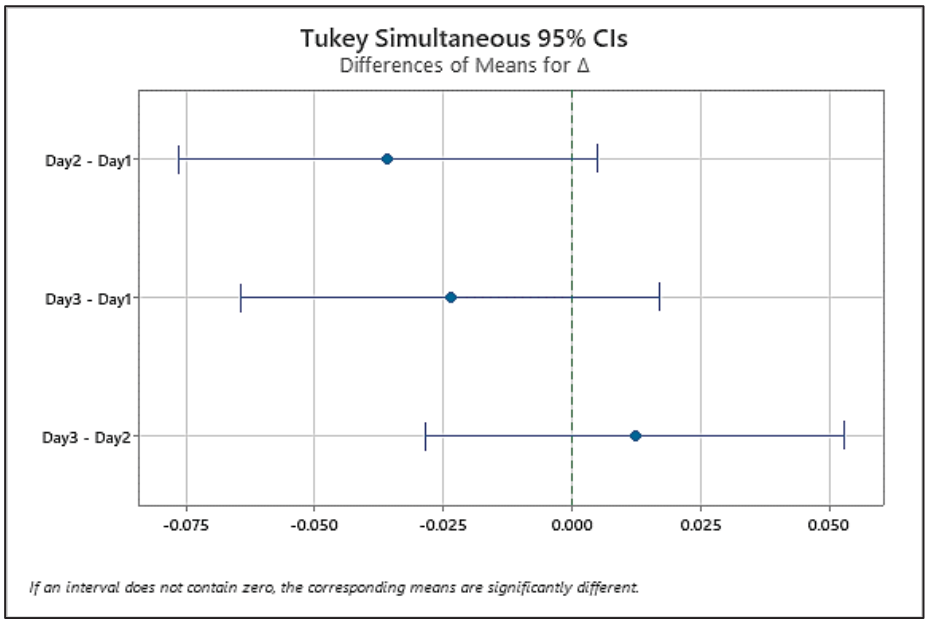

Figure 5.6 Effect of day on iGPS measurement uncertainty

ii. **Effect of Time on Measurement Uncertainty**: The results show that the elapsed time after iGPS calibration does not have a statistically significant effect on measurement uncertainty. Although measurements were taken immediately after calibration and several hours later, the observed differences in the mean uncertainty remain within random variability and do not indicate any systematic drift in system performance.

This behavior suggests that, following the initial warm-up and calibration using the i6 Long Reach Probe, the iGPS system maintains stable accuracy and measurement stability over time. Therefore, the post-calibration time effect can be considered negligible within the uncertainty model. (See Figure 5.7 and Figure 5.8).

One-way ANOVA:

Method

Null hypothesis	All means are equal
Alternative hypothesis	Not all means are equal
Significance level	α = 0.05

Equal variances were assumed for the analysis.

Analysis of Variance

Source	DF	Adj SS	Adj MS	F-Value	P-Value
Time	2	0.005	0.002	1.279	0.284
Error	81	0.144	0.002		
Total	83	0.149			

Means

Time	N	Mean	StDev	95% CI
0 Hour	28	0.036	0.048	(0.020, 0.052)
3 Hour	28	0.035	0.015	(0.019, 0.051)
4 Hour	28	0.051	0.053	(0.035, 0.067)

Pooled StDev = 0.0422136

Figure 5.7 Comparison of time effects on measurement uncertainty

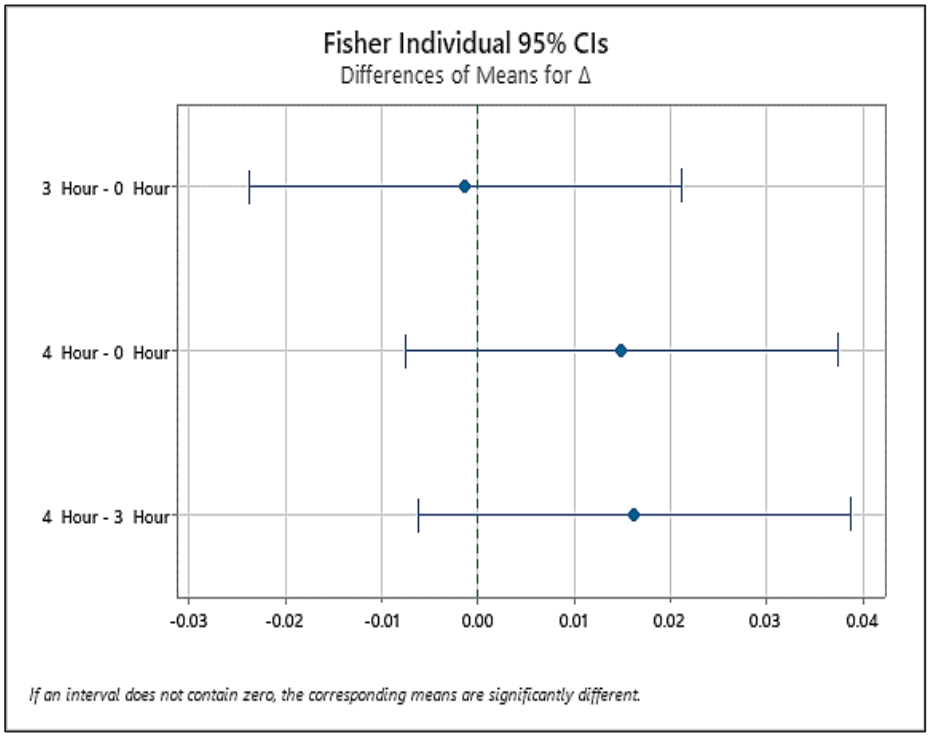

Figure 5.8 Effect of time on uncertainty

iii. **Distance Between Points:** Increased distances between points elevate uncertainty, impacting measurements in both the iGPS and laser tracker systems. The most significant factor affecting measurement results was the distance between points. As the distance increased, so did the uncertainty, impacting measurements in both the iGPS and laser tracker systems (See Figure 5.9 and Figure 5.10).

According to our experiments, distance between the measured points is the dominant driver of measurement uncertainty. Across all runs, changes in evaluation of measurement uncertainty and warm-up time were not statistically significant (p_value > 0.05). These findings were consistent across devices and days, indicating that the distance effect is robust while the other factors are negligible for our setup. Accordingly, the remainder of the analysis concentrates on quantifying the distance effect on uncertainty.

One-way ANOVA:

Method

Null hypothesis	All means are equal
Alternative hypothesis	Not all means are equal
Significance level	α = 0.05

Equal variances were assumed for the analysis.

Analysis of Variance

Source	DF	Adj SS	Adj MS	F-Value	P-Value
Distance Group	6	0.188	0.031	8.704	0.000
Error	245	0.880	0.004		
Total	251	1.067			

Means

DistanceGroup	N	Mean	StDev	95% CI
250.316	63	0.020	0.061	(0.006, 0.035)
500.139	54	0.025	0.055	(0.009, 0.041)
750.502	45	0.040	0.059	(0.022, 0.057)
1000.890	36	0.062	0.059	(0.043, 0.082)
1250.837	27	0.066	0.069	(0.043, 0.089)
1500.418	18	0.075	0.059	(0.048, 0.103)
1752.213	9	0.144	0.058	(0.104, 0.183)

Pooled StDev = 0.0599292

Figure 5.9 Comparison of distance effects on measurement uncertainty across different systems

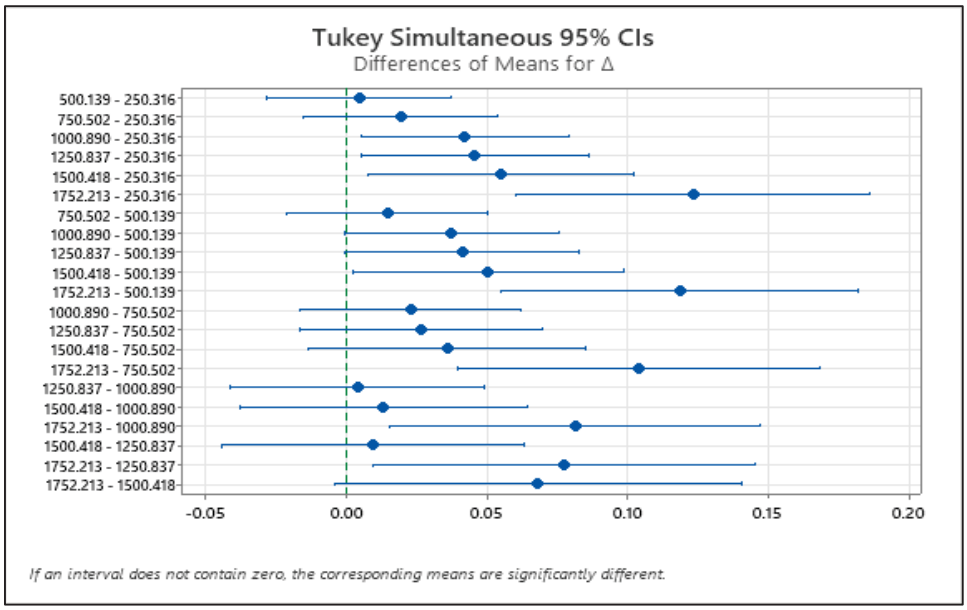

Figure 5.10 Distance effect on uncertainty

Step 4: Calculating Repeatability Uncertainty for iGPS

- The mean coordinates for each point were calculated using Eq. (2.10).
- The standard deviation of these coordinates was then computed using Eq. (2.11).

Step 5: Determining Device Uncertainty for iGPS

The maximum device uncertainty for the iGPS, specified as $\pm 200\mu m + 20\mu m$, was calculated using Eq (2.14).

Step 6: Combining Standard Uncertainties for Each Point

- Uncertainty Combination: The total standard uncertainty for each point includes repeatability uncertainty, device uncertainty, and reference uncertainty (the maximum point uncertainty measured by the laser tracker along the x-axis) determined in the previous step. These standard uncertainties are combined using Eq (2.5).

Step 7: Calculating the Uncertainty of the Distance Between Two Points

- Point Uncertainty Combination: The uncertainty of the distance between two points is calculated by combining the uncertainties of both points involved, using Eq (4.4).

- Adjustment for Confidence Level: This value is multiplied by 2 to reflect a 95% confidence level.

This approach provides a complete and accurate assessment of the iGPS performance and highlights the factors that affect measurement precision.

The iGPS reflectors were placed at the same predefined locations used by the laser-tracker measurements. After calibration, iGPS measurements were taken.

The standard uncertainty along the X, Y, and Z axes was computed for each point within the work volume. For each pair of points, the combined uncertainty of the corresponding Euclidean distance was then calculated along the relevant axis. To ensure adequate spatial coverage, two lines were evaluated along the X-axis (A–B and C–D), two along the Y-axis (A–C and B–D), and four along the Z-axis (A–E, B–F, C–G, and D–H), as illustrated in Figure 5.11 to Figure 5.16.

For each axis, maximum combined uncertainty was taken as the representative uncertainty of each axis by applying a $k \approx 2$ (for 95% confidence). The resulting representative uncertainties for each axis are reported at the end of this section.

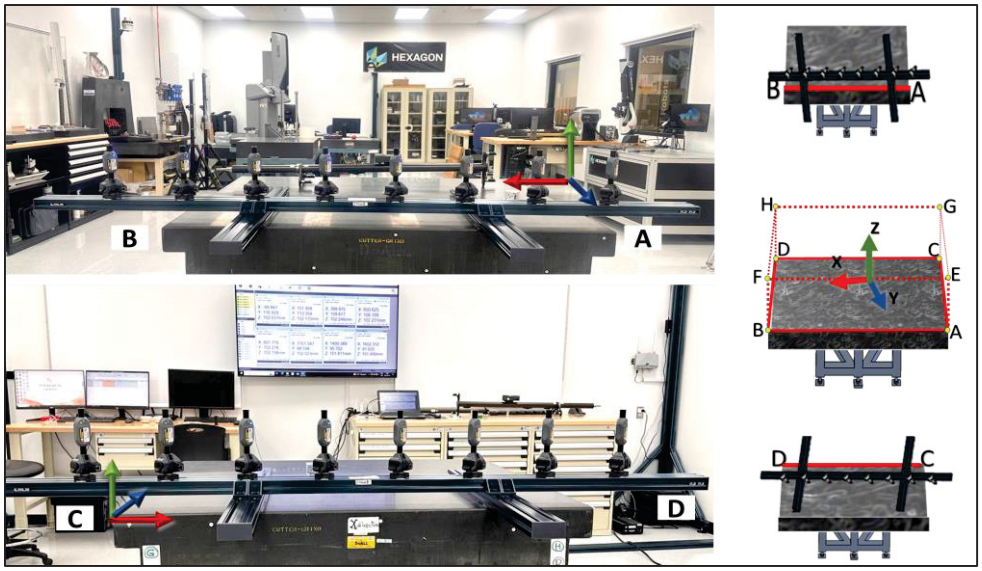

Figure 5.11 X Setup with eight iGPS detectors on AB and CD along the X-axis

To assess the iGPS uncertainty along the X-axis, the setup shown in Figure 5.11 was used. Eight detectors were positioned along two parallel lines (A–B and C–D) on the reference bar. These two lines were selected to verify repeatability and to ensure that the measurement uncertainty remained stable across different positions along the same axis. Both sets of measurements were performed under identical conditions after calibration of the iGPS system, using the same reference points as those established by the laser tracker.

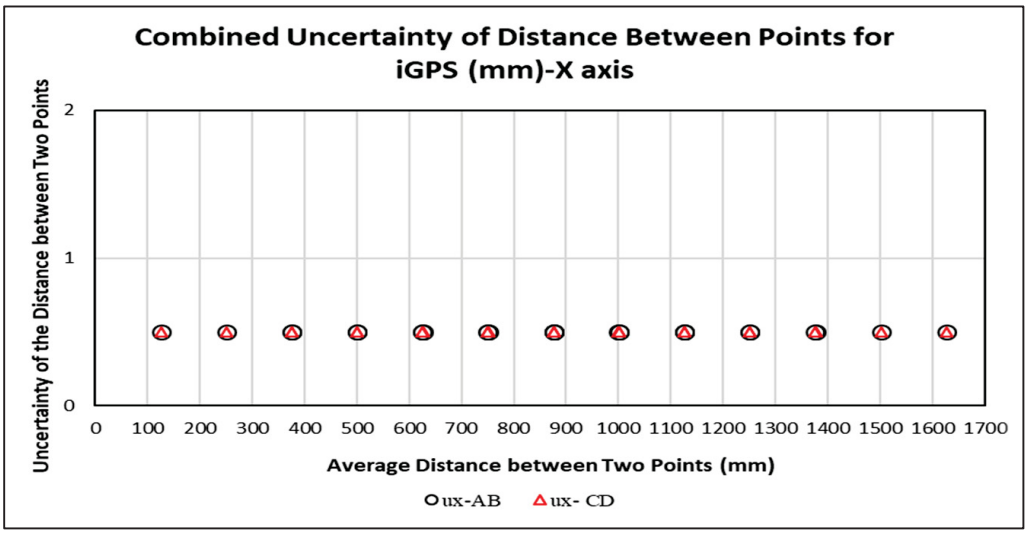

Figure 5.12 Compares combined distance uncertainties across AB and CD along the X-axis

Figure 5.12 presents the corresponding combined uncertainty of distance for the A–B and C–D lines. The uncertainty values remain consistent along the axis, indicating that distance has a negligible influence on the iGPS performance in the X direction. The maximum value obtained was considered as the representative uncertainty of the X-axis.

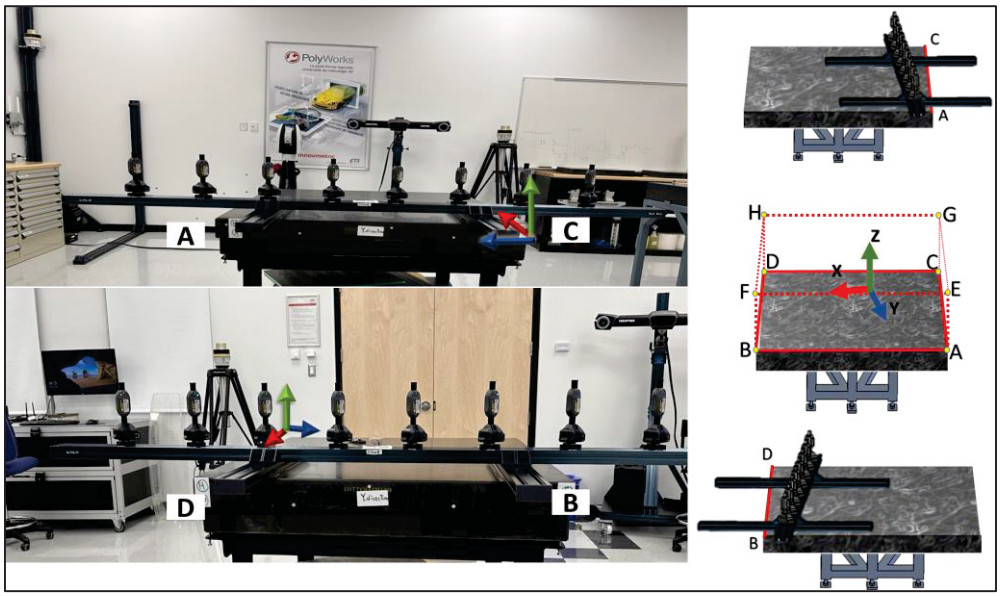

Figure 5.13 Y Setup with eight iGPS detectors on AC and BD along the Y-axis

To evaluate the system's behavior along the Y-axis, the detectors were arranged as shown in Figure 5.13, along two perpendicular lines (A–C and B–D). This configuration extends the measurement coverage across the second horizontal direction of the work volume. The alignment of these lines allows assessment of the spatial uniformity of the iGPS uncertainty in the Y direction.

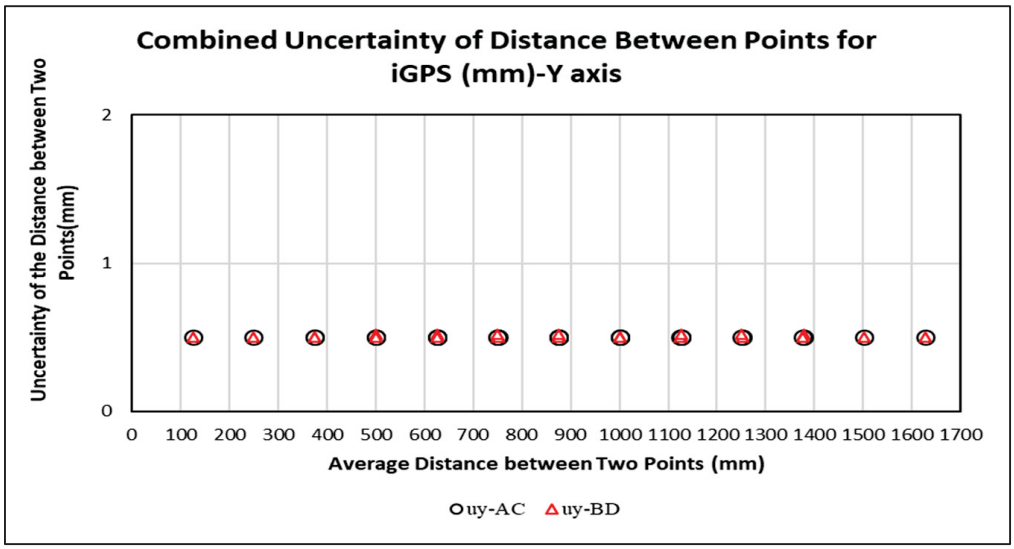

Figure 5.14 Compares combined distance uncertainties across AC and BD along the Y-axis

The corresponding results are displayed in Figure 5.14, where the combined uncertainties for the A–C and B–D lines are compared. The curves demonstrate very similar trends with minimal variation, confirming that the iGPS system maintains stable precision along the Y-axis as well.

Figure 5.15 Setup with eight iGPS detectors on AE, BF, CG, DH along the Z-axis

Finally, for the Z-axis, the setup shown in Figure 5.15 includes four vertical lines (A–E, B–F, C–G, and D–H). This configuration was designed to examine the effect of height and detector position on the iGPS performance, as well as to verify consistency across the vertical direction.

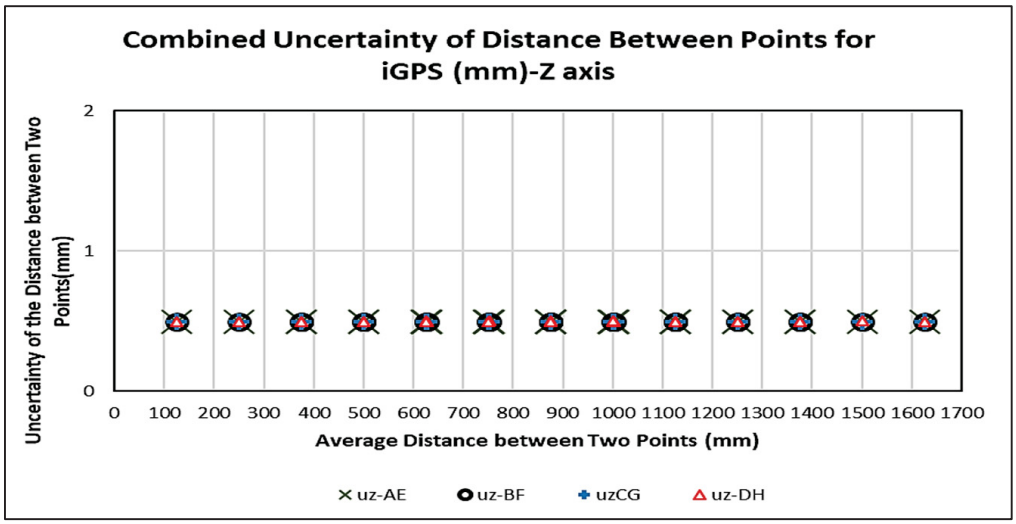

Figure 5.16 Compares uncertainties across the AE, BF, CG, DH along the Z-axis

Figure 5.16 illustrates the combined uncertainty of distance for these four lines. The uncertainty values are uniform throughout the entire height range. The maximum combined uncertainty among these four configurations is taken as the representative uncertainty of the Z-axis.

The plots show that the largest iGPS uncertainty occurs between point 1 and point 8. Across the tested distances (within the defined volume), the uncertainty values are stable and do not change meaningfully with the distance. These outcomes align with our expectations and confirm that, in the defined work volume, the iGPS system provides consistent measurement uncertainty on all three axes. The values, reported relative to the laser-tracker reference, are:

X-axis: U_X = 0.4985 mm
Y-axis: U_Y = 0.5182 mm
Z-axis: U_Z= 0.4992 mm

These representative uncertainties are used as inputs in the next section to quantify how measurement error propagates to key assembly characteristics.

5.2 Propagation Uncertainty of Position as a KCs in MAA by Using iGPS

After estimating the iGPS system uncertainty for each single measurement point, we assess how that uncertainty propagates through the assembly process when using iGPS. In this section, we analyze uncertainty propagation for one key assembly characteristic position.

5.2.4 Design of the Artifact

A hexagonal aluminum plate with a central circular through-hole (nominal radius 50 mm) was fabricated. Six detector reference seats were CNC-machined on a concentric pitch-circle of radius 117.5 mm and permanently marked 1–6 on the plate surface (See Figure 5.17).

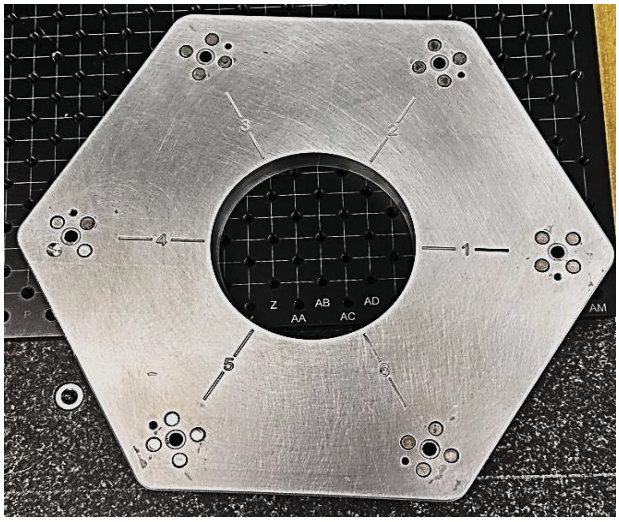

Figure 5.17 CNC-fabricated aluminum artifact with concentric reference seats

5.2.5 Experimental Setup

The CMM established the A|B|C datum reference frame, with the center of the large circular hole defined as the origin at (0, 0, 0). The six detector locations were measured and exported as nominal points for import into Surveyor®.

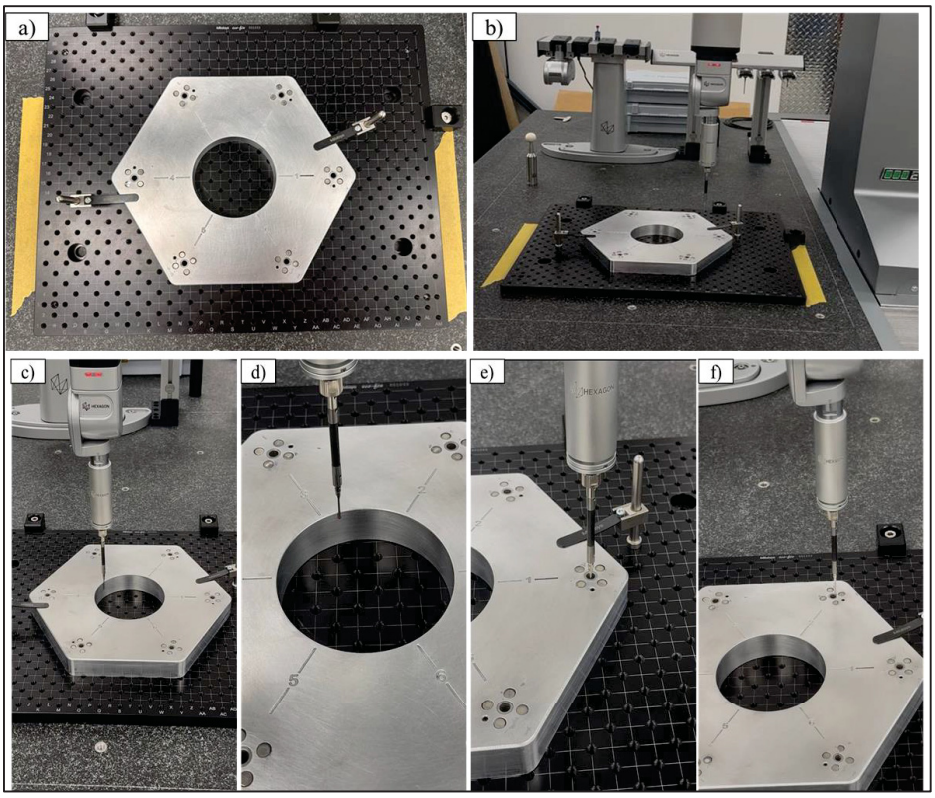

Figure 5.18 CMM measurement setup for defining the reference frame and nominal coordinates of the detector artifact

As shown in Figure 5.18(a–f), the artifact was inspected on a CMM to define the A|B|C datum frame and to extract the nominal coordinates of the detector holes. The artifact was rigidly mounted on the CMM table (a, b). The top surface of the artifact Figure 5.18(b) was probed to define Datum A (plane); the central hole Figure 5.18(c, d) was measured to establish Datum B (axis); and detector hole #1 Figure 5.18(e) was probed to define Datum C, constraining in-plane rotation. Finally, all six detector holes were measured (f), and the coordinates were exported as nominal data for import into Surveyor® iGPS.

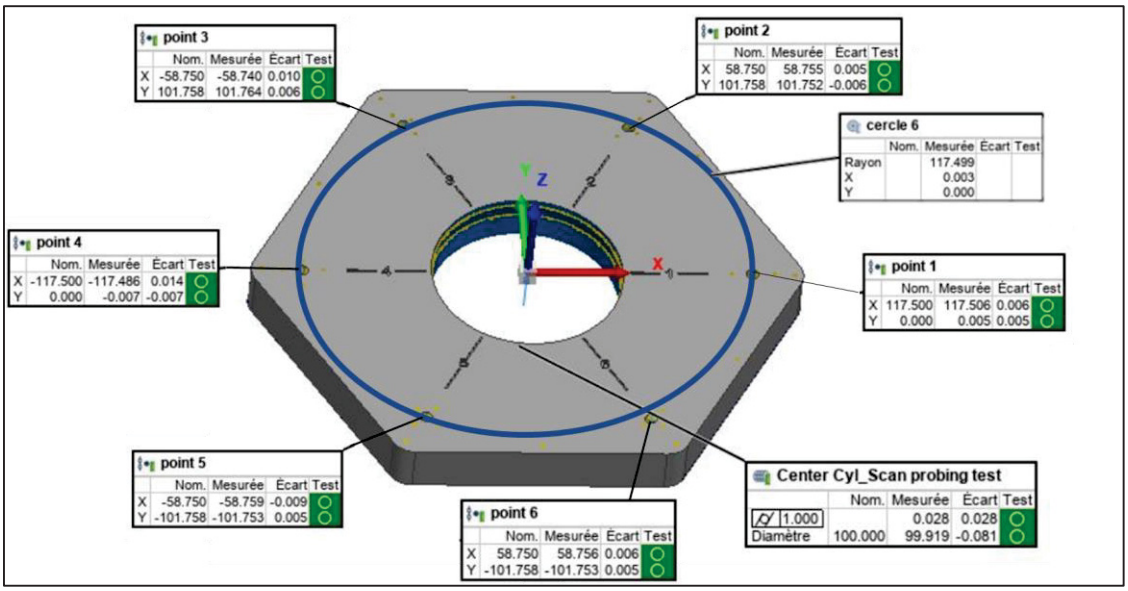

Figure 5.19 CMM results for the artifact and nominal coordinates

For measurement preparation, the iGPS system was powered on and allowed to warm up for one hour. Figure 5.19 shows the nominal coordinates of the six detector holes and the central reference hole, as obtained from the CMM inspection. The coordinate frame (X, Y, Z) was established based on the defined datums A, B, and C described earlier. Calibration was then performed using the i6 scale bar, with a Plane–Line–Line alignment of the coordinate system, following the manufacturer's procedure. To remove the scale-bar offset, the same calibrated fixture described in the methodology was used. Its orthogonal edges were aligned with the coordinate axes, and the offset corrections were applied and zeroed in the software to ensure that the (X, Y) axes were perfectly aligned.

Figure 5.20 iGPS setup for calibration and offset alignment

The artifact was placed on the laboratory's granite surface plate. Figure 5.20 illustrates the iGPS experimental setup used for calibration and offset alignment. The setup includes the granite plate; the artifact fitted with reflectors; the iGPS detectors; and the i6 Long Reach Probe. Using the tool described earlier, the XY plane was established and the i6 Long Reach Probe offset was removed. The detectors were then arranged around the work volume to ensure complete coverage. Five target locations (X, Y) were randomly selected within the usable area of the granite plate, the same work volume used for Objective 1, to ensure full coverage of the work volume during the experiments. The minimum edge clearance was respected. Table 5.2 lists the nominal X–Y coordinates of the selected target points, which were used as reference positions for relocating the artifact during each measurement repetition. In each repetition, the artifact is moved from the coordinate origin toward the selected target, is guided as close as possible to the nominal position, and is then fixed at that location.

Table 5.2 Randomly selected target locations on the work volume

Point ID	Nominal X (mm)	Nominal Y (mm)
P1	548.000	496.000
P2	700.000	400.000
P3	835.000	1028.000
P4	1013.000	330.000
P5	1365.000	615.000

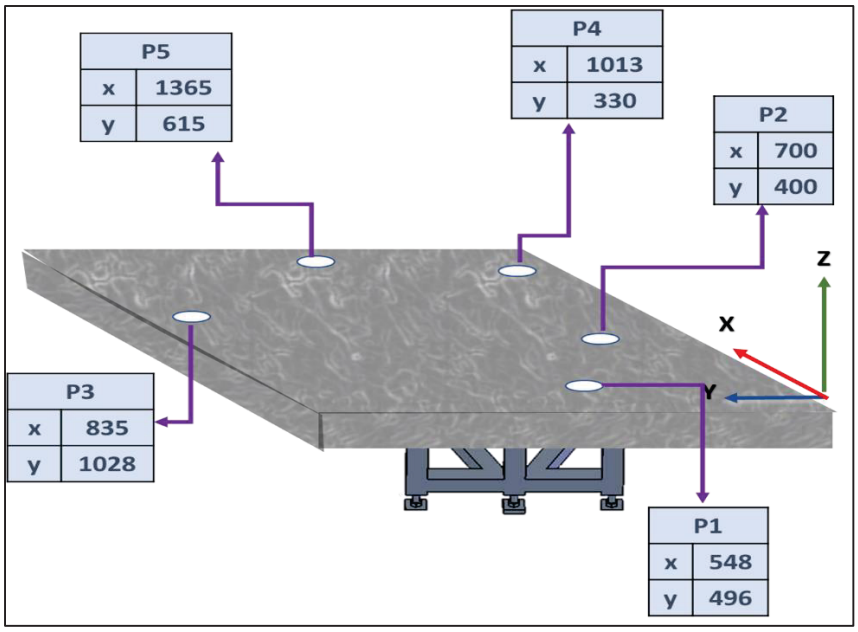

Figure 5.21 Layout of randomly selected target location within the work volume

Figure 5.21 shows the layout of five randomly selected target location (P1–P5) within the measurement work volume. These points represent different spatial positions used to evaluate the propagation of uncertainty across the table surface.

Figure 5.22 presents the configurations of the detector placement scenarios used in the experiments, labeled 3i5, 4i5, 5i5, and 6i5. Each scenario corresponds to the number of active iGPS detectors employed for data collection. These configurations were used to study how

increasing the number of detectors affects the measurement precision and stability within the same work volume.

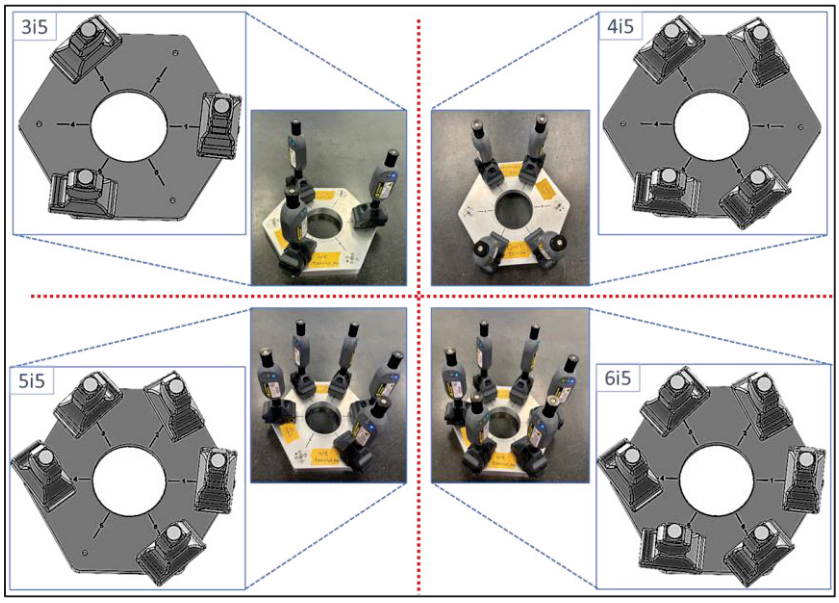

Figure 5.22 Configurations of detector placement scenarios (3i5–6i5) on the artifact

As shown in Figure 5.22, four detector-number scenarios were tested to assess whether adding detectors improves the accuracy of the estimated position as a key characteristic (KCs). Detector locations follow the numbers engraved on the artifact: 3-detector (1, 3, 5), 4-detector (2, 3, 5, 6), 5-detector (1, 2, 3, 4, 6), and 6-detector (1-6). The order of the scenarios and the detector-location assignments were randomized.

For each target location and each detector scenario, three repetitions are performed. In each repetition, only the detectors assigned to that scenario collect data at the target, and the resulting measurements are used as inputs to the Monte Carlo simulation.

In PolyWorks®, a Plane-Line-Line alignment was applied to align the Laser Tracker (LT) coordinate frame with that of the iGPS system for validation purposes.

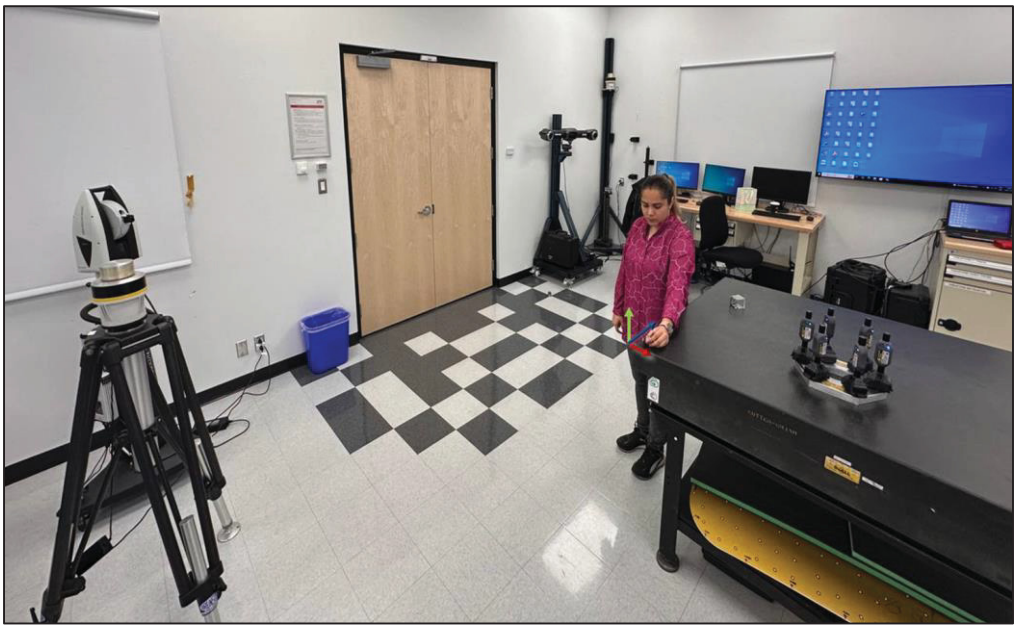

Figure 5.23 Laser Tracker validation setup

Figure 5.23 shows the experimental setup used for Laser Tracker (LT) validation. The LT was positioned facing the granite plate and the artifact, allowing direct comparison between the two measurement systems. The same coordinate frame alignment (Plane–Line–Line in PolyWorks®) ensured that both systems measured the same reference geometry within the defined work volume.

The next section uses the Monte Carlo method to evaluate the propagation of uncertainty for each scenario and target.

5.2.6 Monte Carlo Method Propagates Uncertainties

Five random target locations were selected on the granite table within the work volume (Figure 5.21, Table 5.2). At each location, four detector configurations were tested (Figure 5.22). Each configuration was measured in three independent repetitions, for a total of sixty best-fit circles (See Figure 5.24).

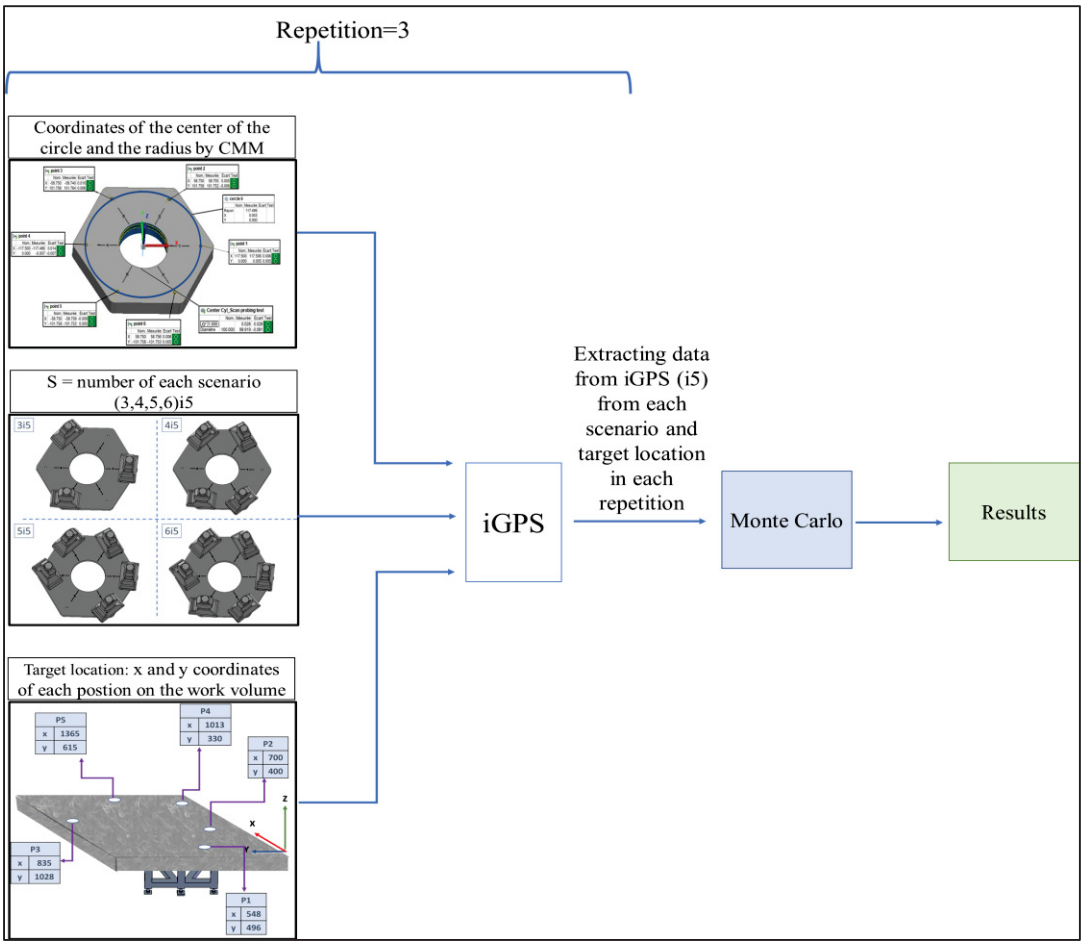

Figure 5.24 Experimental workflow for evaluating the effect of detector-number scenarios on uncertainty propagation

For each run, iGPS points were perturbed by Monte Carlo sampling using the uncertainties (U_X, U_Y, U_Z) from Objective 1 section 5.1.

X-axis: U_X = 0.4985 mm

Y-axis: U_Y = 0.5182 mm

Z-axis: U_Z= 0.4992 mm

Because the circle is estimated in the (XY) plane, the per-axis inputs were scaled by $(1/2\sqrt{2})$, consistent with Objective 1. Cross-axis correlations were assumed zero. Each realization was then refitted to a least squares best-fit circle in (XY); the measurement model and objectives are given in the Methodology (Eq (4.6)-(4.9)).

Convergence of the mean, standard deviation, and RMSE of the radius and center coordinates were monitored. Stabilization was observed at approximately 6,000 iterations; nevertheless, each Monte Carlo run used 10,000 iterations with a step of 10 (diagnostics and stored samples every 10 iterations) to provide a margin. Results are reported at the 95% confidence level. Figures display $\pm 2\sigma$ bands around the Monte Carlo means.

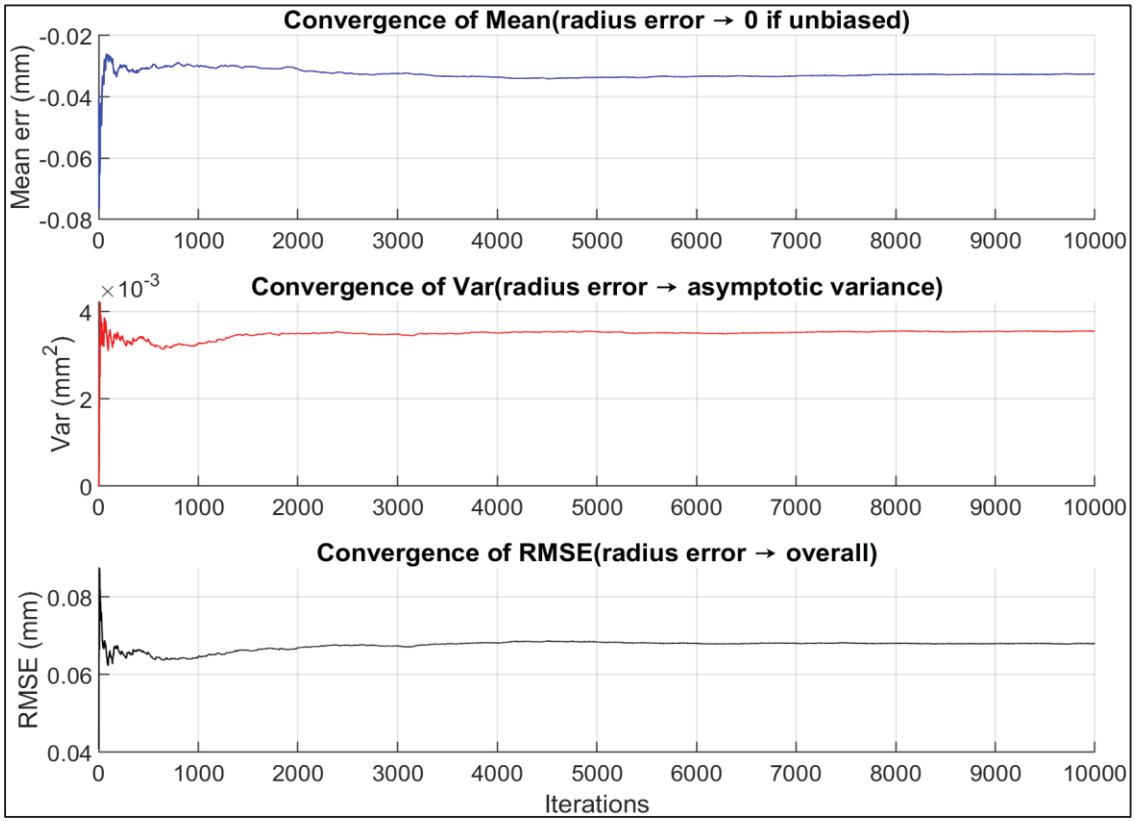

Figure 5.25 Convergence of Monte Carlo estimates for the circle radius of target location of P5 with 6-detector configuration

The convergence behavior of the Monte Carlo simulation for target location of P5 is illustrated in Figure 5.25. The mean error, variance, and RMSE of the estimated radius were monitored over 10,000 iterations (step = 10). All three quantities stabilized after approximately 6,000 iterations, indicating that the sampling process had reached statistical steadiness. This confirms

that the Monte Carlo simulation provided a consistent and repeatable propagation of measurement uncertainty for radius estimation.

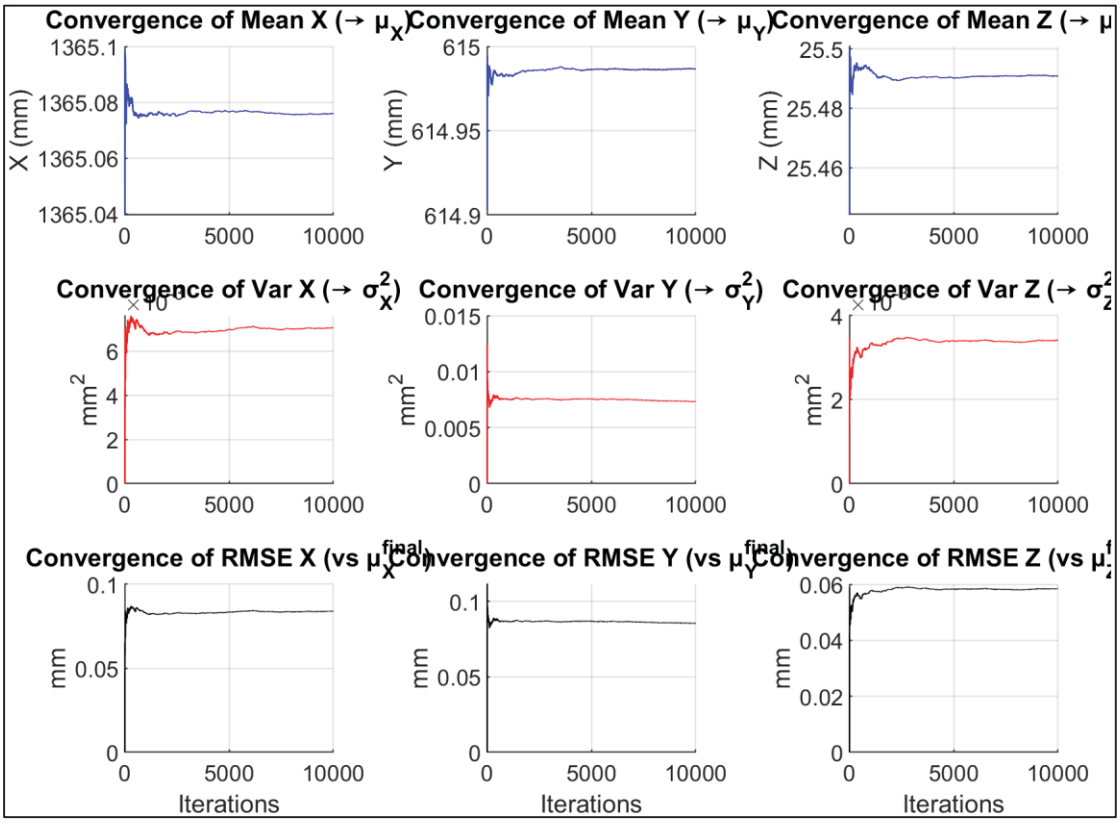

Figure 5.26 Convergence of Monte Carlo estimates for the circle center of target location of P5 with 6-detector configuration

Figure 5.26 shows the evolution of the mean (top), variance (middle), and RMSE (bottom) of the X, Y, and Z center coordinates over 10,000 iterations.

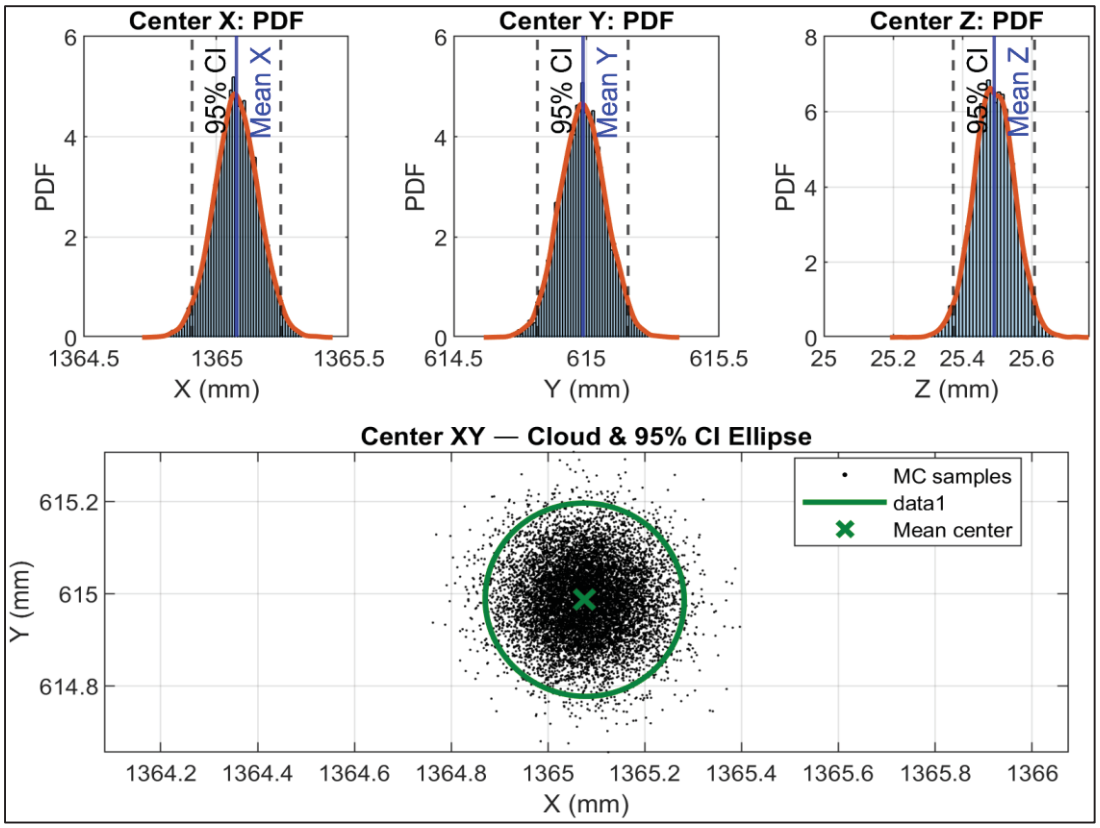

Figure 5.27 Monte Carlo simulation results for target location P5 with 6-detector configuration

In Figure 5.27 Probability density functions (PDFs) of the estimated circle-center coordinates (X, Y, Z) obtained from 10,000 Monte Carlo samples with a step of 10. The blue histograms represent the simulated distributions, the orange curves the fitted PDFs, and the dashed lines indicate the 95% confidence intervals around the mean values. The bottom plot shows the 2D distribution of the simulated center positions in the XY plane together with the 95% confidence ellipse and the mean center (green cross).

For every test, three radii were compared: the nominal CMM radius(R_{CMM}), the LT radius (R_{LT}), and the iGPS Monte Carlo mean (R_{iGPS}). In addition, the circle centers from iGPS and LT were compared at each location and repetition after coordinate alignment; the (X), (Y) deviations are reported with 95% confidence intervals. LT data were used solely for validation.

Figure 5.28 to Figure 5.32 present the comparison between the iGPS (blue) and Laser Tracker (LT, orange) measurements for the five random target locations (P1–P5) under the 3-detector configuration, each repeated three times.

For each target, the top plots show the estimated circle centers in the (XY) plane, while the lower plots compare the corresponding radii measured by iGPS, LT, and CMM.

The 95% confidence intervals (CI) are shown as error bars, allowing a direct visualization of measurement repeatability and uncertainty overlap.

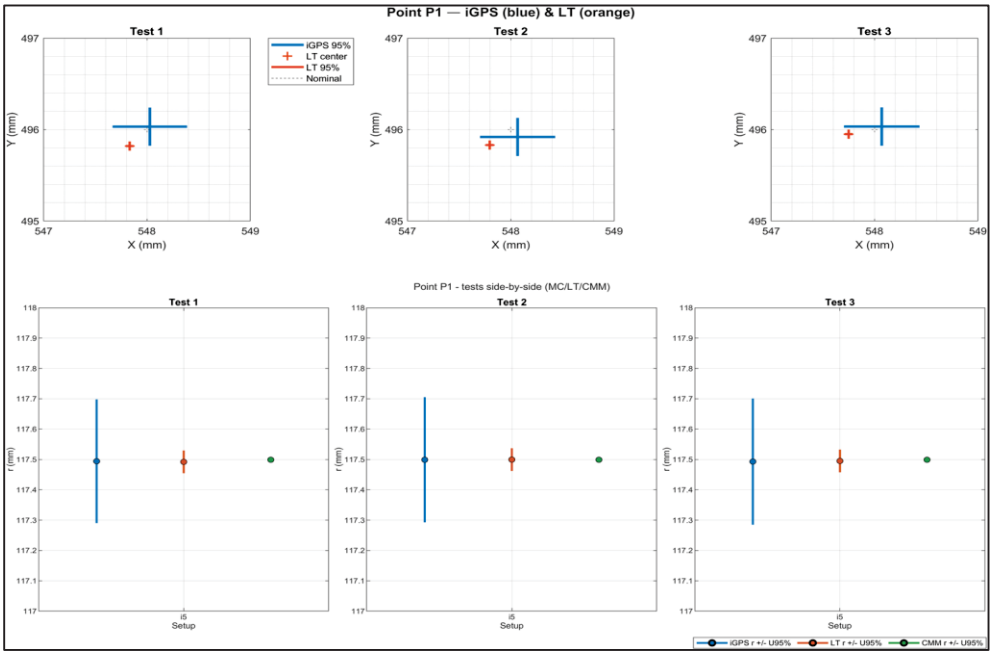

Figure 5.28 Point P1 - iGPS (blue) vs. LT (orange), 3-detector configuration

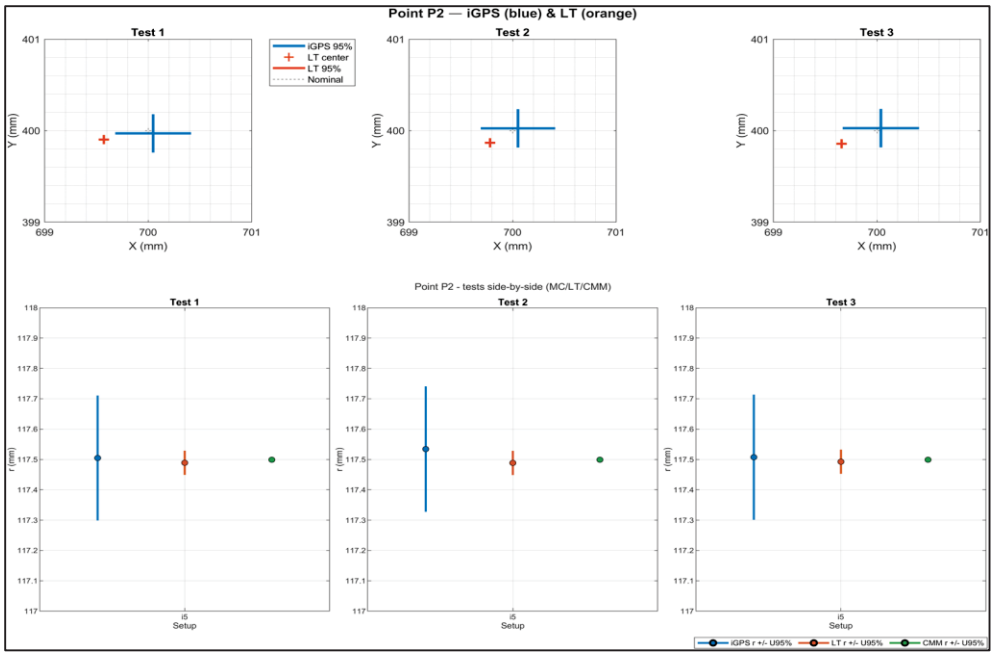

Figure 5.29 Point P2 - iGPS (blue) vs. LT (orange), 3-detector configuration

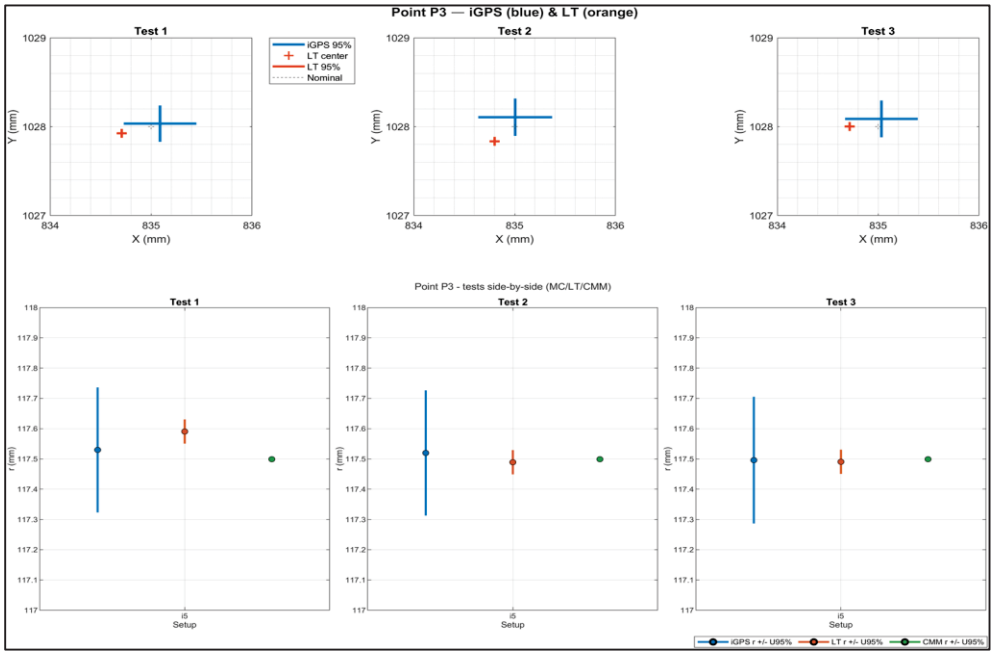

Figure 5.30 Point P3- iGPS (blue) vs. LT (orange), 3-detector configuration

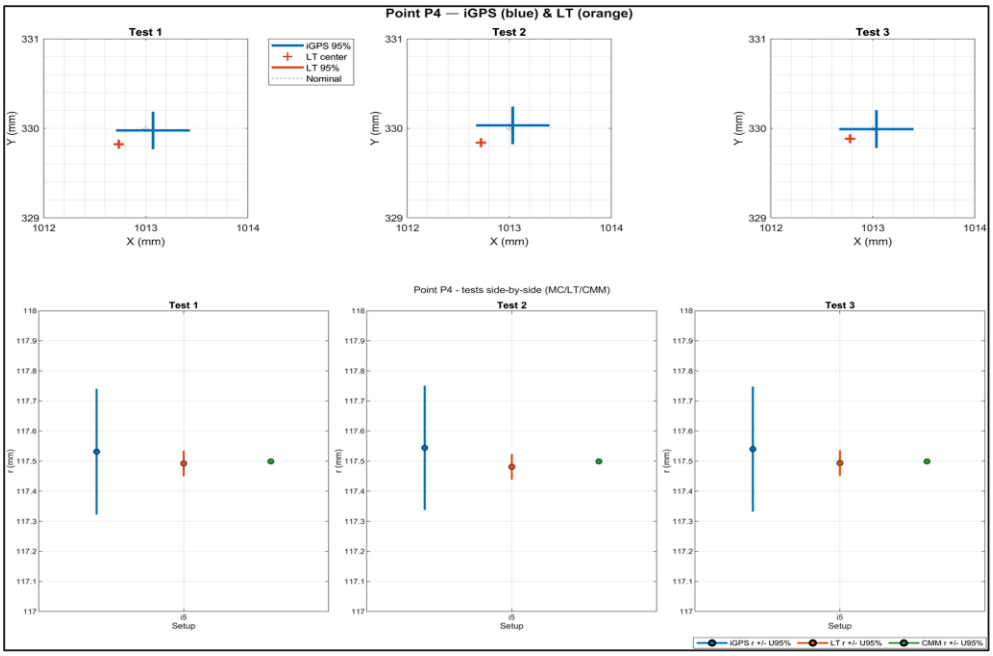

Figure 5.31 Point P4- iGPS (blue) vs. LT (orange), 3-detector configuration

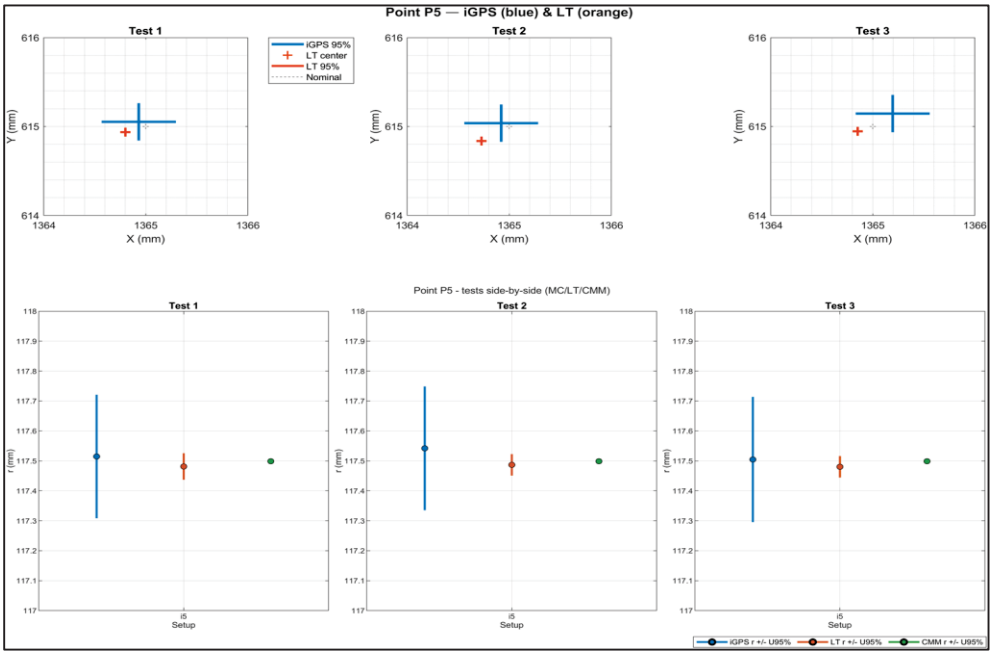

Figure 5.32 Point P5 - iGPS (blue) vs. LT (orange), 3-detector configuration

The results obtained from all five target locations (P1–P5) under the 3-detector configuration demonstrate that the iGPS system can successfully reconstruct both the circle center and radius within the expected uncertainty limits. Across all points, the mean differences between the iGPS and LT centers were typically below 0.3 mm, while the mean radius deviations remained within 0.15 mm relative to the LT and CMM references.

These deviations fall well inside the 95% confidence interval predicted by the Monte Carlo uncertainty propagation. The 95% confidence intervals of the iGPS estimates are consistently wider than those of LT, which is expected due to the lower geometric redundancy of the 3-detector setup. However, all LT centers lie within the iGPS confidence regions, confirming that the uncertainty model correctly represents the system's measurement behavior.

Regarding the radius estimation, the iGPS results show excellent consistency across the three repetitions for each target. Although the iGPS intervals are wider, the mean radius values for all points align closely with those from LT and CMM. The repetitions demonstrate that the measurement process is stable and that the propagated uncertainties effectively capture both random and geometric variations in the setup.

Figure 5.33 to Figure 5.37 show the results for the 4-detector configuration. Each plot presents the iGPS (blue) and LT (orange) comparisons for P1–P5. The top plots show the estimated circle centers, and the lower ones compare radii with CMM references. The 95 % CI are indicated as error bars.

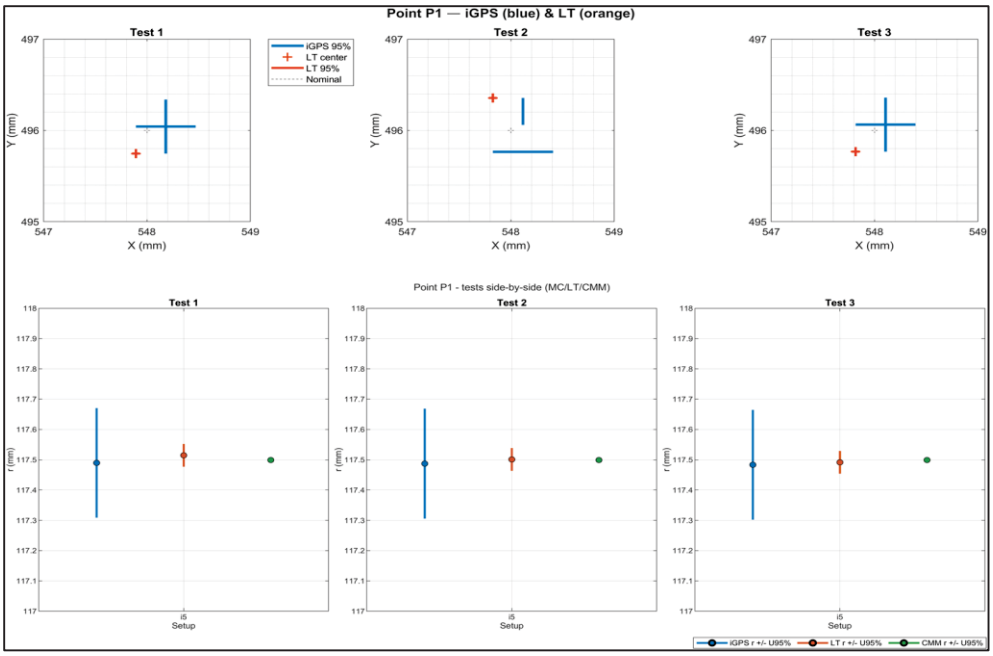

Figure 5.33 Point P1 - iGPS (blue) vs. LT (orange), 4-detector configuration

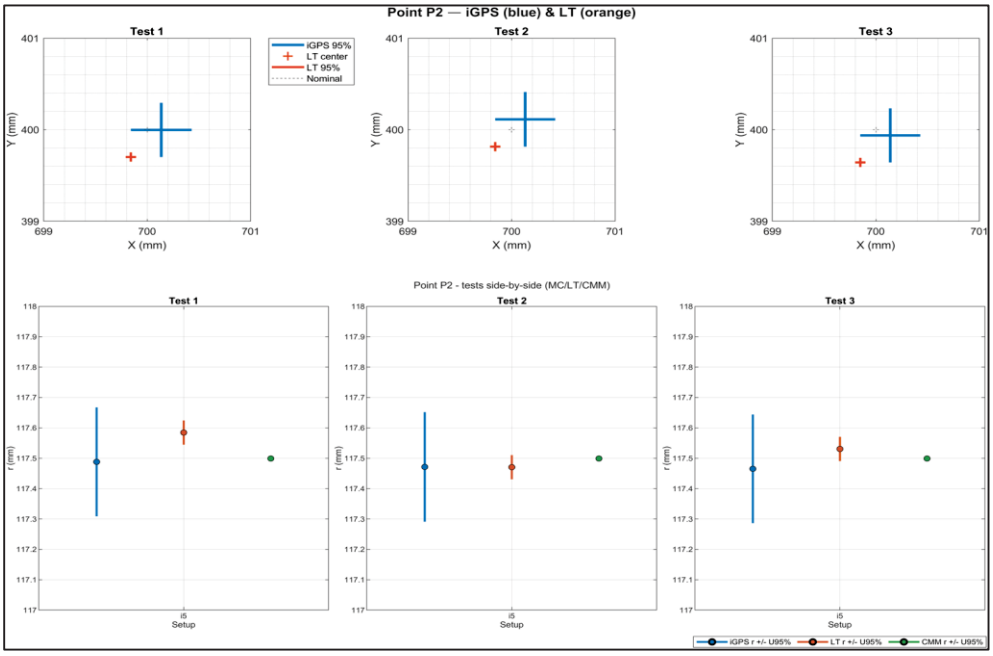

Figure 5.34 Point P2 - iGPS (blue) vs. LT (orange), 4-detector configuration

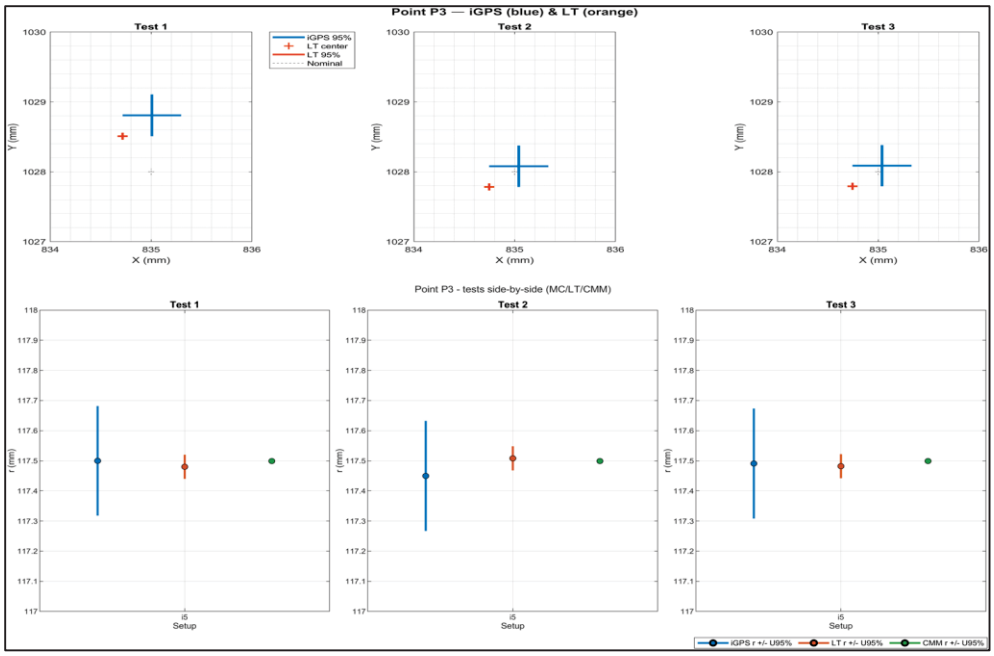

Figure 5.35 Point P3 - iGPS (blue) vs. LT (orange), 4-detector configuration

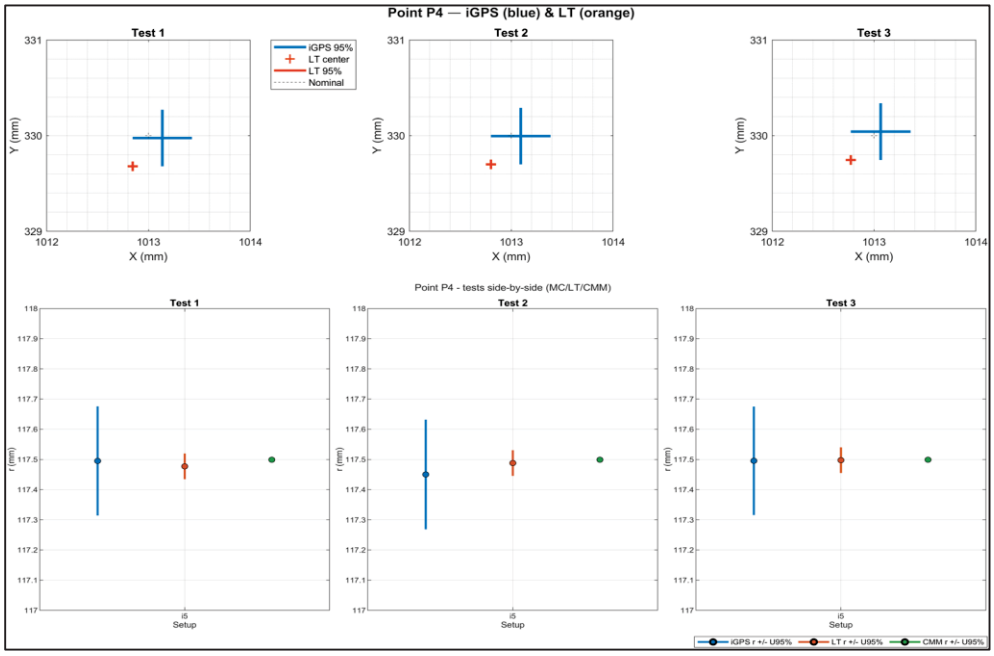

Figure 5.36 Point P4 - iGPS (blue) vs. LT (orange), 4-detector configuration

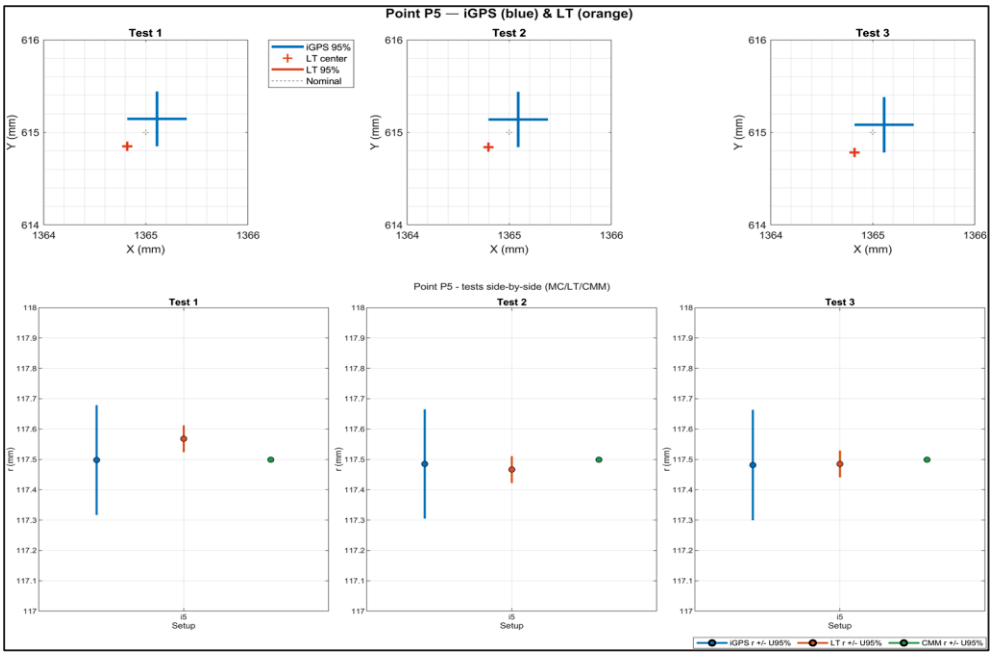

Figure 5.37 Point P5 - iGPS (blue) vs. LT (orange), 4-detector configuration

The results obtained under the 4-detector configuration show a clear improvement in measurement stability and accuracy compared to the 3-detector setup.

For all five points (P1–P5), the iGPS centers exhibit tighter alignment with the LT references. The mean differences across the work volume were typically below 0.25 mm in both X and Y axes (significantly better than the 3-detector scenario). The 95% confidence ellipses are noticeably smaller, particularly in central locations like P3 and P4, indicating better geometric constraint due to the increased spatial redundancy.

Radius comparisons reveal strong consistency among iGPS, LT, and CMM, with deviations typically within 0.1 mm. The overlap of the 95% confidence intervals confirms that the Monte Carlo propagated uncertainties effectively represent the true measurement dispersion. Across all repetitions, the variation between tests remains minimal, showing robust repeatability.

In summary, the 4-detector configuration provides a significant enhancement in both precision and reliability of iGPS measurements. The reduced uncertainty bounds and closer agreement with LT and CMM demonstrate that the addition of a fourth detector notably improves the

triangulation geometry and minimizes random dispersion in the reconstructed circle parameters.

Figure 5.38 to Figure 5.42 show the results for the 5-detector configuration, again comparing iGPS (blue) and LT (orange) for P1–P5. The upper plots show the estimated centers, while the lower plots compare the measured radii versus CMM and LT references.

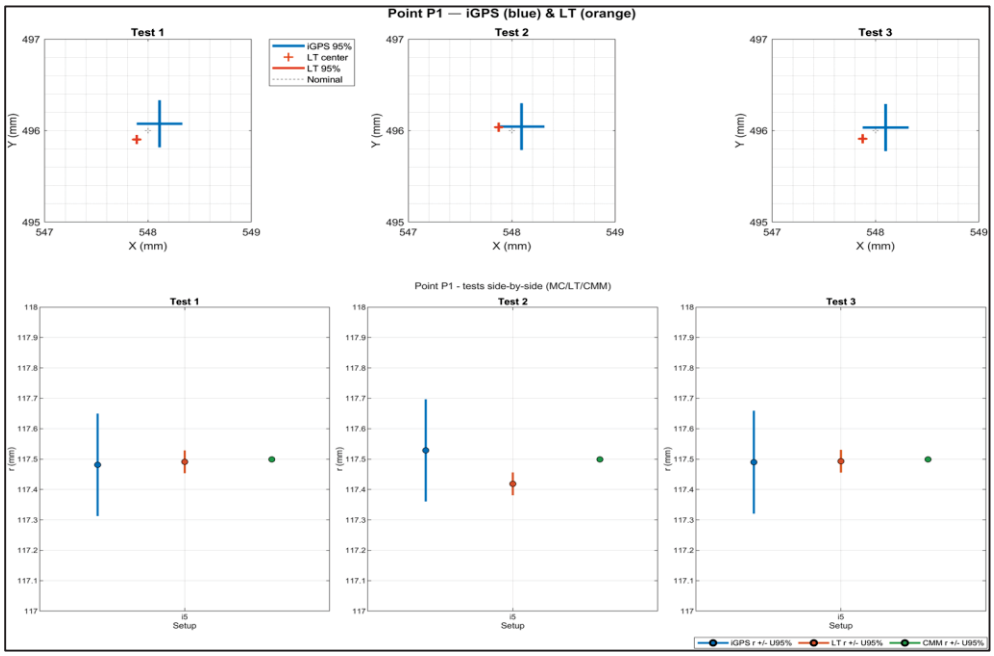

Figure 5.38 Point P1 - iGPS (blue) vs. LT (orange), 5-detector configuration

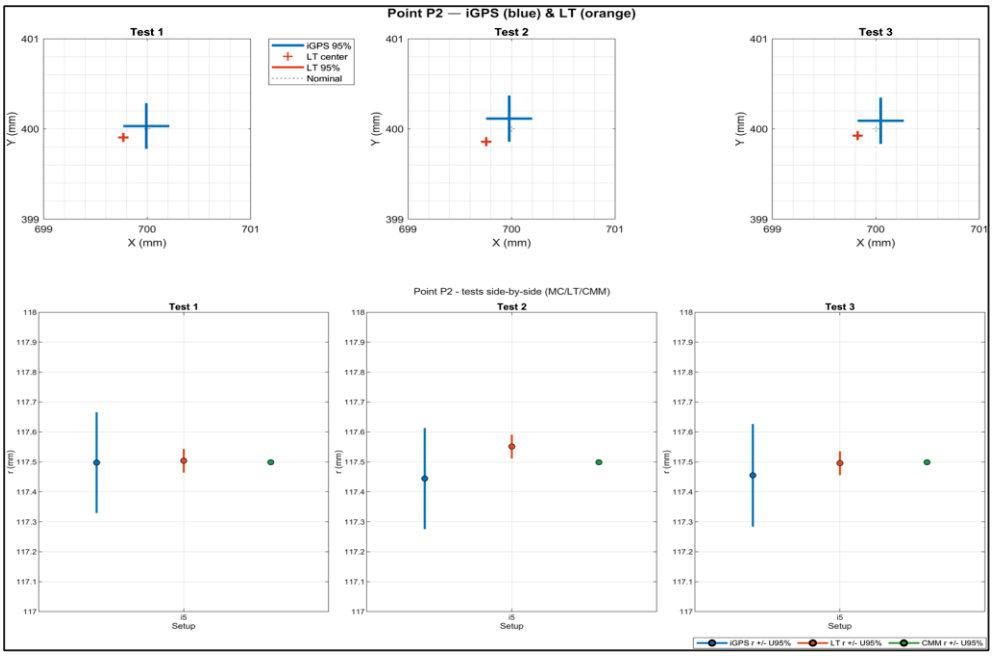

Figure 5.39 Point P2 - iGPS (blue) vs. LT (orange), 5-detector configuration

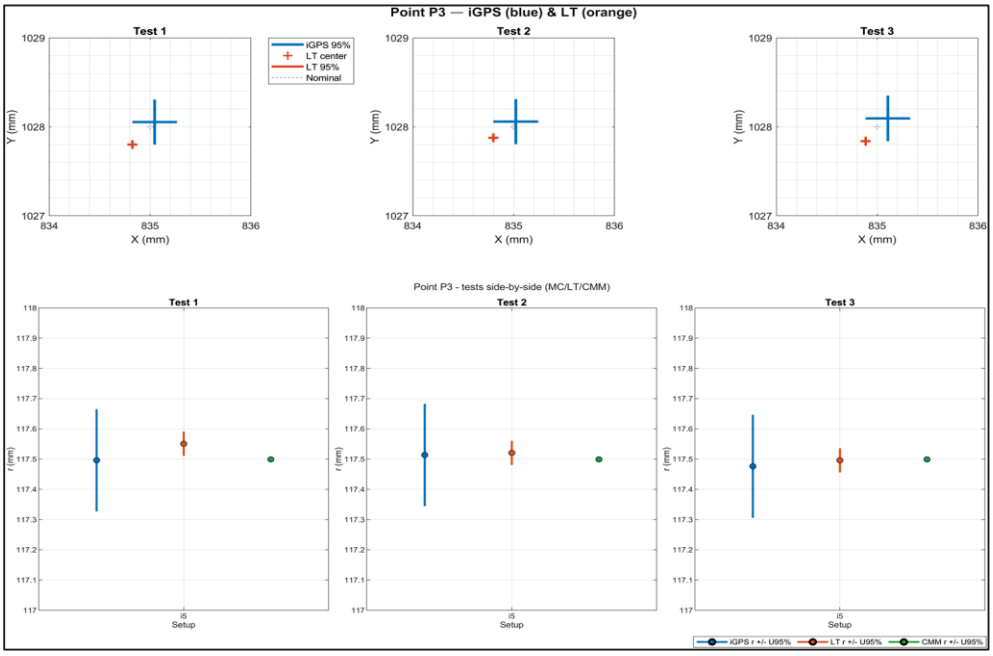

Figure 5.40 Point P3 - iGPS (blue) vs. LT (orange), 5-detector configuration

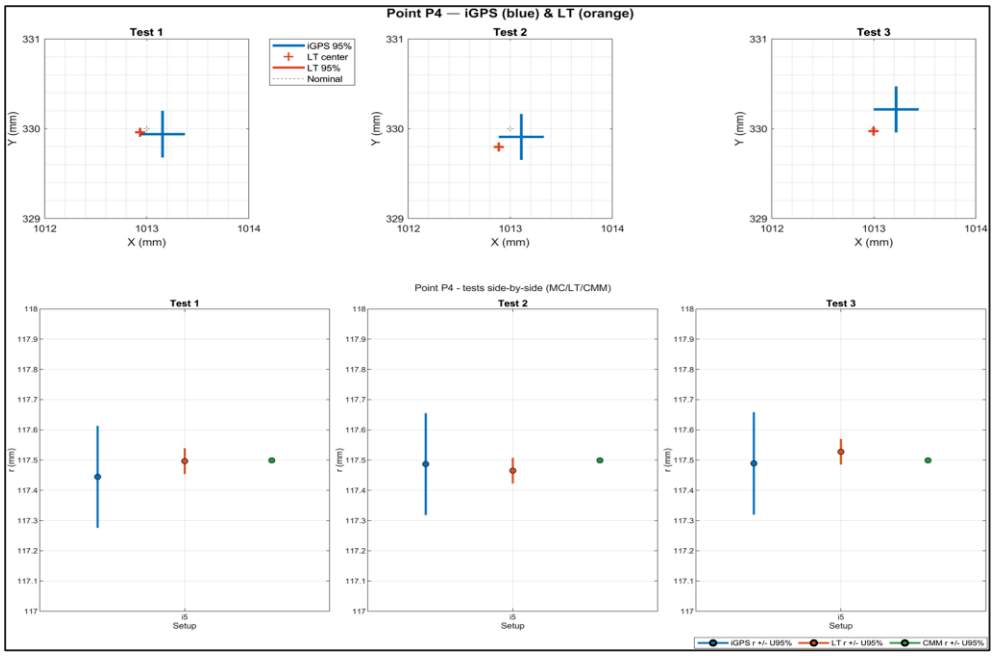

Figure 5.41 Point P4 - iGPS (blue) vs. LT (orange), 5-detector configuration

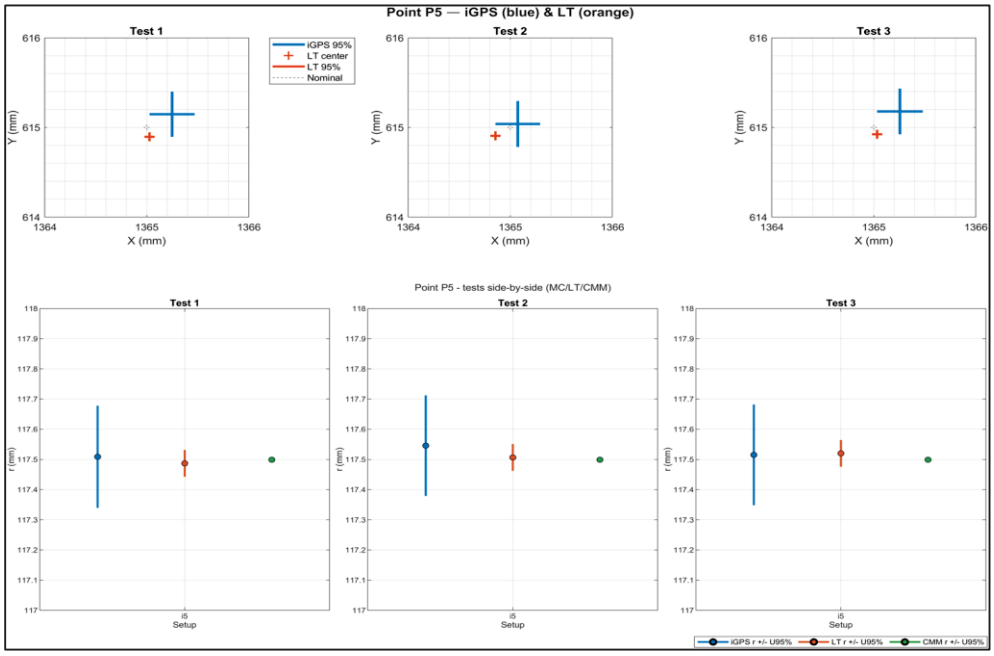

Figure 5.42 Point P5 - iGPS (blue) vs. LT (orange), 5-detector configuration

The results obtained under the 5-detector configuration demonstrate a further improvement in both precision and spatial stability compared to the 4-detector scenario.

Across all five target locations (P1–P5), the iGPS centers show strong alignment with LT references. The mean differences are typically below 0.2 mm in both X and Y axes, with the 95% confidence interval becoming noticeably smaller and more symmetric compared to previous setups. This indicates higher geometric redundancy and significantly reduced triangulation errors due to the addition of the fifth detector.

Regarding the radius values, the agreement among iGPS, LT, and CMM is excellent. As observed in the test results, the deviations generally remain under 0.05 mm relative to the references. The 95% confidence intervals of iGPS fully encompass the CMM reference and overlap with the LT intervals, confirming that the propagated uncertainties correctly represent the system's measurement behavior. Compared to the 4-detector configuration, the dispersion of the iGPS data has decreased notably, especially for peripheral points like P2 and P4, where the uncertainty regions have now stabilized.

The repeatability among the three tests per point remains consistent and stable, showing that the iGPS system performs reliably under this configuration. Overall, the 5-detector setup provides an optimal balance between system complexity and uncertainty reduction, yielding high accuracy in both radius and center estimation.

Figure 5.43 to Figure 5.47 display the results for the 6-detector configuration, the most geometrically stable arrangement tested. As in previous setups, the top plots represent circle centers, and the lower ones compare radius estimates from iGPS, LT, and CMM with 95 % CI.

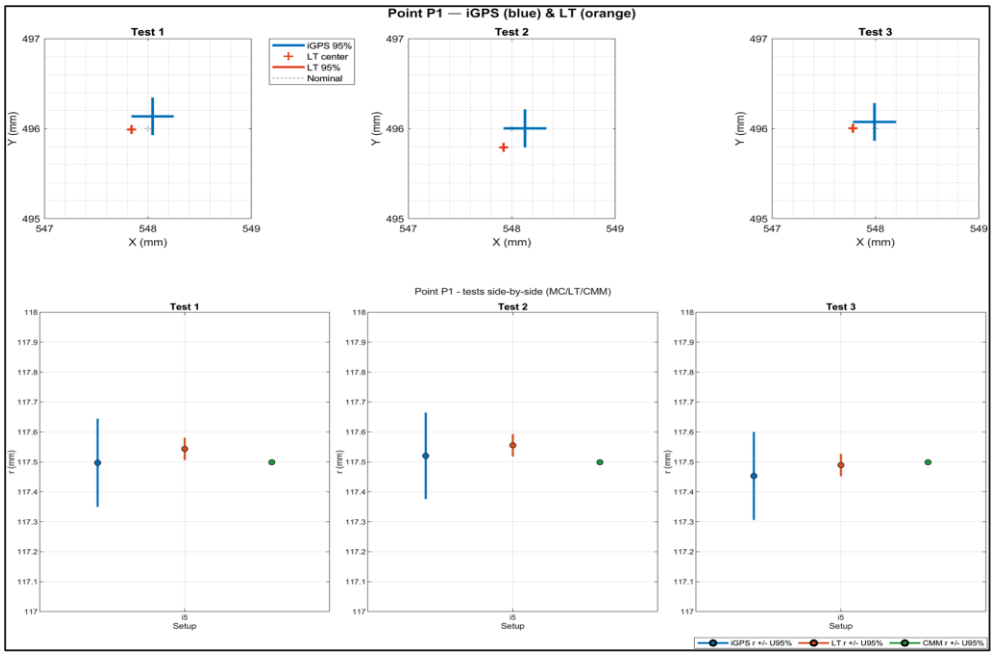

Figure 5.43 Point P1 - iGPS (blue) vs. LT (orange), 6-detector configuration

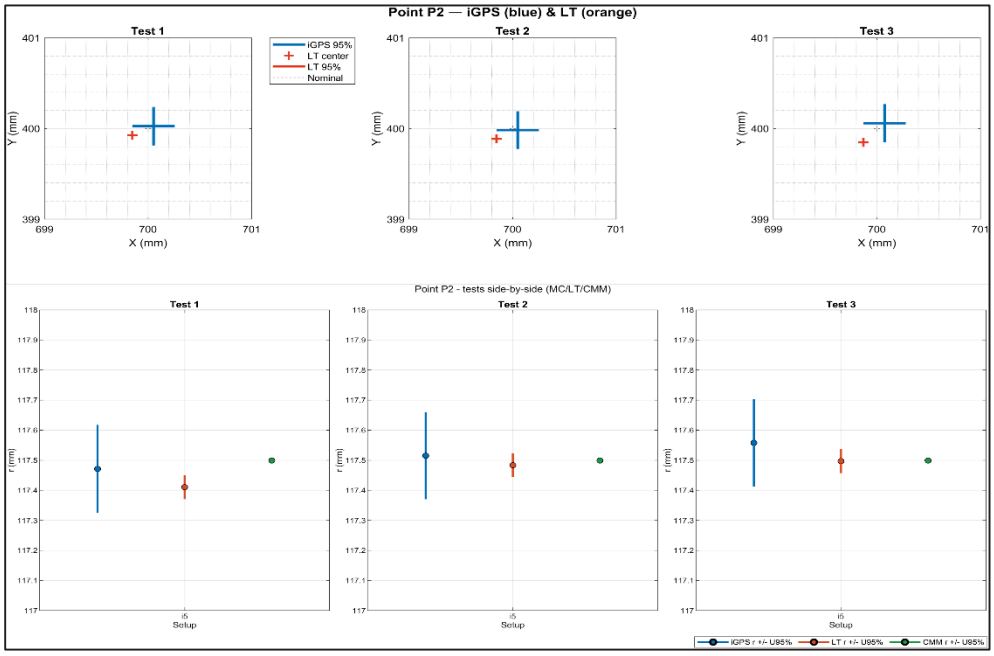

Figure 5.44 Point P2 - iGPS (blue) vs. LT (orange), 6-detector configuration

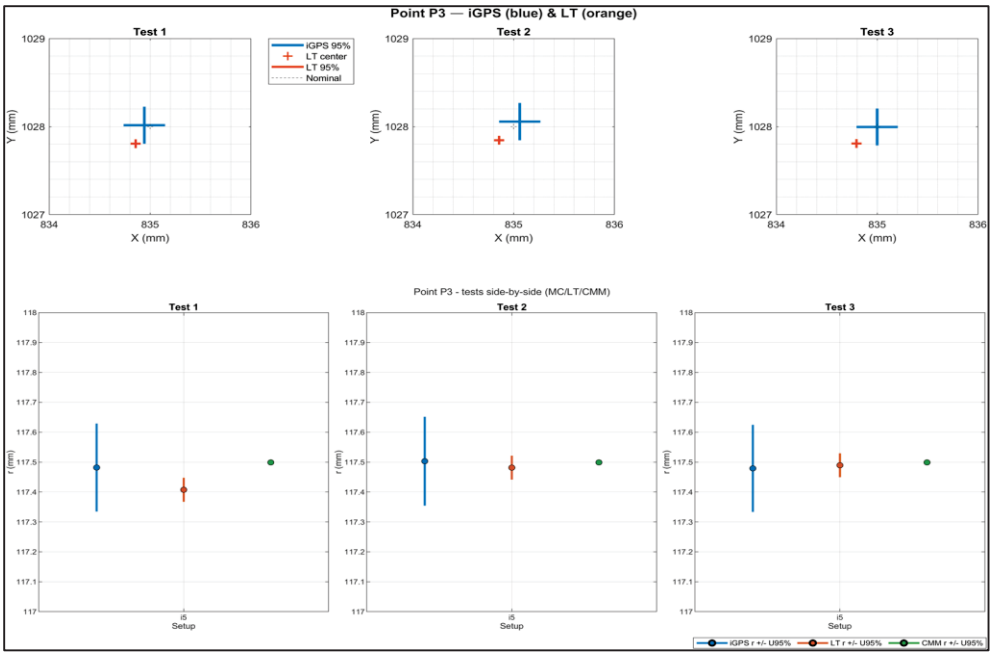

Figure 5.45 Point P3 - iGPS (blue) vs. LT (orange), 6-detector configuration

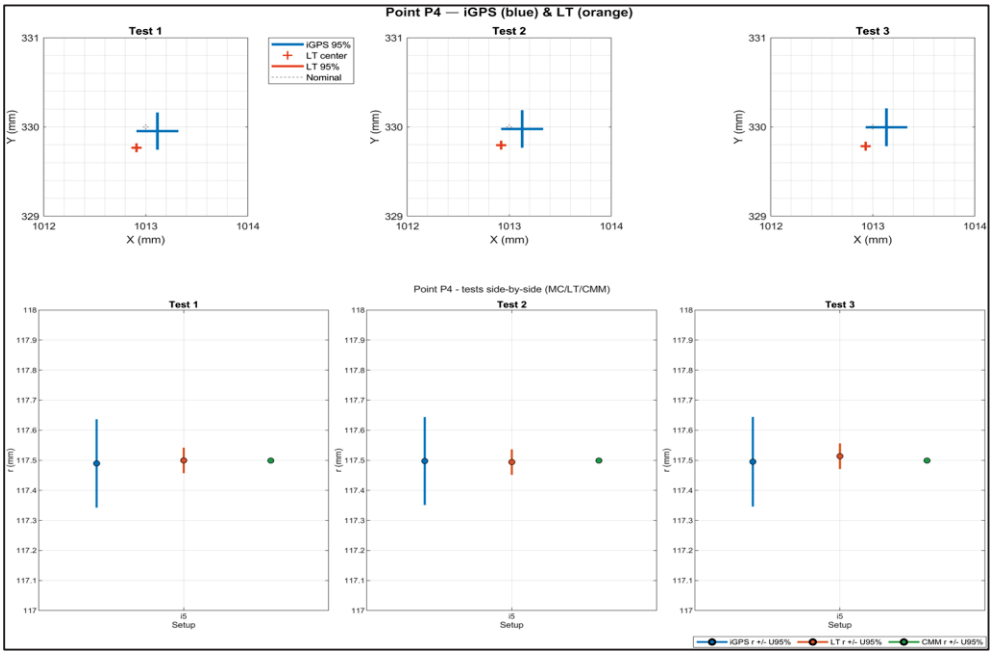

Figure 5.46 Point P4 - iGPS (blue) vs. LT (orange), 6-detector configuration

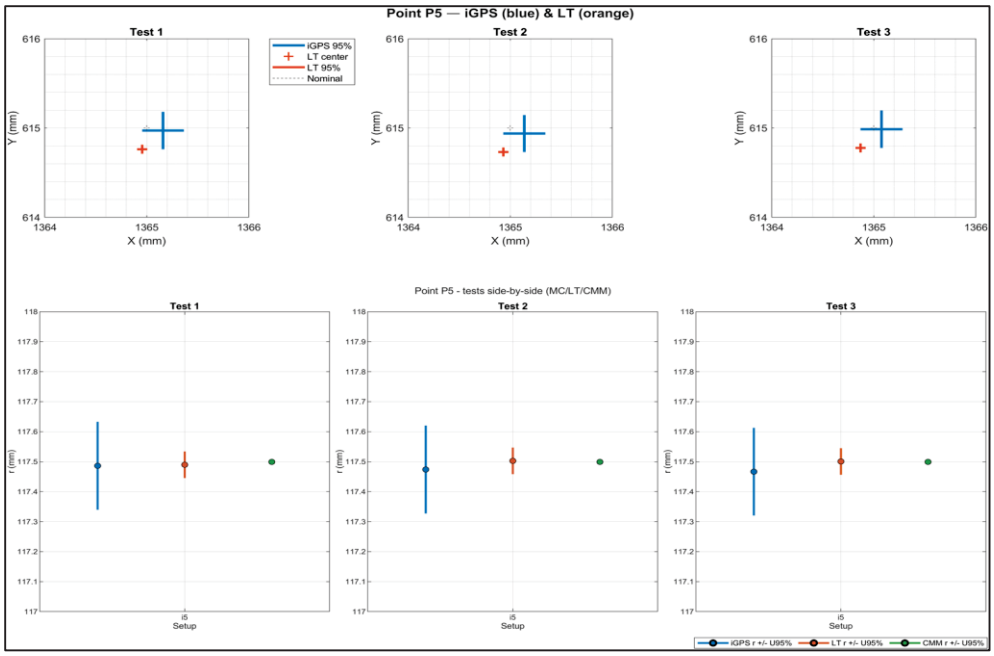

Figure 5.47 Point P5 - iGPS (blue) vs. LT (orange), 6-detector configuration

The 6-detector configuration represents the most geometrically stable and accurate arrangement tested. Across all five points (P1–P5), the iGPS centers exhibit near-perfect alignment with the LT references. The mean deviations are consistently below 0.15 mm in both X and Y directions. The 95% confidence interval are compact and almost perfectly circular, indicating that the maximum detector redundancy substantially enhances spatial constraint and minimizes the propagation of measurement uncertainty.

Regarding the radius results, the iGPS estimates show exceptional accuracy. As observed in the plots, deviations remain typically within 0.05 mm relative to the LT and CMM references, with their 95% confidence intervals overlapping completely. This confirms not only high accuracy but also the strong reliability of the Monte Carlo propagated uncertainty model. Furthermore, the consistency across the three repetitions per point suggests excellent repeatability and measurement stability.

Comparatively, the improvement from 5-detector to 6-detector configuration is modest but significant.

As expected, the 6-detector configuration achieves the lowest uncertainty, highest repeatability, and strongest agreement with LT and CMM references, establishing it as the most precise configuration among all tested setups. This configuration can therefore serve as high-precision iGPS-based assembly measurements where submillimetre accuracy is required.

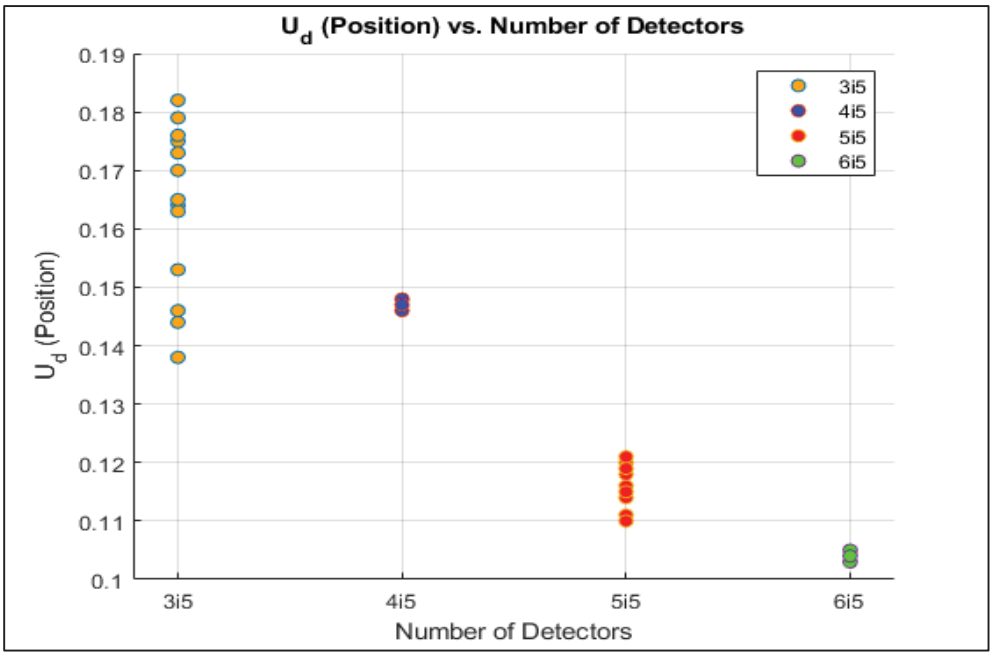

Figure 5.48 Effect of detector configuration on the Euclidean position difference between iGPS and Laser Tracker

Figure 5.48 shows the Euclidean distance difference between the positions obtained from the iGPS system and the Laser Tracker across the different detector configurations.

The experimental data confirms that increasing the number of detectors from 3 to 6 steadily decreases the combined position uncertainty (U_d) and enhances the measurement repeatability. While the 6-detector setup offers the ultimate precision, the sharpest gain in performance is realized at the 5-detector level, which balances system complexity with significant uncertainty reduction.

CONCLUSION

The main objective of this research was to develop a practical and traceable framework for jigless assembly based on 3D metrology. The intent was to reproduce the accuracy traditionally provided by physical jigs while improving flexibility, reducing costs, and enabling real time, measurement-assisted operations. To that end, two goals were pursued: first, to quantify the measurement uncertainty of each measurement point of iGPS system along the X, Y, and Z axes within a defined working volume using a Laser Tracker (LT) as the reference and in accordance with the Guide to the Expression of Uncertainty in Measurement (GUM); and second, to propagate those uncertainties to Key Characteristic (KC) (Euclidean distance and position) using Monte Carlo simulations, results are validated experimentally with Laser Tracker measurements.

Within the working volume, expanded uncertainties at the 95% confidence level were obtained for each axis, namely U_X = 0.4985 mm, U_Y = 0.5182 mm, and U_Z= 0.4992 mm. Statistical analysis identified the distance between points as the dominant factor influencing measurement uncertainty, while time and day had no statistically significant effects (p-value > 0.05). The Laser Tracker as a reference showed stable behavior, and the maximum reference uncertainty was incorporated when combining components, ensuring alignment with GUM principles. For propagation to position, the analysis was implemented for a circular feature in the XY plane, a Monte Carlo simulation with 10,000 iterations reached convergence after about 6,000 iterations. For each target location and detector configuration (3i5, 4i5, 5i5, 6i5), the circle's center and radius were estimated and compared with Laser Tracker and CMM reference data.

The results demonstrate that the proposed uncertainty model accurately represents real measurement behavior. Across all configurations, mean center deviations between iGPS and Laser Tracker were $\leq$ 0.3 mm for 3i5, $\leq$ 0.25 mm for 4i5, $\leq$ 0.2 mm for 5i5, and $\leq$ 0.15 mm for 6i5, while radius differences between iGPS and Laser Tracker /CMM decreased from roughly ±0.15 mm (3i5) to ±0.05 mm (6i5). Increasing the number of detectors improved geometric stability: confidence ellipses for the estimated centers became smaller, with the 6-

detector configuration providing the most accurate and stable results and a modest but meaningful improvement over the 5-detector case. Practically, these findings show that submillimetre accuracy is achievable in jigless assembly when uncertainty is explicitly quantified and propagated, enabling decisions about alignment, gap, and positioning to be based on confidence intervals rather than nominal values, and thereby reducing cost and improving flexibility without sacrificing accuracy.

Scientifically and technically, this work delivers a standardized estimation procedure for iGPS uncertainty within a working volume, combining repeatability, device, and reference components according to GUM and validating them against Laser Tracker. It establishes a complete uncertainty propagation chain from axis uncertainties to positional KCs using Monte Carlo, with explicit convergence monitoring and reporting at the 95% confidence level. It systematically analyzes geometric redundancy by quantifying the benefit of increasing the detector count from 3i5 to 6i5 on the size and confidence ellipses. It also provides dual validation with Laser Tracker and CMM that extends beyond calibration to the full-propagation chain, confirming statistical agreement between simulated and measured data. Together, these contributions constitute a comprehensive and reproducible methodology for implementing Metrology-Assisted Assembly (MAA) in a jigless assembly.

The industrial implications are direct. The results support the adoption of MAA in large-scale assembly by showing that using five to six detectors yields geometrically robust setups with small and reliable positional estimation. Expressing results as 95% confidence intervals gives process engineers a probabilistic measure of KC conformity that supports informed decisions at the line. For sectors such as automotive and aerospace, where product variability is high and tolerances are strict, this approach reduces dependence on jigs, shortens reconfiguration time, and maintains dimensional quality through data-driven control.

This study has limitations. The experiments were performed within a specific working volume and detector geometry, so extending the approach to other setups requires recalibration. Inter-axis correlations were assumed negligible. Importantly, the bias between iGPS and Laser

Tracker was computed but not included in the uncertainty propagation model; details are documented in the Appendix for transparency. Consequently, the reported uncertainties primarily represent random components and may slightly underestimate total uncertainty.

In conclusion, a carefully calibrated iGPS-based metrology system, combined with explicit uncertainty quantification and propagation, can effectively replace mechanical jigs in large-scale assemblies. From estimating U_X, U_Y and U_Z to Monte Carlo propagation and dual validation with Laser Tracker and CMM, the framework achieves submillimetre precision and repeatability.

RECOMMENDATIONS

Based on the findings and limitations of this research, several recommendations are proposed to guide future work and industrial implementation of jigless assembly supported by 3D metrology and uncertainty management.

First, it is recommended to incorporate bias estimation into the uncertainty propagation model. Although bias between the iGPS and Laser Tracker (LT) was analyzed, it was not included in the Monte Carlo simulation due to atypical patterns. A bias-aware Monte Carlo framework should be developed to integrate both random and systematic components, providing a more realistic representation of total measurement uncertainty.

Second, the proposed uncertainty propagation method should be extended to other GD&T features, such as 3D position, flatness, and parallelism, as well as to multi-stage assemblies. These extensions would allow the methodology to cover a broader range of industrial scenarios and further validate its robustness.

Third, it is advised to develop a real-time metrology dashboard for assembly operators. This system should display the 95% confidence intervals of key characteristics (KCs), provide visual indicators of conformity or deviation, and suggest corrective actions during the process. Integrating uncertainty visualization into the assembly interface would make the methodology more intuitive and immediately usable on the production floor.

Finally, it is recommended to integrate the developed framework into real industrial assembly environments in collaboration with manufacturers in the aerospace or automotive sectors. This would provide a realistic assessment of the system’s robustness, repeatability, and cost effectiveness in operational conditions.

By following these recommendations, future research can complete the transition from geometry constrained by physical jigs to geometry controlled by measurement and data,

strengthening the reliability, flexibility, and traceability of modern assembly systems within the framework of Industry 4.0.

APPENDIX A

BIAS ESTIMATION BETWEEN IGPS AND LASER TRACKER

In this appendix, the procedure used to estimate and examine the bias between the iGPS and the Laser Tracker (LT) is described. To ensure a valid comparison, both measurement systems were aligned as closely as possible in their coordinate frames. A Plane–Line–Line alignment was performed according to the manufacturer's procedure, and the origins and primary axes were synchronized in the software environment.

After alignment, a series of points was selected along the X-axis, which were measured by both instruments: the LT using a 1.5in Red Ring probing and the iGPS using its detector. Each point was measured three times with each device, ensuring repeatability. The bias for each coordinate was then computed as the difference between the iGPS and LT measurements $(X_{\text{iGPS}} - X_{LT})$, $((Y_{\text{iGPS}} - Y_{LT})$. Initially, a small number of alignment features were used, followed by an increased number of reference points for both the plane and the line to verify whether the results would change. However, the bias pattern remained consistent.

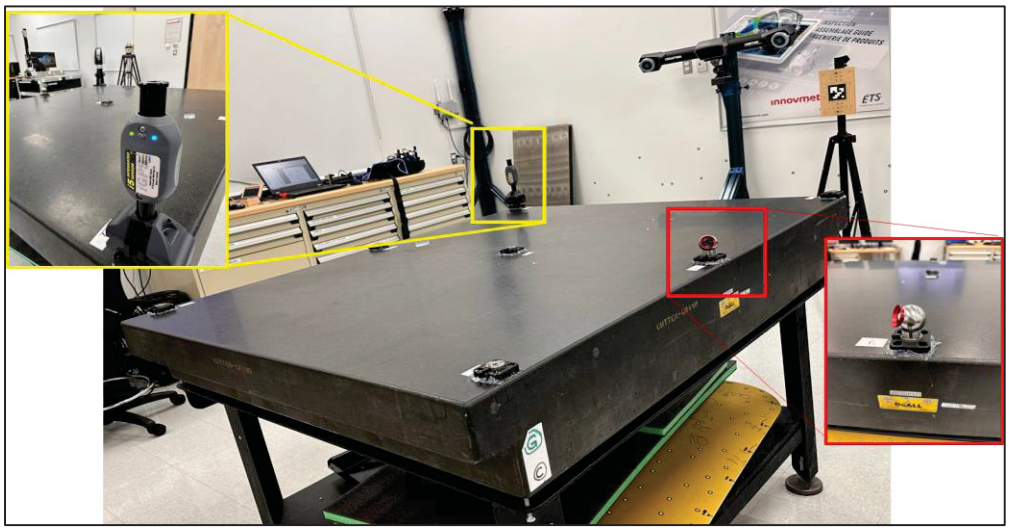

Figure AA.1 Integrated setup for bias estimation between the iGPS and Laser Tracker

Table AA.1 Point iGPS–LT comparison and component bias

	iGPS		LT		Bias	
	X	Y	X	Y	X	Y
Point1-Test1	97.037	32.910	96.636	32.743	0.401	0.167
Point1-Test2	97.004	32.860	96.627	32.733	0.377	0.127
Point1-Test3	97.424	32.410	97.121	32.352	0.303	0.058
Point2-Test1	759.907	33.632	759.507	33.608	0.400	0.024
Point2-Test3	761.981	33.042	761.694	32.974	0.287	0.068
Point3-Test1	1500.100	30.417	1499.554	30.432	0.546	-0.015
Point3-Test2	1500.010	30.311	1499.533	30.420	0.477	-0.109
Point3-Test3	1500.061	30.430	1499.547	30.426	0.514	0.004
Point4-Test1	102.530	1192.847	101.903	1192.795	0.627	0.052
Point4-Test2	102.480	1192.878	101.925	1192.770	0.555	0.108
Point4-Test3	102.519	1192.834	101.937	1192.780	0.582	0.054
Point5-Test1	800.231	1193.074	799.699	1193.000	0.532	0.074
Point5-Test2	800.325	1193.016	799.712	1193.007	0.613	0.009
Point5-Test3	800.283	1193.005	799.693	1193.024	0.590	-0.019
Point6-Test1	1500.720	1187.436	1500.139	1187.581	0.581	-0.145
Point6-Test2	1500.694	1187.472	1500.134	1187.595	0.560	-0.123
Point6-Test3	1500.711	1187.537	1500.136	1187.593	0.575	-0.056
Average					0.373	0.051

The results showed that the bias along the X-axis was stable and consistently positive. For point separations between approximately 100 mm and 800 mm, the X-bias values ranged between 0.30 and 0.63 mm, while for the largest interval around 1500 mm, the bias ranged from 0.47 to 0.58 mm.

The Y-component of bias oscillated around zero and remained relatively small in magnitude, typically between −0.15 mm and +0.17 mm, indicating no significant systematic deviation. The Z-component was not considered for bias estimation because the XY plane.

To eliminate the effect of coordinate frame alignment and isolate the metrological behavior, a second approach was applied. The Euclidean distance between pairs of points on the reference scale bar (Objective 1) was measured using both systems, each repeated three times. For the X-axis pair, the iGPS coordinates were:

Table AA.2 iGPS coordinates X,Y-axis pair

iGPS- X axis				
	FrameName	X	Y	Z
Point 1-rep1	i5IS_0104952316	1327.259	173.821	102.196
Point 2-rep1	i5IS_0104952315	80.281	173.750	102.047
Point 1-rep2	i5IS_0104952316	1327.263	173.823	102.196
Point 2-rep2	i5IS_0104952315	80.288	173.750	102.045
Point 1-rep3	i5IS_0104952316	1327.262	173.827	102.189
Point 2-rep3	i5IS_0104952315	80.278	173.751	102.041
iGPS- Y axis				
	FrameName	X	Y	Z
Point 1-rep1	i5IS_0104952316	116.513	49.489	102.039
Point 2-rep1	i5IS_0104952315	116.899	1296.484	101.893
Point 1-rep2	i5IS_0104952316	116.514	49.490	102.036
Point 2-rep2	i5IS_0104952315	116.893	1296.486	101.892
Point 1-rep3	i5IS_0104952316	116.509	49.487	102.044
Point 2-rep3	i5IS_0104952315	116.900	1296.491	101.898

Table AA.3 LT coordinates X,Y-axis pair

Laser Tracker X axis			
	X	Y	Z
Point 1-rep1	79.813	173.643	133.785
Point 2-rep1	1326.912	173.662	133.937
Point 1-rep2	79.826	173.639	133.782
Point 2-rep2	1326.92	173.644	133.93
Point 1-rep3	79.835	173.634	133.768
Point 2-rep3	1326.918	173.647	133.933
Laser Tracker Y axis			
	X	Y	Z
Point 1-rep1	116.485	1296.352	133.601
Point 2-rep1	116.101	49.249	133.755
Point 1-rep2	116.497	1296.358	133.628
Point 2-rep2	116.097	49.249	133.748
Point 1-rep3	116.493	1296.343	133.624
Point 2-rep3	116.082	49.234	133.757

Table AA.4 Euclidean distance comparison on X,Y-axis pair: iGPS vs LT

	ED i,j-iGPS- X axis	ED i,j-LT- X axis	
point i,j	d ij	d ij	d IGPS- d LT
Point1,2-Rep1	1246.978	1247.099	-0.121
Point1,2-Rep2	1246.976	1247.094	-0.118
Point1,2-Rep3	1246.985	1247.083	-0.098
	ED i,j-iGPS- Y axis	ED i,j-LT- Y axis	
point i,j	d ij	d ij	d IGPS- d LT
Point1,2-Rep1	1246.995	1247.103	-0.108
Point1,2-Rep2	1246.996	1247.109	-0.113
Point1,2-Rep3	1247.005	1247.109	-0.104

The difference in measured distances was taken as a metric of length bias. This approach is independent of coordinate translation or rotation and provides a direct assessment of the comparative measurement behavior of the two systems over distance.

Figure AA.2 Experimental setup for bias evaluation along X and Y-axes

These distance-based results are consistent across axes and repetitions and, importantly, are independent of any residual rotation or translation between frames. In both the X-pair and Y-pair analyses the iGPS distance is shorter than the LT distance by about one tenth of a millimeter. The mean distance bias is approximately -0.112 mm on the X-pair and -0.108 mm on the Y-pair, with small spreads across the three repetitions, indicating good repeatability of the estimate. The negative sign means that, on the length scale of ~1.25 m, iGPS slightly underestimates the true distance compared to LT. For transparency, we report these distance differences here and, as stated in the main text, we did not incorporate this bias into the

uncertainty propagation model; instead, it is documented in this appendix as a stable, axis-agnostic indicator (≈ -0.11 mm over ~1.25 m) to inform future bias modeling and calibration.

LIST OF BIBLIOGRAPHICAL REFERENCES

Analysis of Variance for Completely Randomized Designs. (2024, 9 mars). Repéré à https://pub.aimind.so/analysis-of-variance-for-completely-randomized-designs-8065177953d4

Chen, Z., & Du, F. (2017). Measuring principle and uncertainty analysis of a large volume measurement network based on the combination of iGPS and portable scanner. *Measurement*, *104*, 263-277. https://doi.org/10.1016/j.measurement.2017.03.037

de Mello, J. M. G., Trabasso, L. G., Reckevcius, A. C., Palmeira, A. L. O. A., Reiss, P., & Caraca, W. (2020). A novel jigless process applied to a robotic cell for aircraft structural assembly. *The International Journal of Advanced Manufacturing Technology*, *109*(3), 1177-1187. https://doi.org/10.1007/s00170-020-05700-4

Drouot, A., Zhao, R., Irving, L., Sanderson, D., & Ratchev, S. (2018). Measurement Assisted Assembly for High Accuracy Aerospace Manufacturing∗. *IFAC-PapersOnLine*, *51*(11), 393-398. https://doi.org/10.1016/j.ifacol.2018.08.326

Émond-Girard, L. (2022). *Analyse de l'erreur du positionnement assisté par la métrologie 3D sans contact*. masters. École de technologie supérieure. Repéré à https://espace.etsmtl.ca/id/eprint/3011/

Ferri, C., Mastrogiacomo, L., & Faraway, J. (2010). Sources of variability in the set-up of an indoor GPS. *International Journal of Computer Integrated Manufacturing*, *23*(6), 487-499. https://doi.org/10.1080/09511921003642147

Fiedler, F., Ehrenstein, J., Höltgen, C., Blondrath, A., Schäper, L., Göppert, A., & Schmitt, R. (2024). Jigs and Fixtures in Production: A Systematic Literature Review. *Journal of Manufacturing Systems*, *72*, 373-405. https://doi.org/10.1016/j.jmsy.2023.10.006

Franceschini, F., Galetto, M., Maisano, D., & Mastrogiacomo, L. (2014). Large-scale dimensional metrology (LSDM): from tapes and theodolites to multi-sensor systems. *International Journal of Precision Engineering and Manufacturing*, *15*(8), 1739-1758. https://doi.org/10.1007/s12541-014-0527-2

Francis, A., Maropoulos, P., Mullineux, G., & Keogh, P. (2016). Design for Verification. *Procedia CIRP*, *56*, 61-66. https://doi.org/10.1016/j.procir.2016.10.017

Fukuda, T., Dobashi, H., Nagano, H., Tazaki, Y., Katayama, R., & Yokokohji, Y. (2023). Jigless assembly of an industrial product by a universal robotic hand mounted on an industrial robot. *Robotica*, *41*(8), 2464-2488. https://doi.org/10.1017/S0263574723000474

Ganguly, B., Dey, B. K., Pareek, S., & Sarkar, B. (2023). Cost-Effective Imperfect Production-Inventory System under Variable Production Rate and Remanufacturing. *Mathematics*, *11*(15), 3417. https://doi.org/10.3390/math11153417

Han, R., Dunker, T., Trostmann, E., & Xu, Z. (2024). Research on high-precision tracking and localization of industrial robots based on iGPS. *Measurement Science and Technology*, *35*(6), 065006. https://doi.org/10.1088/1361-6501/ad2f08

https://7dkmetrology.com/. (2024, 16 octobre). 6th Generation Technology Further Increases iGPS Usability & Performance. *6th Generation Technology Further Increases iGPS Usability & Performance*. Repéré à https://7dkmetrology.com/7dk-1/products

JCGM - Joint Committee for Guides in Metrology. (2008). Repéré à https://www.iso.org/sites/JCGM/GUM-introduction.htm

Maisano, D. A., Jamshidi, J., Franceschini, F., Maropoulos, P. G., Mastrogiacomo, L., Mileham, A. R., & Owen, G. W. (2008). Indoor GPS: system functionality and initial performance evaluation. *International Journal of Manufacturing Research*, *3*(3), 335. https://doi.org/10.1504/IJMR.2008.019214

Mei, Z., & Maropoulos, P. G. (2014). Review of the application of flexible, measurement-assisted assembly technology in aircraft manufacturing. *Proceedings of the Institution of Mechanical Engineers, Part B: Journal of Engineering Manufacture*, *228*(10), 1185-1197. https://doi.org/10.1177/0954405413517387

Metrolog X4 - Metrologic Group. (2019, 9 janvier). Repéré à https://www.metrologic.group/metrolog-x4/

Mochizuki, T. (2010). Application of Reverse Engineering to Product Development. *Applied Mechanics and Materials*, *42*, 5-8. https://doi.org/10.4028/www.scientific.net/AMM.42.5

Moses, A., Golos, D., & Bennett, C. (2015). An Alternative Approach to Early Literacy: The Effects of ASL in Educational Media on Literacy Skills Acquisition for Hearing Children DOI 10.1007/s10643-015-0690-9. *Early Childhood Education Journal*, *43*. https://doi.org/10.1007/s10643-015-0690-9

Mozzillo, R., Iaccarino, P., Vitolo, F., & Franciosa, P. (2019). Design and development of jigless assembly process: the case of complex aeronautical systems. Dans *2019 II Workshop on Metrology for Industry 4.0 and IoT (MetroInd4.0&IoT)* (pp. 132-136). https://doi.org/10.1109/METROI4.2019.8792874

Muelaner, J. E., Martin, O. C., & Maropoulos, P. G. (2013). Achieving Low Cost and High Quality Aero Structure Assembly through Integrated Digital Metrology Systems. *Procedia CIRP*, *7*, 688-693. https://doi.org/10.1016/j.procir.2013.06.054

Muelaner, J. E., Wang, Z., Jamshidi, J., & Maropoulos, P. G. (2010). Verification of the Indoor GPS System by Comparison with Points Calibrated Using a Network of Laser Tracker Measurements. Dans G. Q. Huang, K. L. Mak, & P. G. Maropoulos (Éds), *Proceedings of the 6th CIRP-Sponsored International Conference on Digital Enterprise Technology* (pp. 607-619). Berlin, Heidelberg : Springer. https://doi.org/10.1007/978-3-642-10430-5_47

Muelaner, Jody E, Kayani, A., Martin, O., & Maropoulos, P. (2011). Measurement Assisted Assembly and the Roadmap to Part-To-Part Assembly: 7th International Conference on Digital Enterprise Technology (pp. 11-19). Repéré à http://www.lms.mech.upatras.gr/DET2011/

Naing, S., Burley, G., Odi, R., Williamson, A., & Corbett, J. (2000). Design for tooling to enable jigless assembly - An integrated methodology for jigless assembly. *SAE Technical Papers*. https://doi.org/10.4271/2000-01-1765

Nicksch, C., Sabzehi, M., & Schmitt, R. H. (2022). Virtual indoor-GPS for measurement uncertainty determination in reconfigurable environments. *Production Engineering*, *16*(4), 545-560. https://doi.org/10.1007/s11740-022-01111-4

Pilati, F., Lelli, G., Regattieri, A., & Ferrari, E. (2022). Assembly line balancing and activity scheduling for customised products manufacturing. *The International Journal of Advanced Manufacturing Technology*, *120*(5), 3925-3946. https://doi.org/10.1007/s00170-022-08953-3

Ren, Y., Fu, Y., Liu, F., & Zhang, F. (2019). Multilateration with laser tracker applied in large-scale coordinate calibration. Dans *Optical Metrology and Inspection for Industrial Applications VI* (Vol. 11189, pp. 107-113). SPIE. https://doi.org/10.1117/12.2539646

Schmitt, R. H., Peterek, M., Morse, E., Knapp, W., Galetto, M., Härtig, F., … Estler, W. T. (2016). Advances in Large-Scale Metrology – Review and future trends. *CIRP Annals*, *65*(2), 643-665. https://doi.org/10.1016/j.cirp.2016.05.002

Tang, X., & Chen, Z. (2015). A Multi-dimensional Model for Computer-Aided Measuring Planning (CAMP) in Digital Manufacturing. Dans A. Fred, J. L. G. Dietz, K. Liu, & J. Filipe (Éds), *Knowledge Discovery, Knowledge Engineering and Knowledge Management* (pp. 56-65). Berlin, Heidelberg : Springer. https://doi.org/10.1007/978-3-662-46549-3_4

Ted Hessing. (2014, 13 septembre). Measurement Systems Analysis (MSA). *Six Sigma Study Guide*. Repéré à https://sixsigmastudyguide.com/measurement-systems-analysis/

Turnadge, C., Mallants, D., & Peeters, L. (2018). *Overview of aquitard and geological fault simulation approaches in regional scale assessments of coal seam gas extraction impacts*. (S.l.) : (s.n.).

Wang, Z., Mastrogiacomo, L., Franceschini, F., & Maropoulos, P. (2011). Experimental comparison of dynamic tracking performance of iGPS and laser tracker. *The International Journal of Advanced Manufacturing Technology*, *56*(1), 205-213. https://doi.org/10.1007/s00170-011-3166-0

Zhao, G., Zhang, P., & Xiao, W. (2018). Coordinate alignment of combined measurement systems using a modified common points method. *Journal of Instrumentation*, *13*(03), P03021. https://doi.org/10.1088/1748-0221/13/03/P03021

Zhu, X., Zheng, L., & Tang, X. (2016). Configuration Optimization of Laser Tracker Stations for Large-scale Components in Non-uniform Temperature Field Using Monte-carlo Method. *Procedia CIRP*, *56*, 261-266. https://doi.org/10.1016/j.procir.2016.10.078